Technical Report

TR-99-34

Mechanical failure of SKB spent fuel disposal canisters

Mathematical modelling and scoping calculations

Hiroyasu Takase, Steven Benbow, Peter Grindrod
QuantiSci

Oktober 1998

Svensk Kärnbränslehantering AB
Swedish Nuclear Fuel
and Waste Management Co
Box 5864
SE-102 40 Stockholm Sweden
Tel 08-459 84 00
+46 8 459 84 00
Fax 08-661 57 19
+46 8 661 57 19

Mechanical failure of SKB spent fuel disposal canisters

Mathematical modelling and scoping calculations

Hiroyasu Takase, Steven Benbow, Peter Grindrod
QuantiSci

October 1998

Executive Summary

According to the current design of SKB, a copper overpack with a cast steel inner component will be used as the disposal canister for spent nuclear fuel. A recent study considered the case of a breach in the copper overpack, through which groundwater could enter the canister. It has pointed out that hydrogen gas generated by an anaerobic corrosion could cushion the system and reduce or eventually stop further infiltration of water into the breached canister, and thence the spent fuel.

One potential pitfall in this previous study lies in the fact that it did not consider any processes which might violate the following assumptions which are essential for the gas "cushioning":

1. Hydrogen gas accumulated in the annular gap in the canister forms a free gas phase which is stable indefinitely into future;

2. Elevated gas pressure in the canister prevents further supply of groundwater except for diffusion of vapour.

In the current study we developed a set of mathematical models for the above problem and applied it to carry out an independent assessment of the long-term behaviour of the canister. A key aim in this study was to clarify whether there are any alternative processes which may affect the result obtained by the previous study by violating one of the assumptions listed above. For this purpose, a scenario development exercise was conducted. The result supported the concept described in the previous study. One exception is that possible intrusion of bentonite gel followed by its desaturation could leave paths both for the gas and water simultaneously without forming a gas cushion. This is summarised in the first part of the report.

In the second part, development of mathematical models and their applications are described. The key results are:

1. The model describing behaviour of gas and pore water in the canister and the buffer material reproduced the main results of the previous study;

2. The model considering intrusion of the bentonite gel pointed out possibility where the gas cushion fails to form and water keeps coming into the canister from the buffer. However, even in this case, significant deformation of the copper overpack due to accumulation of magnetite takes very long time;

3. The model for corrosion of the steel inner container by vapour supported the main results obtained by the previous study.

In summary, prolonged containment time after failure of the outer copper overpack is justifiable and can be incorporated in a safety assessment provided a robust view is taken considering the conceptual and the parameter variations investigated in this study.

Sammanfattning

Enligt SKBs gällande förvarsdesign kommer ett kopparhölje med gjutjärnsinsats att användas som förvaringskapsel för använt bränsle. En tidigare studie betraktade fallet med en skada i kopparhöljet, genom vilken grundvatten kunde komma in i kapseln. Det har poängterats att vätgas från anaerobisk korrosion skulle kunna dämpa systemet genom att reducera och slutligen stoppa ytterligare inflöde av vatten in i den skadade kapseln och följaktligen till det använda bränslet.

En potentiell begränsning i den tidigare studien var att den inte studerade några processer som kunde förändra följade randvillkor, vilka är nödvändiga för "gasdämpningen":

1. Vätgasen som samlas i spalten mellan hölje och insats bildar en fri gasfas som är stabil för all framtid;

2. Förhöjt gastryck i kapseln förhindrar ytterligare vattentillförsel, förutom genom diffusion i ångfas.

I den här studien har vi utvecklat en uppsättning matematiska modeller för ovannämnda problem och tillämpat dem för att genomföra en oberoende analys av kapselns långtidsfunktion. Ett huvudmål i den här studien var att klargöra om det finns alternativa processer som skulle kunna påverka resultatet från den tidigare studien genom att avvika från något av de tidigare nämnda randvillkoren. För detta ändamål genomfördes en scenarioutvecklingsstudie. Resultatet från denna stöder de valda förutsättningarna i den tidigare studien. Det enda undantaget är inträngning av bentonitgel, vilket skulle kunna bilda samtidiga transportvägar för vatten och gas utan att en gaskudde bildas. Detta beskrivs i den första delen av rapporten.

I den andra delen beskrivs utvecklingen av de matematiska modellerna och tillämpningen av dessa. Huvudresultaten är:

1. Modellen som beskriver beteendet av gas och porvatten i kapseln och buffertmaterial återskapar huvudresultat från den tidigare studien.

2. Modellen som beskriver inträngning av bentonitgel pekar ut en möjlighet där en gaskudde inte bildas och vatten fortsätter att strömma in i kapseln från bufferten. Även i detta fall tar det dock mycket lång tid innan kopparhöljet börjar att deformeras på grund av uppbyggnad av magnetit.

3. Modellen av korrosion av stålinsatsen från vattenånga stöder resultaten från den tidigare studien.

Sammanfattningsvis, förlängd isoleringstid efter en skada i kopparhöljet är försvarbart och kan används i säkerhetsanalyser, om ett robust synsätt tillämpas, med tanke på de konceptuella- och parametervariationerna i denna studie.

Summary

According to the current design of SKB, a copper overpack with a cast steel inner component will be used as the disposal canister for spent nuclear fuel. A recent study conducted by AEA Technology **[1]** considered the case of a breach in the copper overpack, through which groundwater could enter the canister. The report **[1]** concluded that, due to the hydrogen gas cushion generated by an anaerobic corrosion process, infiltration of water into the breached canister, and thence the spent fuel, is reduced and eventually stops in a finite time.

One potential pitfall in this previous study lies in the fact that it did not consider any processes which might violate the following assumptions which are essential for the gas "cushioning":

1. Hydrogen gas accumulated in the annular gap in the canister forms a free gas phase which is stable indefinitely;

3. Elevated gas pressure in the canister prevents further supply of groundwater except for diffusion of vapour.

As a consequence, it is not at all clear what conditions are required for the gas cushioning to take place although it seems fairy unlikely that the stable gas phase can form all values of certain parameters such as size of the hole(s) through the copper canister.

In the current study we developed a set of mathematical models for the above problem and applied it to carry out an independent assessment of the long term behaviour of the spent fuel disposal canister. A key aim in this study was to clarify whether there are any alternative processes which may affect the result obtained by the previous study by violating one of the assumptions listed above.

The first part of the report summarises an independent scenario development exercise addressing the above issue. As a result of the event tree analyses, we obtained the following conclusions similar to **[1]**:

- As long as there exists water as liquid in the canister, steel corrosion will be dominated by anaerobic reaction with it and, as a result, the system will exhibit a complicated behaviour driven by coupled water flow, steel corrosion and gas transport;

- Coupled behaviour of the flow, steel corrosion and gas transport can vary considerably depending on key parameters such as height and size of the penetration through the copper overpack, rate of the steel corrosion and so on;

- The flux of water flowing into the canister will decrease as the internal gas pressure rises, and will eventually become less than the amount of water consumed by corrosion. After all the (liquid) water is consumed, steel corrosion will continue with supply of water vapour.

In addition the following two issues that were not considered in **[1]** were identified:

- Depending on the position of the crack(s) through the steel inner container relative to the maximum height of the water table in the annular gap between the copper overpack and the inner container, the coupled flow-corrosion-gas transport behaviour may become more complicated than considered in **[1]** and can affect the results obtained in **[1]**;

- Through the penetration that was assumed in **[1]**, bentonite gel may enter the canister rather than water on its own. In this scenario, steel corrosion and water out-flow increases the density of the bentonite that entered the canister as a gel and, as a result, the gas desaturates a small number of preferential paths and escapes, leaving the compressed bentonite behind. The corrosion will continue by "sucking" the water through connected water body in the compressed bentonite inside and outside the canister.

In the second part of the report we summarise results of the consequence analyses.

Firstly we developed three conceptual models depending on the different locations of the cracks through the inner steel container to describe coupled groundwater flow, steel corrosion and gas generation/migration during resaturation and desaturation of the annular gap and the fuel channels due to the gas pressure rise. The models are refered to as CT (where the crack is near the top), CB (where the crack is near the bottom) and CTB (where there are cracks near both the top and bottom). Similar to the treatment in **[1]**, we represent the conceptual models as a set of box models and numerically solve the resulting system of ordinary differential equations. A key difference from the model in **[1]** is that we explicitly model the channels within the steel inner container. This leads to a more realistic description of the behaviour of the coupled processes in the case where the crack is positioned only at the bottom of the steel container. The results of the calculations are summarised in Table 1.

The results shown in Table 1 agree with those obtained in **[1]**, for most of the cases where available. However there is a significant difference between **[1]** and the current study for the model CT (with penetration at 4.3 m, penetration area 5.0 e-6 m^2 and corrosion rate of 0.01 μm/yr) both in terms of the estimated time when water inventory is used up and the maximum thickness of the magnetite achieved by then. The reason for this is that contribution of vapour driven corrosion on the inner channel surface to consumption of water was ignored in **[1]**.

A model corresponding to the scenario where bentonite gel flows into the annular gap was developed as well. A number of calculations were carried out assuming that density of the initial bentonite gel and the critical bentonite density for gas breakthrough via preferential paths are 1,300 kg/ m^3 and 1,800 kg/ m^3 respectively. In the case where position of the penetration through the copper canister is sufficiently low (see Table 2 for details), the bentonite gel is consolidated due to loss of water content due to flow and corrosion before the gel surface falls below the penetration. This causes gas migration through preferential pathways in the bentonite to the exterior of the canister. In this scenario, since a water body connecting the steel surface with the external bentonite pore water is left behind the gas pathways, a gas cushion will not be formed and the corrosion continues by sucking water through the connected water body until the magnetite layer fills the annular gap.

Table 1 Summary of the results for scenarios where only water enters the canister

	Model CTB	Model CT	Model CB
1	• 0.427m at 7.3e3y • 0.327mm at 1.5e4y • yes	• 0.079m at 6.0e3y • 0.272mm at 1.3e4y • yes	• 0.463m at 7.4e3y • 0.167mm at 1.5e4y • yes
2	• 0.427m at 7.3e3y • 0.709mm at 3.3e4y • no	• 0.079m at 6.0e3y • 0.426mm at 2.0e4y • yes	• 0.463m at 7.4e3y • 0.365mm at 2.8e4y • no
3	• 0.427m at 7.3e3y • 0.709mm at 3.3e4y • no	• 0.079m at 6.0e3y • 0.535mm at 2.5e4y • no	• 0.463m at 7.4e3y • 0.445mm at 3.4e4y • no
4	• 0.877m at 6.8e3y • 0.321mm at 3.4e4y • yes	• 0.488m at 5.8e3y • 0.484mm at 3.4e4y • yes	• 0.963m at 7.1e3y • 0.167mm at 1.5e4y • yes
5	• 0.877m at 6.8e3y • 1.256mm at 5.8e4y • no	• 0.488m at 5.8e3y • 0.799mm at 3.3e4y • yes	• 0.963m at 7.1e3y • 0.383mm at 2.8e4y • no
6	• 0.877m at 6.8e3y • 1.256mm at 5.8e4y • no	• 0.488m at 5.8e3y • 0.972mm at 4.5e4y • no	• 0.963m at 7.1e3y • 0.469mm at 3.6e4y • no
7	• 0m • approach 0.103mm • no	• 0m • approach 0.103mm • no	• 0m • approach 0.103mm • no
8	• 0m • approach 0.103mm • no	• 0m • approach 0.103mm • no	• 0m • approach 0.103mm • no
9	• 0m • approach 0.103mm • no	• 0m • approach 0.103mm • no	• 0m • approach 0.103mm • no
10	• <0.02m • approach 0.1mm • no	• <0.02m • approach 0.1mm • no	• 0m • approach 0.1mm • no
11	• <0.02m • approach 0.1mm • no	• <0.02m • approach 0.1mm • no	• 0m • approach 0.1mm • no
12	• <0.02m • approach 0.1mm • no	• <0.02m • approach 0.1mm • no	• 0m • approach 0.1mm • no

Note

- maximum water level in channel and time
- maximum magnetite thickness when water is exhausted
- whether water is expelled from canister or not

Case Description

1: Penetration at 0 m, Penetration area;5e-6m^2, Corrosion rate;0.01 μm/y
2: Penetration at 2.235 m, Penetration area;5e-6m^2, Corrosion rate;0.01 μm/y
3: Penetration at 4.3 m, Penetration area;5e-6m^2, Corrosion rate;0.01 μm/y
4: Penetration at 0 m, Penetration area;2e-5m^2, Corrosion rate;0.01 μm/y
5: Penetration at 2.235 m, Penetration area;2e-5m^2, Corrosion rate;0.01 μm/y
6. Penetration at 4.3 m, Penetration area;2e-5m^2, Corrosion rate;0.01 μm/y
7: Penetration at 0 m, Penetration area;5e-6m^2, Corrosion rate;0.1 μm/y
8: Penetration at 2.235 m, Penetration area;5e-6m^2, Corrosion rate;0.1 μm/y
9: Penetration at 4.3 m, Penetration area;5e-6m^2, Corrosion rate;0.1 μm/y
10: Penetration at 0 m, Penetration area;2e-5m^2, Corrosion rate;0.1 μm/y
11: Penetration at 2.235 m, Penetration area;2e-5m^2, Corrosion rate;0.1 μm/y
12: Penetration at 4.3 m, Penetration area;2e-5m^2, Corrosion rate;0.1 μm/y

Table 2 Summary of the results for scenarios where betonite gel enters the canister

	Model CTBi
Penetration area; 5.0 e-6 m^2 Corrosion rate; 0.01 μm/y	• 0.094 m • 9.2 e4 years
Penetration area; 2.0 e-5 m^2 Corrosion rate; 0.01 μm/y	• 0.165 m • 9.2 e4 years
Penetration area; 5.0 e-6 m^2 Corrosion rate; 0.1 μm/y	• Not obtained • 9.2 e3 years*
Penetration area; 2.0 e-5 m^2 Corrosion rate; 0.1 μm/y	• Not obtained • 9.2 e3 years*

Note

- Upper bound of the penetration height for which gas breakthrough via preferential paths to take place
- Time when the annular gap is blocked by the magnetite layer

Remark

* The time when the annular gap is filled by the magnetite layer was derived from rescaling results for the other cases since the equation was too stiff to solve. Rescaling is very straight forward and justifiable since the time should be inversely proportional to the corrosion rate provided all the other parameters are fixed at the same value.

Secondly we developed a model for diffusion-limited corrosion of the steel container and expansion of the magnetite, that was identified in the scenario analysis in the first part of this report as well as in **[1]** as the controlling factor for canister life time in the scenarios where gas "cushioning" occurs. In the model, the following processes are taken into account;

- transport of water vapour from the saturated bentonite surrounding the canister into the annular gap by diffusion,
- anaerobic corrosion of steel by vapour which results in cosumption of water, generation of hydrogen gas and production of magnetite,
- outward flow of hydrogen gas generated by anaerobic corrosion of steel and advective transport of vapour associated with it,
- change of the gap width due to growth of the magnetite layer,
- suppression of corrosion due to growth of a protective magnetite layer.

The key difference between the current model and the one developed in **[1]** is that it can handle the dependence of corrosion rate on the vapour density (or saturation level, in other words) as well as the magnetite thickness. By virtue of this feature, calculated spatial profiles for the vapour density and the magnetite thickness possess "smoothness", avoiding the discontinuity of the first spatial derivative at the outer boundary of the support (called "corrosion radius" in **[1]**) which is not reasonable either from mathematical or physical point of view.

Using this model we conducted a series of calculations for some of the cases in Table 1 regarding their end points as the initial conditions for the subsequent calculations for diffusion-limited corrosion whose results are summarised in Table 3.

Table 3 Summary of the calculations on diffusion-limited corrosion

Penetration at 0 m Penetration area; 5.0e-6m^2 Initial corrosion rate; 0.01 μm/y Corrosion suppression length;1mm	Model CT	• 7.6 e4 yrs • 0.85
Penetration at 0 m Penetration area; 5.0e-6 m^2 Initial corrosion rate; 0.01 μm/y Corrosion suppression length;0.1mm	Model CT	• 4.8 e5 yrs • 0.92
Penetration at 0 m Penetration area; 5.0e-6 m^2 Initial corrosion rate; 0.1 μm/y Corrosion suppression length;1mm	Model CT	• 8.3 e3 yrs • 0.56
Penetration at 0 m Penetration area; 5.0e-6 m^2 Initial corrosion rate; 0.1 μm/y Corrosion suppression length;0.1mm	Model CT	• 4.7 e4 yrs • 0.83
Penetration at 0 m Penetration area; 5.0e-6 m^2 Initial corrosion rate; 0.1 μm/y Corrosion suppression length;1mm	Model CB	• 6.8 e3 yrs • 0.53
Penetration at 0 m Penetration area; 5.0e-6 m^2 Initial corrosion rate; 0.1 μm/y Corrosion suppression length;0.01mm	Model CB	• 4.8 e5 yrs • 0.95
Penetration at 0 m Penetration area; 2.0e-5 m^2 Initial corrosion rate; 0.01 μm/y Corrosion suppression length;1mm	Model CT	• 6.9 e4 yrs • 0.88
Penetration at 0 m Penetration area; 2.0e-5 m^2 Initial corrosion rate; 0.01 μm/y Corrosion suppression length;0.01mm	Model CT	• 4.6 e6 yrs • 0.98

Note

- Time when the annular gap is blocked by the magnetite layer
- Average thickness/ Maximum magnetite thickness

As can be seen from Table 3, the time required for the magnetite layer to block the annular gap varies over three orders of magnitude and appears to be most sensitive to the initial corrosion rate and the corrosion suppression length. The corrosion suppression length also affects the spatial profile of the magnetite layer, i.e., the larger the suppression length, the more localised the magnetite accumulation. This spatial pattern of the magnetite growth may affect the mode of mechanical failure of the copper overpack discussed in **[1]**.

In summary, there are a number of alternatives at different levels within the assessment, i.e., scenarios, mathematical models, and parameter values. These variations can make the system's behaviour bifurcate both qualitatively and quantitatively. Hence, in order to identify a set of robust system responses, it is essential either to conservatively bound the impacts of these alternatives (if we assume that the critical thickness of the magnetite layer to open up the penetration through the overpack is about 20 mm, then conservative estimate of the containment time would be in the order of 10^5years) or to conduct further R&D and answer the questions such as:

- Whether can bentonite gel migrate into the canister through penetration and stay in the annular gap without being fully expelled by the gas pressure;
- How large the long term corrosion rate of the steel is and, in particular, how the magnetite layer acts as a protective layer against further corrosion.

In order to answer the first question, it is essential to specify possible causes of the penetration through the copper overpack, and its size and shape. For example, if the penetration is a narrow (< a few tens of microns) circumferential one, then it is very unlikely that bentonite gel will intrude. Key to the second question, on the other hand, is the accumulation of data obtained by long-term corrosion experiments conducted under conditions relevant to the expected repository environment.

Considering the hierarchical structure of the performance assessment through both of the two possible ways forward mentioned above may play positive roles by providing support from one to the other.

Contents

Part I Scenario development

Part II Consequence analysis

Part I Scenario development

1 Introduction

According to the current design considered by SKB, a copper canister with a cast steel inner component will be used as the disposal canister for spent nuclear fuel. A recent study conducted by AEA Technology **[1]** considered the case of a breach in the copper overpack, through which groundwater could enter the canister. The study concluded that increased pressure within the canister, due to the hydrogen gas generated by an anaerobic corrosion process, could cushion the system and reduce or eventually stop further infiltration of water into the breached canister, and thence the spent fuel.

One potential pitfall in this previous study lies in the fact that it did not consider any processes which might violate the following assumptions which are essential for the gas "cushioning":

1. Hydrogen gas accumulated in the annular gap in the canister forms a free gas phase which is stable indefinitely into future;

2. Elevated gas pressure in the canister prevents further supply of groundwater except for diffusion of vapour.

As the consequence, it is not at all clear what conditions are required for the gas "cushioning" to take place although it seems fairy unlikely that the stable gas phase can form for all values of certain parameters (e.g., size of the hole(s) through the copper canister).

In the current study we will develop a mathematical model for the above problem and apply it to carry out an independent assessment of the long term behaviour of the spent fuel disposal canister. A key aim in this study is to clarify whether there are any alternative processes which may affect the result obtained by the previous study by violating one of the assumptions listed above.

The first part of the report summarises the result of an independent scenario development exercise addressing the above issue, which is the first task of the QuantiSci's work programme in the financial year 1998.

2 System specification

2.1 Engineered Barrier System

The disposal concept for the spent nuclear fuel rods in Sweden is based on the multi-barrier principle. The spent fuel rods will be encapsulated within canisters which will be placed in vertical boreholes drilled from galleries in the granitic host rock at a depth of about 500m.

The canister consists of an inherently corrosion resistant copper overpack of 50 mm thickness, 4.47 m internal depth and 0.525m outer radius and a thick cast steel inner container designed to provide mechanical strength and to keep individual fuel bundles at a safe distance from another, minimising the risk of criticality. The primary loading on the container will be a pressure of about 10 MPa which is sum of the hydrostatic pressure of 5 MPa and the bentonite swelling pressure of 5 MPa. The steel container is fitted inside the copper overpack with a 2 mm annular gap which is required for handling purposes. In the BWR canister type depicted in Figure 2.1, the spent fuel is contained in 12 square vertical channels of width 0.156 m. On closure, the remaining void volume in the inner container is 0.4 m^3.

The cast steel canister will be fabricated in two parts, each with half the total length, and welded together in the middle. The copper overpack will be fabricated either as a seamless tube by extrusion, or from two plates that have been formed into tube halves and welded together by longitudinal electron beam welds. A steel lid will be fixed onto the steel container by a bolt while the copper overpack and its lid will be welded together.

Each canister will be surrounded by compacted bentonite clay. The bentonite swells as it takes up water and self-seals to achieve very low hydraulic conductivity. Thus the bentonite clay acts as the primary barrier against the groundwater flow.

In the scenario development exercise to be described in the later sections, we consider the case where there is a hole(s) or a crack(s) within the copper canister. In this case, we represent the EBS structure by a simple box model (Figure 2.2) consisting of

1. vertical channels in the steel container in which the spent fuel assemblies are placed,
2. hole(s) or crack(s) through the steel container,
3. annular gap between the steel container and the copper overpack,
4. hole(s) or crack(s) through the copper canister,
5. buffer material (bentonite clay).

2.2 Mass transfer and relevant processes

In what follows, we concentrate on the "post-thermal" period when the thermal gradient developed by the decay heat in the spent fuel is negligible. We also assume that, initially, the bentonite clay surrounding the copper overpack is fully saturated with water.

In the presence of (reducing) groundwater, steel corrodes anaerobically to magnetite (Fe_3O_4), consuming water and generating hydrogen **[2]**

$$3Fe + 4H_2O \rightarrow Fe_3O_4 + 4H_2.$$

The hydrogen gas thus generated exists initially in the aqueous phase and form a free gas phase once solubility is achieved.

When the vicinity of the steel surface is not saturated with groundwater, water still exists mainly as vapour which also contributes to the above corrosion mechanism. Partial pressure of the vapour is determined by the balance between evaporation and condensation, and it can be assumed to establish equilibrrium in the long term, which depends on the temperature. The corrosion rate of the steel can be galvanically enhanced if it is wet.

Spent fuel contained in the vertical channels in the steel container will, by the

$$Fe + \tfrac{1}{2}O_2 + H_2O \rightarrow Fe(OH)_2,$$

α-radiation, split nearby water into oxidising and reducing compounds (α-radiolysis) **[3]**. The reducing compounds are mostly hydrogen that will diffuse away or transfer to the gaseous form. The remaining oxidising compounds can oxidise the uranium oxide in the fuel and make it more soluble **[4]**. In many cases the rate of consumption of the oxidising compounds is smaller than the rate of its generation and, thus, a net oxidising condition can be formed around the fuel rods **[3]**. In these circumstances, the following aerobic mode of corrosion **[2]** which also consumes groundwater but does not generate hydrogen will take place where the oxidizing compounds are denoted by O_2 collectively as in **[4]**.

2.3 Mobile forms and transport mechanisms

As a result of physico-chemical processes summarised in the previous section, the following fluids and solutes are involved in the system

1. water,
2. water vapour,
3. oxidising compounds (O_2),
4. H_2 (aqueous),
5. H_2 (gaseous),
6. bentonite.

The water is transported predominantly by advection driven by the pressure gradient across the system. Because of its low permeability, the bentonite clay will provide the largest resistance to the flow into and out of the canister.

Water vapour will exist in the vertical channels within the steel container and in the annular gap if the gaps are not fully saturated. The vapour will be transported by diffusion in the unsaturated part of the gaps and through the layers of steel corrosion products which will have non-zero porosity accessible to it. However, it is possible for the corrosion product layer to act as a "protective layer" against the further corrosion by restricting the diffusive flux of vapour across it.

The oxidising compounds generated by the α-radiolysis will react with the reducing agents (iron, corrosion products, etc.) and will be consumed while they migrate. Thus the redox condition in the system will develop a front-like structure connecting the two chemical equilibria corresponding to oxidising and reducing conditions (often called as a "redox front" **[3]**). Transport of the oxidising compounds will be dominated by advection and diffusion, and propagation of the front will be retarded by the redox reactions.

Transport of the hydrogen in the aqueous phase will also be driven by diffusion and advection. Since the hydrogen is not chemically reactive in the aqueous phase, it will be transported as a conservative solute unless there is a significant pressure change which causes mass transfer between gaseous and aqueous phases.

Hydrogen gas is a much less viscous fluid than water and the hydrogen gas generated by anaerobic corrosion of the steel canister will migrate very quickly through even tiny pores provided they are dry. However this is not the case in the media which are saturated with water (or other viscous fluids). In order to migrate through these media, gas needs to desaturate some part or sometimes the whole region. When the

gas is slowly pushing a fluid of low viscosity (e.g., water), the gas-fluid interface moves retaining a smooth planar geometry. In this case, no water is left behind the interface. However, if viscosity of the invaded fluid increases or the gas is generated more rapidly, then the difference in the viscosities generates the Saffman-Taylor instability **[5]** which leads to formation of a "viscous fingering" **[6]**. In this case, the gas will migrate through preferential paths leaving the viscous fluid behind. As an extreme, gas will migrate through a small number of desaturated capillaries in a porous medium **[7]**. Pores desaturated after a gas migration experiment through bentonite represent only a few percent of the total porosity or even less **[8]**. As we discuss later, bentonite with wide range of bentonite to water ratios (from "bentonite gel" to compacted bentonite) may exist in the waste package, and migration of the gas through them can be highly variable.

The bentonite clay is regarded as a porous medium if the bentonite to water ratio is sufficiently high. However, with larger amount of water content, it behaves as a gel which is more appropriately modelled by a viscous fluid. The bentonite gel can be formed at a free surface of the compacted bentonite placed in water, and it migrates through a crack of width less than 1 mm **[9]** if there is a negative gradient of the gross pressure (gas, water pressure and swelling pressure of the bentonite with varying density) into the crack. When the sign of the gross pressure gradient is reversed, the less viscous fluid (e.g., gas) starts pushing the gel interface back, causing compression of the gel by squeezing out the excess water from it until the clay density reaches a critical value above which the gas desaturates pores to make its preferential paths in the bentonite rather than pushing the bulk interface of clay-water mixture.

Table 2.1: Mobile form of mass transport mechanisms

Mobile form	Transport mechanism
water	**advection**
vapour	**diffusion**
oxidants (O2)	diffusion + advection
H2 (aq)	diffusion + advection
H2 (gas)	**expansion of gas "cushion", permeation through bentonite**
bentonite	migration of gel, compression

bold letters : considered in **[1]**

3 Scenario development

3.1 Performance measures and relevant state variables

According to the results of the previous study, the release of the nuclides in the groundwater due to dissolution of the fuel matrix will be significantly delayed by the formation of the "gas cushion", until build-up of the steel corrosion product mechanically damages the copper overpack and the nuclides can diffuse out of the canister. This will provide substantial prolongation in the containment time. Hence we consider the following as the performance measures in the subsequent analysis of the long term performance of the spent fuel canister

1. time and amount of water flowing out of the disposal canister,

2. time of the mechanical failure of the copper overpack.

Water flux (possibly containing radioactive nuclides) out of the canister is driven by a pressure difference between inside and outside the canister. Hence, it becomes necessary to monitor changes in the following state variables in order to describe future evolution(s) of the system

- gas pressure in the gaps,
- water pressure in the gaps,
- water pressure in and outside the bentonite clay cylinder.

In order to define the mass balance for the gas and the water, the following set of variables play dominant roles

- hydraulic transmissivity across the hole(s) in the copper overpack,
- rates of anaerobic and aerobic corrosion respectively.

Considering the mode of corrosion (anaerobic or aerobic), availability of the oxidising compounds in the canister also becomes important. Since the α-radiolysis can be initiated only after contact of water with the fuel assemblies, it is necessary to consider

- water level in the annular gap relative to the hole(s) through the steel container,

which may provide another important bifurcation of the system's evolution, together with the following parameters which will control on the net available amount of the oxidising compounds

- generation rate of oxidising compounds by the α-radiolysis,
- consumption rate of oxidising compounds by UO_2 oxidisation.

With respect to the gas release out of the canister, the following variable will affect the mechanism of gas migration (see 2.3)

- density of bentonite (gel) in the gaps.

Finally, whether the copper overpack is mechanically damaged or not critically depends on

- amount of corrosion product built-up in the gaps.

3.2 Analysis of sequence of events

A series of simple event tree analyses have been conducted and, as a result, a number of scenarios are developed as sequences of events which are, in other words, changes in the key state variables listed in 3.1 caused by the mass transfer and/or mass transport described in 2.2 and 2.3 respectively.

These scenarios are summarised in Figure 3.1. As one can see in the figure, all the scenarios considered in the previous study are included (boxes highlighted by the shadow).

Returning to the original objective of this scenario development exercise, the following two scenarios are identified as the possibilities that the "gas cushion", which always worked in the analysis within the previous study **[1]**, fails to prolong the containment time

1. Steel corrosion and water out-flow increases bentonite density which entered into the canister as a gel and, as a result, the gas desaturates a small number of preferential path and escapes, leaving the compressed bentonite behind (Figure 3.2). The corrosion will continue by "sucking" the water through connected water body in the compressed bentonite inside and outside the canister **(Scenarios 122, 2122, 22122);**

2. Aerobic corrosion consuming the oxidising compounds generated by the _-radiolysis generates corrosion product rapidly without generating the hydrogen gas and the gas cushion, and it mechanically damages the copper overpack much earlier than in the other scenarios **(Scenario 222)**.

3.3 Screening

After having developed the initial set of scenarios as in Figure 3.1, a review has been conducted focusing on physical or chemical plausibility of processes and consequences within each scenario. As the result of this, bifurcation of **Scenario 222** at **Joint 221/222** is considered to be implausible since the α-radiolysis caused by the UO2 matrix generates reducing compounds such as H2 **[3][4]** , and, if we take this into account, it is clear that the aerobic corrosion triggered by the α-radiolysis also generates H2 gas whose amount per unit mass of steel corroded has to be comparable with that for the anaerobic corrosion.

4 Conclusion of scenario analysis

A scenario development exercise was carried out for long term behaviour of the spent fuel canister, and a class of alternative scenarios (**Scenario 122, 2122, 22122**) which were not considered in the previous study were identified as the possibilities that the "gas cushion" fails to prolong the containment time. These alternative scenarios together with the scenarios that were considered in the previous study and identified to be relevant also in the current exercise form a comprehensive scope of the mathematical modelling which is to be attempted in this project.

The key issues to be tackled in the subsequent quantitative analysis is to answer the following questions

1. Can the alternative scenarios happen?

2. What is the necessary condition for the gas cushion to prolong the containment time of the disposal canister?

To answer these questions, a number of mathematical models for the relevant processes need to be formulated. In addition, alternative conceptual or mathematical formulation of the processes treated in the previous study should be attempted so that an opportunity of independent comparison is provided.

Figure 2.1: Cross section of the EBS

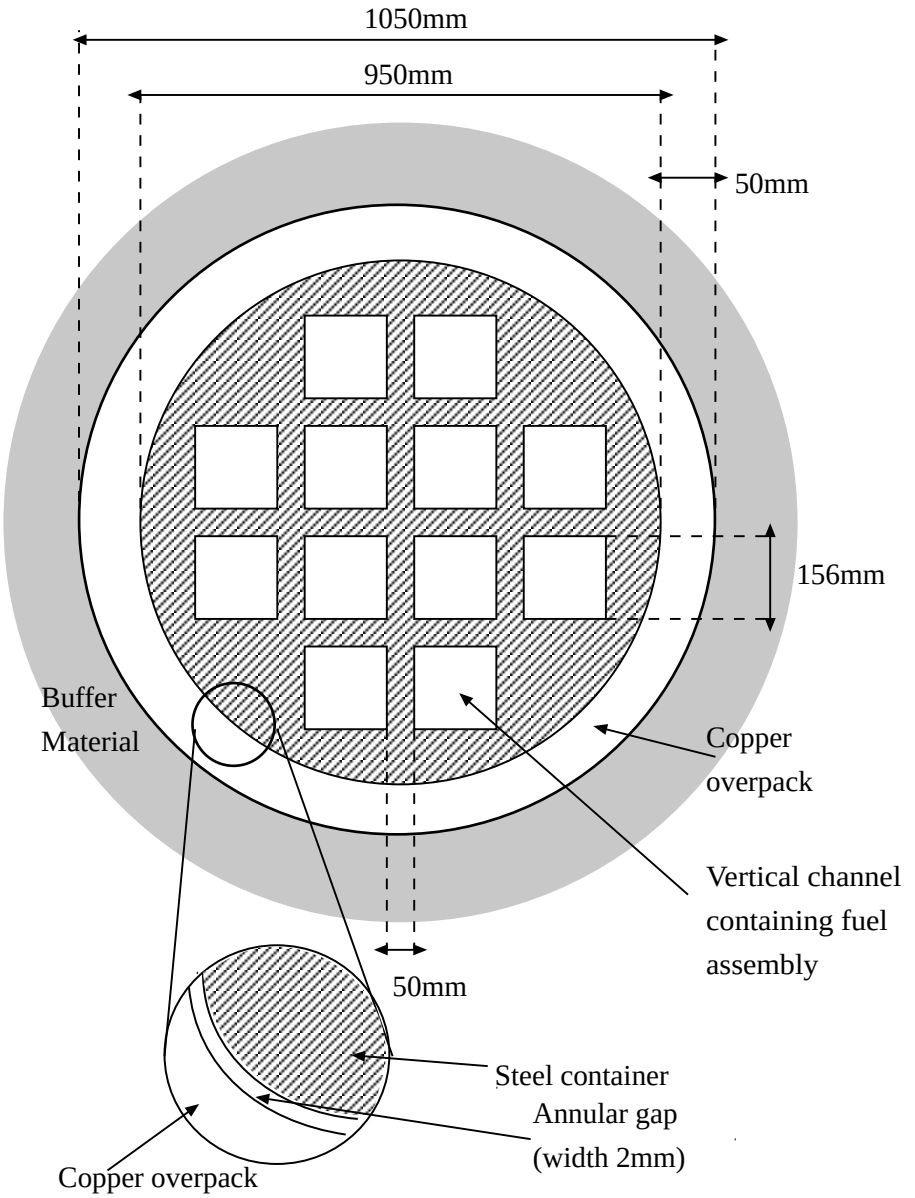

Figure 2.2: A conceptual (box) model representation of the system

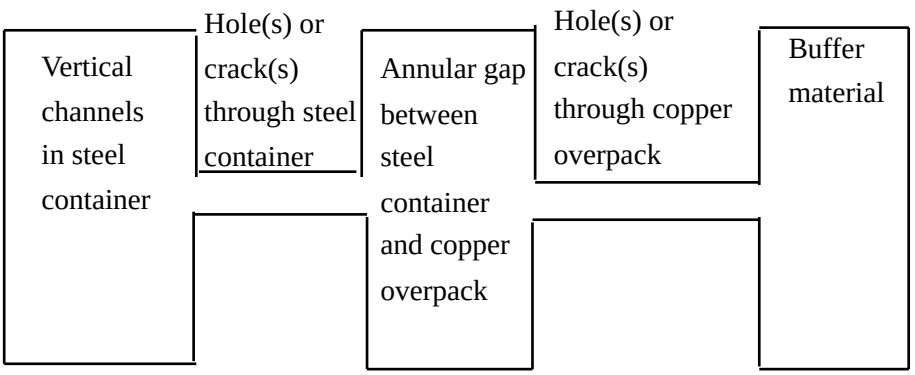

Figure 2.3:
Mass transport diagram

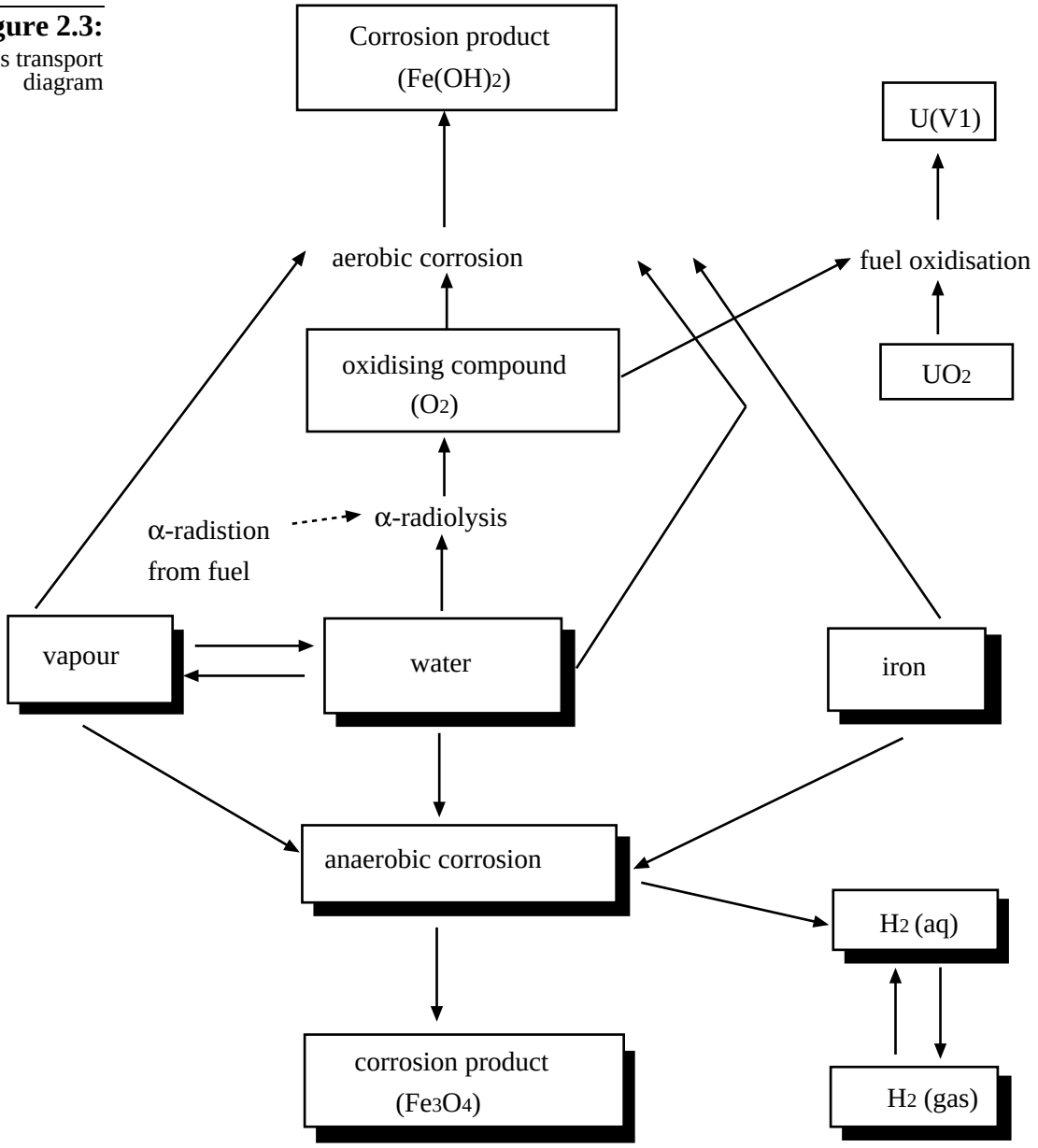

Figure 3.1:
Sequence of events (1)

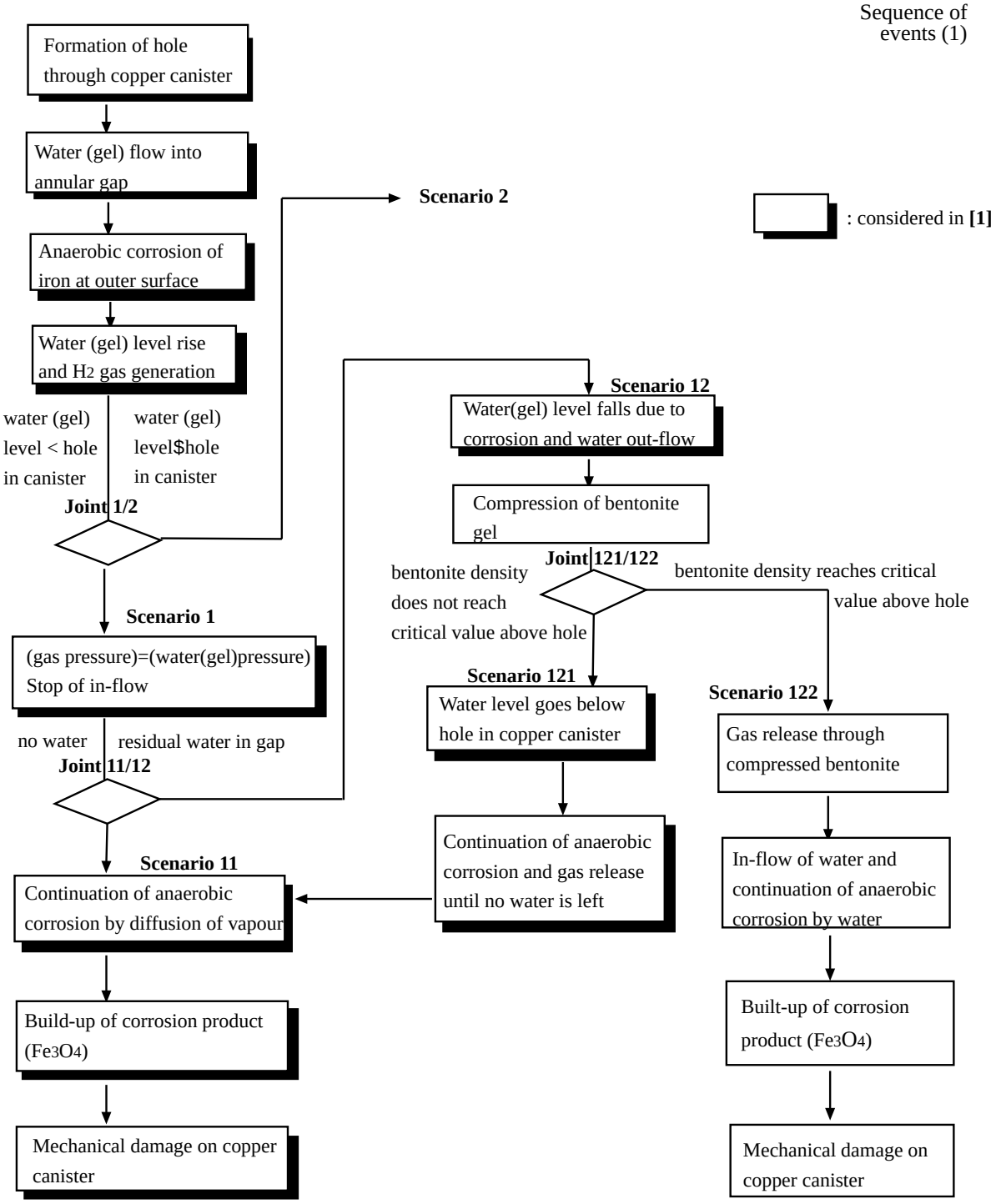

Figure 3.1: Sequence of events (2)

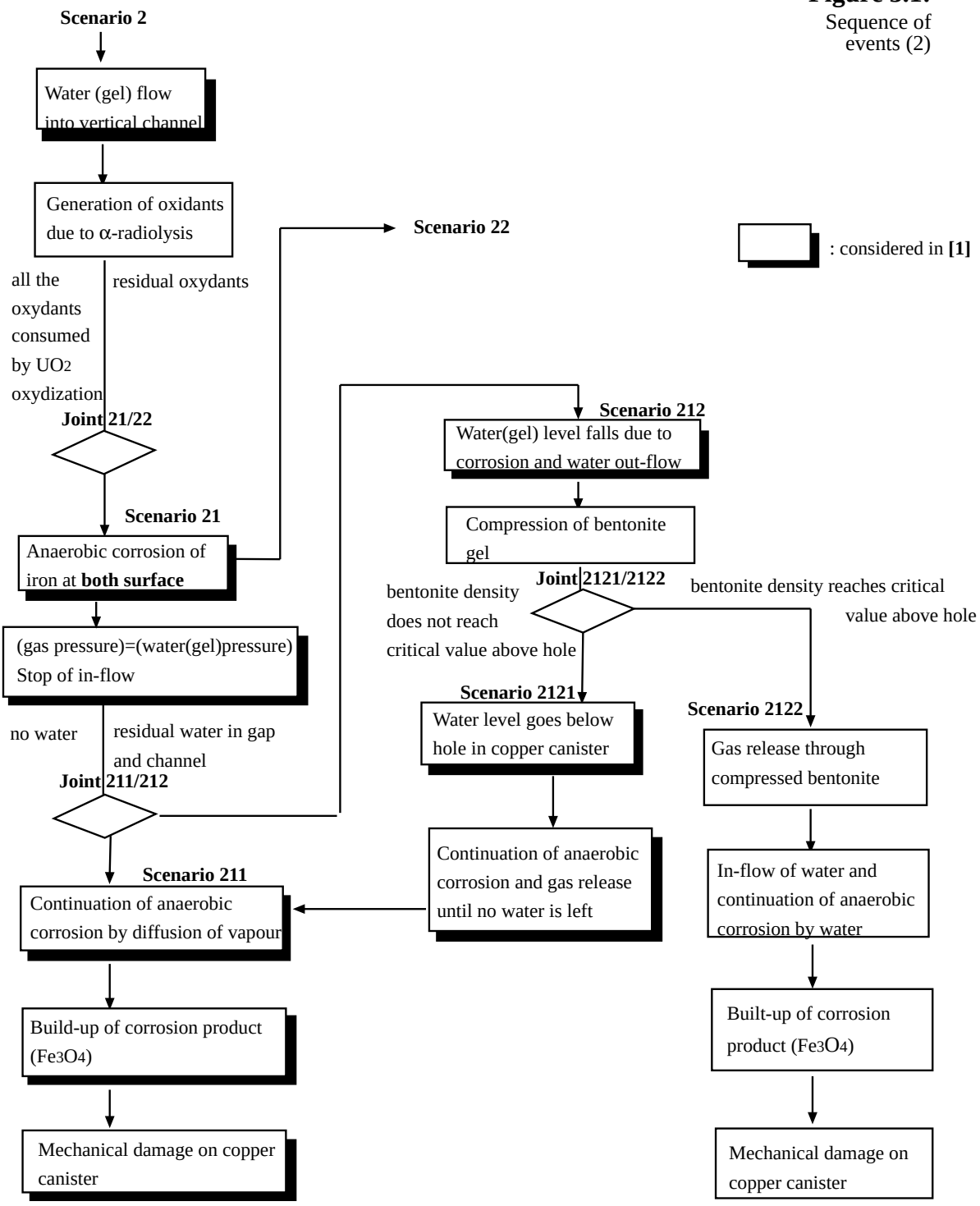

Figure 3.1:
Sequence of events (3)

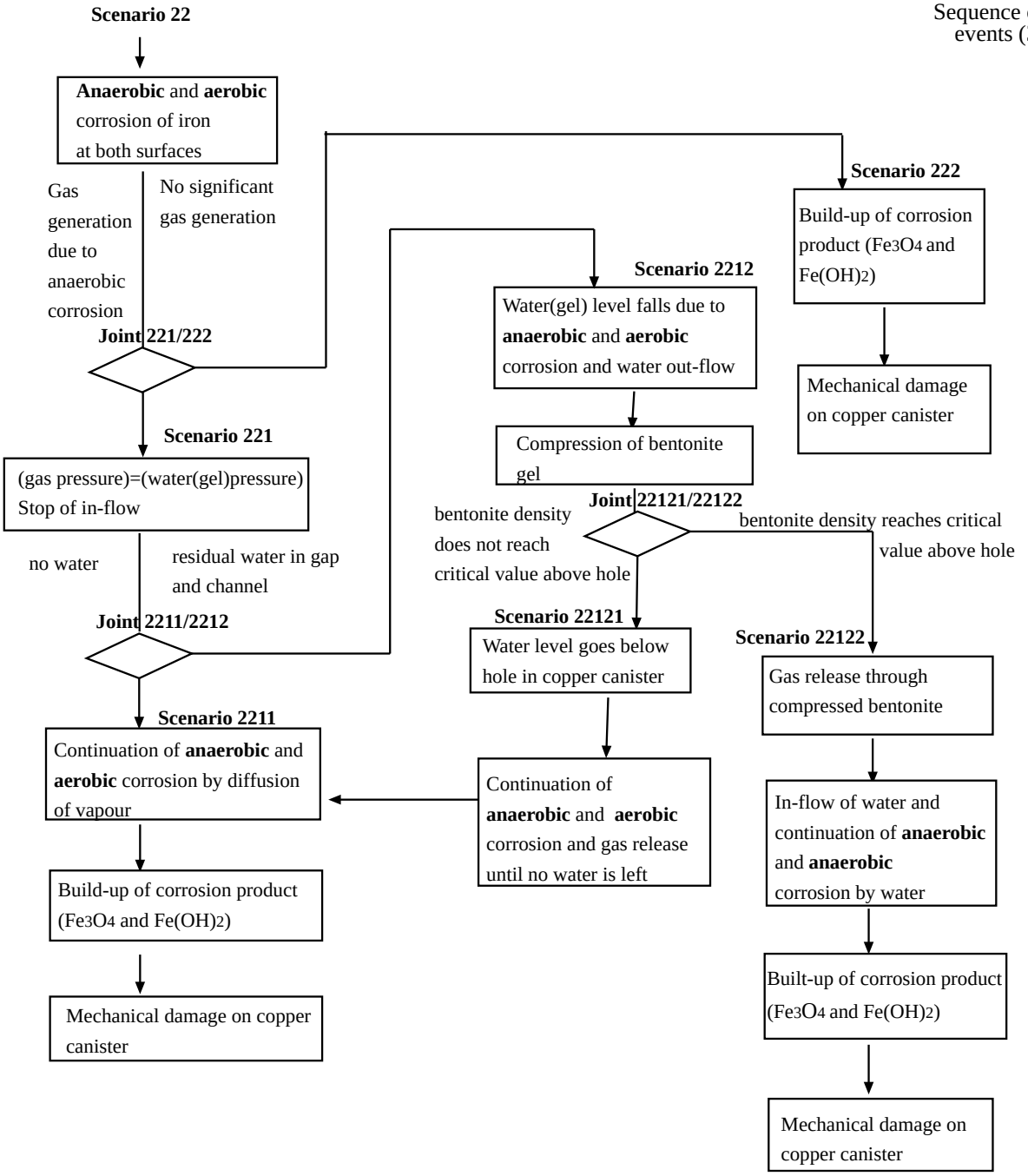

Figure 3.2:
Two possible modes of gas release from the canister
(a) Scenarios 121,2121,22121
(b) Scenarios 122,2122,22122

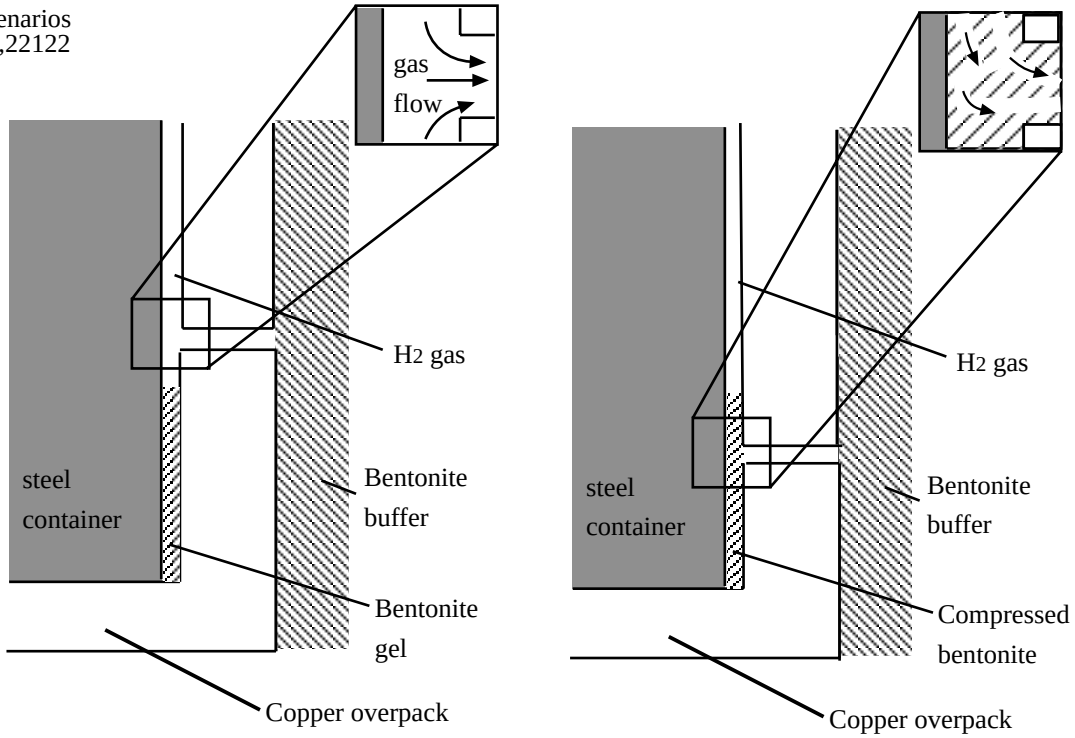

Part II Consequence analysis

1 Introduction

Scenario development exercise described in Part I identified a number of scenarios including alternative processes and features that are not considered in **[1].** Objective of the study in Part II is to develop a series of mathematical models corresponding to the FEPs identified in the scenario analysis and to conduct quantitative assessment of long-term behaviour of the SKB disposal canister whose results can be compared with that of **[1]**.

In section 2, we develop three conceptual models depending on the different locations of the crack(s) through the inner steel container to describe coupled groundwater flow, steel corrosion, and gas generarion/migration during resaturation and desaturation of the annular gap and the fuel channels due to the gas pressure rise. Similar to the treatment in **[1]**, we represent the conceptual models as a set of box models and numerically solve the resulting system of ordinary differential equations. A key difference from the model in **[1]** is that we explicitly model the channels within the inner steel container. This leads to more realistic description of the behaviour of the coupled processes in the case where the crack is limited at the bottom of the steel container.

In addition, we develop a model corresponding to the scenario where bentonite gel flows into the annular gap rather than water on its own. In the case where the position of the penetration through the copper canister is sufficiently low, the bentonite gel is consolidated due to loss of water content due to flow and corrosion before the gel surface falls below the penetration, causing gas migration through the bentonite without making clear interface. In this scenario, since a water body connecting the steel surface with the external bentonite pore water is left behind the gas pathways, a gas cushion does not form and the corrosion continues sucking the water through the connected body.

In section 3, we model the diffusion-limited corrosion of the steel canister and the expansion of magnetite that are identified, in section 2 as well as in **[1]**, as the controlling factors of canister life time in the scenarios where gas “cushion” occurs. In the model, the following processes are taken into account;

1. transport of vapour from the saturated bentonite surrounding the canister into the annular gap by diffusion,

2. anaerobic corrosion of steel by vapour which results in consumption of water, generation of hydrogen gas and production of magnetite,

3. outward flow of hydrogen gas generated by anaerobic corrosion of steel and advective transport of vapour associated with it,

4. change of the gap width due to growth of the magnetite layer,

5. suppression of corrosion due to growth of "protective" magnetite layer.

The key difference of the current model from the one developed in **[1]** is that it can handle dependence of corrosion rate on the vapour density (or saturation level) as well as the magnetite thickness. By virtue of this feature, calculated spatial profiles for the vapour density and the magnetite thickness possess "smoothness", avoiding the discontinuity of the first derivatives at the outer boundary of the support (called "corrosion radius" in **[1]**) which is not reasonable either from mathematical or physical point of view.

2 Corrosion of steel container during resaturation/desaturation

2.1 Mathematical modelling

The failure for the copper overpack is broken down into three main modes, depending on the location of the circumferential crack(s) in the inner steel container. The three possibilities considered are a crack at the top and bottom (CTB), a single crack at the top (CT) and a single crack at the bottom (CB). The report **[1]** treats only two of these cases, single cracks at either the top or the bottom, although the treatment of the case of a single crack at the bottom in **[1]** corresponds to the model CTB here, since in **[1]** there is no distinction between the case of a single crack at the bottom and two cracks, with one at the top and one at the bottom. The reason for the different treatment here is to avoid the assumption (made in **[1]**) that when there is a single crack at the bottom of the container, water levels in both the annulus and the interior will be equal, and will rise and fall together. The model CB allows the water in each compartment (either the annulus or interior) of the canister to be maintained at different levels, governed by the gas volume differentials required to maintain a uniform pressure in the canister.

The three models are developed separately because some models require more/fewer degrees of freedom than others. A breakdown of each model is given below.

(1) Model CTB

Mathematically, CTB is the simplest of the three models. Since there are cracks in both the top and bottom of the steel canister, the water and hydrogen inventories in each compartment are connected and so the total water inventory and total hydrogen inventory can be calculated, rather than calculating separate inventories for each compartment. The canister geometry that is being modelled is described by the following figure :

Figure 2.1:
Canister geometry
for model CTB

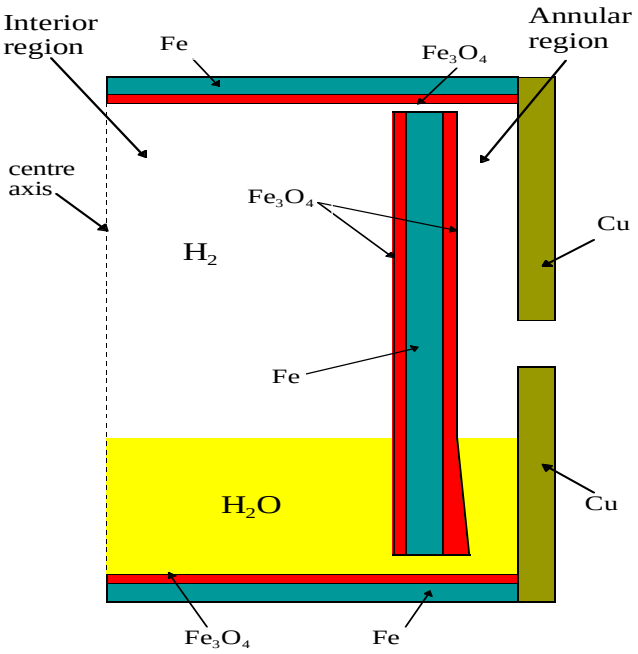

The interior region is not shown to contain any fuel rods because all calculations are performed using the interior void space that remains after the fuel rods are in place, which is taken to be 0.4m^3. The surface area of the interior region is taken to be the total surface area of the twelve square-section vertical channels, of width 0.156m, that contain the fuel rods, and the interior cross sectional area is taken to be the interior void volume divided by the height of the canister, which is 4.47m. The width of the annular region is 0.002m and the radius of the steel inner container is 0.473m.

The differential equations describing the evolution of water, hydrogen and magnetite in the system are :

$$
\begin{aligned}
\dot{M}_W &= \{f\} - \gamma\left(R_a + R_i\right) - \{E\}, \\
\dot{M}_H &= C_H\gamma\left(R_a + R_i\right) - \{V\}, \\
\dot{M}_{C_a} &= C_M\gamma R_a, \\
\dot{M}_{C_i} &= C_M\gamma R_i.
\end{aligned}
\qquad (1)
$$

Here, $\dot{M}_W$, $\dot{M}_H$, $\dot{M}_{Ca}$ and $\dot{M}_{Ci}$ represent the rate of change of mass per second (Kg s^{-1}) of water, hydrogen, magnetite in the annulus and magnetite in the interior respectively. The terms $\{\cdot\}$ are condition dependent, f (Kg s^{-1}) represents the mass

flow rate of water into the canister, which depends on the pressure in the canister, and is only non-zero when the external hydrostatic pressure, P_{hydro} (MPa s), exceeds the internal pressure, p (MPa s). f is given by

$$f = \begin{cases} 0, & p \geq P_{\text{hydro}}, \\ 2\pi r_h \dfrac{k}{\mu}\left(P_{\text{hydro}} - p\right)\rho_{\text{H}_2O,} & p < P_{\text{hydro}}. \end{cases} \tag{2}$$

Here, r_h is the radius of the penetration in the copper overpack (m), k is the permeability of the bentonite (m^2), μ is the viscosity of water (MPa s), and ρ_{H_2O} is the density of (liquid) water (Kg m^{-3}). E and V are the mass flow rates of water expelled and hydrogen vented from the canister respectively (Kg s^{-1}), expressions for which will be derived shortly. R_a and R_i (Kg s^{-1}) are the mass per second consumption of water by the corrosion process in the annulus and interior. Given the corrosion rate $\upsilon\ \mu\text{ms}^{-1}$, the mass consumption rates are found as follows. Firstly, the mass consumption of iron per m^2 per second is given by

$$\upsilon\rho_{\text{Fe}}\ \text{Kg m}^{-2}\text{s}^{-1}, \tag{3}$$

and so the mass consumption of water is

$$R = \upsilon\rho_{\text{Fe}} \times \frac{4}{3}\frac{\text{M}_{\text{H}_2\text{O}}}{\text{M}_{\text{Fe}}}\ \text{Kg m}^{-2}\text{s}^{-1}, \tag{4}$$

where $\text{M}_{\text{H}_2\text{O}}$ is molecular weight of water and M_{Fe} is atomic mass of steel.

The term R_i is then

$$R_i = R \times A_i, \tag{5}$$

where A_i is the surface area in the interior of the canister. R_a is found similarly except that the corrosion rate beneath the water level is galvanically enhanced by a factor of two **[1]**, so that

(6) $$R_a = R \times 2\pi r_c \left(h + w_a\right),$$

where r_c is the radius of the canister (m), w_a is the water height in the annulus (m) and h is the height of the canister (m). C_H and C_M are the relative rates of water mass consumption to hydrogen mass and magnetite mass production in the corrosion process,

(7) $$C_{\mathrm{H}} = \frac{\mathrm{M}_{\mathrm{H}_2}}{\mathrm{M}_{\mathrm{H}_2\mathrm{O}}},$$
$$C_{\mathrm{M}} = \frac{\mathrm{M}_{\mathrm{Fe}_3\mathrm{O}_4}}{4\,\mathrm{M}_{\mathrm{H}_2\mathrm{O}}}.$$

γ is a dimensionless number which inhibits the loss of water to the corrosion reaction when there is insufficient water in the canister to maintain corrosion at the specified rate. Whenever (liquid) water is present in the canister or $f \geq R_a + R_i$, γ takes the value 1, otherwise $\gamma = f / \left(R_a + R_i\right)$ and we will say that the corrosion is limited.

Finally we find expressions for E and V. While $p < P_{\mathrm{hydro}}$, E is zero, since the internal pressure must exceed the external hydrostatic pressure before any water can be expelled. When $p \geq P_{\mathrm{hydro}}$ and the water level in the annulus is above the height of the hole (h_h), the pressure differential between the interior and exterior of the canister forces water out of the canister and through the bentonite buffer, similar to the term f for water flowing into the canister, so that E is given by

(8) $$E = \begin{cases} 0, & p < P_{\mathrm{hydro}}, \text{ or } P_{\mathrm{hydro}} \leq p \text{ and } w_a \leq h_h, \\ 2\pi r_h \dfrac{k}{\mu}\left(p - P_{\mathrm{hydro}}\right)\rho_{\mathrm{H}_2O}, & P_{\mathrm{hydro}} \leq p \text{ and } w_a > h_h. \end{cases}$$

While $p < P_{\mathrm{tot}}$ (where $P_{\mathrm{tot}} = P_{\mathrm{hydro}} + P_{\mathrm{swell}}$) V is zero, because the internal pressure must exceed the total external pressure before any hydrogen can be vented. Suppose $p = P_{\mathrm{tot}}$, then if the water level in the annulus is above the height of the hole, water will be expelled at the rate given by E above. Otherwise hydrogen will be vented at

the rate required to equilibrate the pressure in the canister to P_{tot}. Volume in the canister is conserved via the rule

$$\dot{V}_W = -\dot{V}_H - \frac{\alpha - 1}{\alpha}\left(\dot{V}_{Ca} + \dot{V}_{Ci}\right), \tag{9}$$

where V_W, V_H, V_{Ca} and V_{Ci} are the volumes of water, hydrogen, annulus and interior magnetite in the canister. Here,

$$\alpha = \frac{1}{3}\frac{\mathrm{M}_{\mathrm{Fe_3O_4}}}{\mathrm{M}_{\mathrm{Fe}}}\frac{\rho_{\mathrm{Fe}}}{\rho_{\mathrm{Fe_3O_4}}}, \tag{10}$$

is the volumetric ratio of magnetite generated to steel consumed and $(\alpha - 1)/\alpha$ is the fraction of the total magnetite volume that intrudes into the interior of the canister (i.e. the volume that does not occupy space vacated by the steel). Since the pressure remains constant in the canister once $p = P_{\text{tot}}$ and hydrogen is being vented, the ideal gas laws can be used to calculate V_H, and so

$$\frac{\dot{M}_W}{\rho_{\mathrm{H_2O}}} = -\dot{M}_H \frac{\Gamma\tau}{P_{\text{tot}}\,\mathrm{M}_{\mathrm{H_2}}} - \left(\frac{\alpha - 1}{\alpha}\right)\frac{1}{\rho_{\mathrm{Fe_3O_4}}}\left(\dot{M}_{Ca} + \dot{M}_{Ci}\right), \tag{11}$$

where Γ is the gas constant (MPa m^3 K^{-1} mol^{-1}) and τ is the temperature (K). Substituting the expressions for the derivatives into the above equation and solving for V,

$$V = \left(R_a + R_i\right)\left[\frac{P_{\text{tot}}\,\mathrm{M}_{\mathrm{H_2}}}{\Gamma\tau}\left(\left(\frac{\alpha - 1}{\alpha}\right)\frac{C_M}{\rho_{\mathrm{Fe_3O_4}}} - \frac{1}{\rho_{\mathrm{H_2O}}}\right) + C_H\right]. \tag{12}$$

Here the value of the term $[\cdot] \approx 0.106$ at $\tau = 303$. In summary,

$$\begin{pmatrix} E \\ V \end{pmatrix} = \begin{cases} \begin{pmatrix} 0 \\ 0 \end{pmatrix}, & \text{whenever } p \le P_{\text{hydro}}, \text{or } P_{\text{hydro}} < p < P_{\text{tot}} \text{ and } w_a \le h_h, \\ \begin{pmatrix} 2\pi r_h \dfrac{k}{\mu}\left(p - P_{\text{hydro}}\right)\rho_{H_2O}, \\ 0 \end{pmatrix}, & \text{whenever } P_{\text{hydro}} < p \text{ and } w_a > h_h, \\ \begin{pmatrix} 0 \\ \left(R_a + R_i\right)\left[\dfrac{P_{\text{tot}}\, \mathrm{M}_{H_2}}{\Gamma\tau}\left(\left(\dfrac{\alpha - 1}{\alpha}\right)\dfrac{C_M}{\rho_{Fe_3O_4}} - \dfrac{1}{\rho_{H_2O}}\right) + C_H\right] \end{pmatrix} \\ \qquad\qquad \text{whenever } P_{\text{tot}} \le \text{p and } w_a \le h_h. \end{cases}$$

Using the expressions for f, E and V above, the differential equations can be solved using standard solvers. For this report a variable-order multistep method was used.

As well as satisfying the above equations, physical restrictions were also imposed on the solution, such as the canister not being able to contain more water than the actual inner free volume allows, etc.

(2) Model CT

This model is similar to CTB except that now the water inventory is disconnected, and so separate water inventories for the annulus and interior must be calculated. The canister geometry in this case is described in the following Figure 2.2.

Figure 2.2:
Canister geometry for model CT

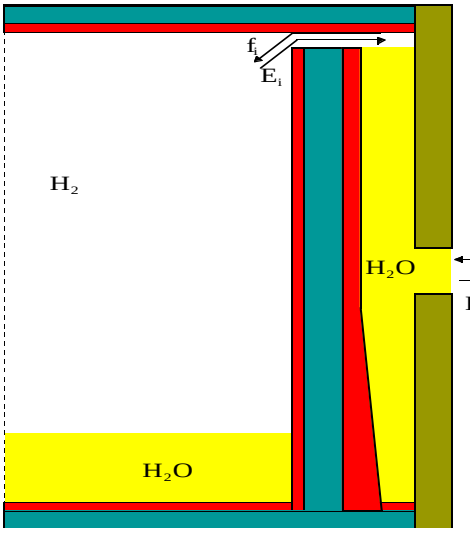

The differential equations that describe the evolution are

$$
\begin{aligned}
\dot{M}_{Wa} &= \{f_a\} - \{E_a\}, \\
\dot{M}_{Wi} &= \{f_i\} - \{E_i\}, \\
\dot{M}_{H} &= C_H \gamma (R_a + R_i) - \{V\}, \\
\dot{M}_{Ca} &= C_M \gamma R_a, \\
\dot{M}_{Ci} &= C_M \gamma R_i .
\end{aligned}
\tag{13}
$$

Here the terms f_a and f_i describe the combined inflow of water due to the pressure differential between the inside and outside of the canister, and loss of water due to corrosion in the annulus and interior. We make the assumption that the water inventory in each compartment is solely responsible for the corrosion in each compartment if each inventory is non-zero. Otherwise, if only a single water inventory is non-zero, that inventory is responsible for the total corrosion in the canister. This is a somewhat simplified assumption. In reality each water inventory would contribute a fraction to the total vapour mass in the canister, and this total vapour mass would be involved in the (non-liquid) corrosion reactions in both compartments. However the difference in solutions when making this assumption was found to be negligible. The terms f_a and f_i are thus given as follows :

$$
\begin{pmatrix} f_a \\ f_i \end{pmatrix} =
\begin{cases}
\begin{pmatrix} \{f\} - \gamma(R_a + R_i) \\ 0 \end{pmatrix} & \text{whenever } w_a < h_c,\ w_i = 0, \\
\begin{pmatrix} 0 \\ \{f\} - (R_a + R_i) \end{pmatrix} & \text{or } w_a = h_c,\ w_i = 0,\ f < R_a + R_i, \\
\begin{pmatrix} \{f\} - \delta R_a \\ -(1-\delta) R_a - R_i \end{pmatrix} & \text{whenever } w_a = h_c,\ f \geq R_a + R_i, \\
\begin{pmatrix} \beta\{f\} - R_a \\ (1-\beta)\{f\} - R_i \end{pmatrix} & \text{whenever } w_a < h_c,\ \ 0 < w_i < h_c, \\
 & \text{whenever } w_a \geq h_c,\ w_i \geq h_c,
\end{cases}
\tag{14}
$$

where

$$
\gamma = \begin{cases} \dfrac{f}{R_a + R_i}, & M_a = 0,\ f < R_a + R_i, \\ 1, & \text{otherwise,} \end{cases}
$$

$$
\delta = \begin{cases} \dfrac{f}{R_a}, & M_a = 0,\ f < R_a, \\ 1, & \text{otherwise,} \end{cases}
$$

$$
\beta = \frac{V_a}{V_{tot}}
$$

and f is defined as for scenario CTB. E_a and E_a are defined in terms of E above,

$$(15)\qquad \begin{pmatrix} E_a \\ E_i \end{pmatrix} = \begin{cases} \begin{pmatrix} 0 \\ 0 \end{pmatrix}, & \text{whenever } p \le P_{\text{hydro}}, \\ & \text{or } \mathrm{P}_{\text{hydro}} < p \text{ and } w_a \le h_h, \\ \begin{pmatrix} E \\ 0 \end{pmatrix}, & \text{whenever } \mathrm{P}_{\text{hydro}} < p \text{ and } \mathrm{h}_{\mathrm{h}} < w_a \le h_c, \\ \begin{pmatrix} \beta E \\ (1-\beta)E \end{pmatrix}, & \text{whenever } \mathrm{P}_{\text{hydro}} < p,\ h_c < w_a \text{ and } h_c < \mathrm{w}_{\mathrm{i}}, \end{cases}$$

where again, $\beta = V_a / V_{\text{tot}}$. The hydrogen venting term V is the same as that given for model CTB, if $w_a > h_c$ then no hydrogen is vented, otherwise it is vented at a rate proportional to $R_a + R_i$. R_a, R_i and γ are the same as in model CTB, as are the constants C_H and C_M.

The switch in f_a, f_i which assigns incoming water to either the annulus or interior, depending on the water height in the annulus, causes the differential equations to be very stiff and difficult to solve at the moment at which the switch occurs. In practise, the solution is evolved until the switch occurs and then a restart is performed.

(3) Model CB

Ideally, to model the case where there is a single crack in the bottom of the canister, the evolution of two separate water and hydrogen inventories would be calculated, with water being transferred from one compartment of the canister to the other in order to balance the pressure in the two hydrogen inventories. A suitable set of differential equations would be,

$$(16)\qquad \begin{aligned} \dot{M}_{Wa} &= \{f\} - R_a - T - \{E\}, \\ \dot{M}_{Wi} &= -R_i + T, \\ \dot{M}_{Ha} &= C_H R_a - B - \{V\}, \\ M_{Hi} &= C_H R_i + B, \\ \dot{M}_{Ca} &= C_M R_a, \\ \dot{M}_{Ci} &= C_M R_i. \end{aligned}$$

(where the corrosion inhibiting term γ has been ignored for brevity, but should be inserted where appropriate). All previously defined terms are as above, the new terms T and B describe the transfer of water between compartments and the 'bubbling' of hydrogen between compartments respectively.

This system cannot be solved with standard solvers because the resulting equations are extremely stiff, essentially because the timescale over which the new terms T and B vary is many of orders of magnitude larger than that of all the other terms. However by making some assumptions on the ultimate location of the hydrogen generated in each compartment and analysing the form of the term T, we can yield sufficient information to perform a simulation of this scenario with fewer degrees of freedom.

To begin with suppose that at a specific timestep of a solver integration, $p < P_{tot}$, and that there is sufficient water in the canister to submerge the crack, for example consider the case in the figure below. If there isn't sufficient water in the canister to submerge the crack, the water height in each compartment can be assumed to be equal and so calculating the water and hydrogen distribution in the canister is trivial in this case. Then all of the hydrogen that has been generated in the canister must still remain inside.

Figure 2.3:
Canister geometry for model CB

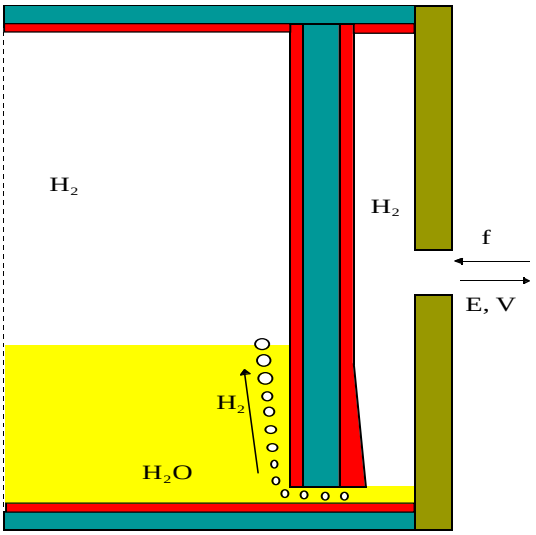

Given M_{Ca} and M_{Ci} we can deduce how much hydrogen was generated in each compartment. If we make the assumption that, once the crack in the canister is submerged, all the hydrogen tends to remain in the compartment in which it was generated, unless the water level in a compartment is sufficiently low so that hydrogen can 'bubble' through the crack and into the other compartment, then the

water inventories in each compartment can be deduced from the total water inventory and total hydrogen inventory as follows.

Firstly, the pressure in the canister is known, since

$$p = \frac{n_H \Gamma \tau}{V_{\text{tot}} - V_W - \left(\frac{\alpha - 1}{\alpha}\right)\left(V_{Ca} + V_{Ci}\right)}, \tag{17}$$

where n_H, the total number of moles of hydrogen, can be found from M_H, the total hydrogen mass. Also, given $M_{Ca}$and M_{Ci}, n_a and n_i, the number of moles of hydrogen generated in each compartment, can be deduced. Suppose further that the net number of moles of hydrogen that have been transferred from the annulus to the interior is n_t. Since the pressure is known, the volumes that these generated gas amounts must occupy can be calculated,

$$V_{Ha}^{*} = \frac{\left(n_a - n_t\right)\Gamma \tau}{p}, \quad V_{Hi}^{*} = \frac{\left(n_i + n_t\right)\Gamma \tau}{p}. \tag{18}$$

These volumes are denoted with a *since they may not be the correct physical volumes of hydrogen in the annulus and interior. Since it is being assumed that the hydrogen tends to remain in the compartment in which it was generated, if there is sufficient space in the annulus to contain V_{Ha}^{*} without forcing the water level to fall below the crack (in which case some hydrogen must have bubbled from the annulus to the interior) then all of the hydrogen that was generated in the annulus is assumed to have remained in the annulus, otherwise as much hydrogen as possible will remain in the annulus, with the water level at the top of the crack, the remainder of the hydrogen is assumed to have bubbled into the interior of the canister, and n_t can be updated. This is the case depicted in the figure above.

Alternatively if V_{Hi}^{*} cannot be contained in the interior without some bubbling of hydrogen from the interior to the annulus, the water height in the interior is set at the top of the crack height, and n_t is updated. Note that it must be possible to contain at least one of the gas volumes in its compartment since we are assuming that there is sufficient water in the canister to submerge the crack. In full, given V_{Ha}^{*} and

V_{Hi}^{*}, the corresponding water heights w_a^* and w_i^* (which could be below the crack height or even negative) can be calculated. Then

If $w_a^* \geq h_c$ *and* $w_i^* \geq h_c$ then the values V_{Ha}^{*}, V_{Hi}^{*}, w_a^* and w_i^* are the actual physical values, so that $V_{Ha} = V_{Ha}^{*}$, $V_{Hi} = V_{Hi}^{*}$, $w_a = w_a^*$ and $w_i = w_i^*$.

If $w_a^* < h_c$ *and* $w_i^* > h_c$ then some hydrogen must have bubbled from the annulus to the interior, so

$$
\begin{aligned}
w_a &= h_c, \\
V_{Ha} &= V_{\mathrm{a}} - V_{Wa} - \left(\frac{\alpha - 1}{\alpha}\right) V_{Ca}, \\
n_a &= \frac{p V_{Ha}}{\Gamma \tau}, \\
n_i &= n_H - n_a, \\
w_i &= V_{\mathrm{i}} - V_{Wi} - \left(\frac{\alpha - 1}{\alpha}\right) V_{Ci}, \\
n_t &= n_t + \left(n_a^* - n_a\right)
\end{aligned}
\qquad (19)
$$

If $w_a^* > h_c$ *and* $w_i^* < h_c$ then some hydrogen must have bubbled from the interior to the annulus, and the treatment is similar to that above.

These three cases encompass all possibilities when there is sufficient water to submerge the crack.

Thus when $p < P_{\mathrm{tot}}$, given M_W, M_H, M_{Ca} and M_{Ci} it is possible to calculate the distribution of hydrogen and water within the canister. When $p = P_{\mathrm{tot}}$ the above argument breaks down since some of the hydrogen may have been vented. However, if we suppose again that there is sufficient water to submerge the crack then, when $p = P_{\mathrm{tot}}$ it is easy to show that

$$
T = R_i \left[1 - C_M \left(\frac{\alpha - 1}{\alpha} \right) \frac{\rho_{\mathrm{H_2O}}}{\rho_{\mathrm{Fe_3O_4}}} - C_H \frac{\Gamma \tau}{P_{\mathrm{tot}}\, \mathrm{M}_{\mathrm{H_2}}} \rho_{\mathrm{H_2O}} \right]. \qquad (20)
$$

(If there were insufficient water to submerge the crack then again, the water levels in the annulus and interior would be equal and this case would be trivial). Here $[\cdot] \approx -13.245$ for $\tau = 303$, and since $R_i \geq 0$, $T \leq 0$. The single-signedness of T allows us to determine the direction of all gas and water flow once the pressure reaches the total external pressure. Once p has reached the total external pressure P_{tot}, water transfer between the compartments is only possible in the direction from the interior to the annulus. (This is indeed obvious, since any transfer in the opposite directions would compress the gas volume in the interior and raise the pressure higher than the total external pressure). If we write $T = -\Psi R_i$ then

(21) $$\dot{M}_{Wa} = \Psi R_i - R_a.$$

R_a assumes its maximum value when the annulus is full of water, since then the galvanically enhanced corrosion effectively doubles the consumption of water in the corrosion reaction . This maximum value is proportional to twice the available (steel) surface area in the annulus, A_a, whilst R_i is proportional to the surface area in the interior, A_i, with the constants of proportion being equal and positive, C say. Thus

(22) $$\dot{M}_{Wa} \geq C\left(\Psi A_i - 2A_a\right) \approx 424.5\ C.$$

Therefore, the water level in the annulus rises as soon as P_{tot} is reached, which prevents any further bubbling from the annulus to the interior. Thus, fixing the value of n_t when P_{tot} is reached, the total volume required by the hydrogen generated in the interior of the canister can be calculated from M_{Ci} and n_t. If this volume leaves enough water volume to submerge the crack, then the remaining water is assigned to the annulus and, depending on the water height in the annulus, a decision on whether to vent hydrogen or expel water can be made. Alternatively, if this gas volume cannot be contained in the interior without revealing the crack, the maximum possible amount of hydrogen is assigned to the interior, whilst still submerging the crack, and the remainder of the hydrogen is assumed to have bubbled to the interior. Again, the water height in the annulus can be calculated, and a decision to vent or expel is made. (We are able to base all calculations on the behaviour in the interior because T is always negative).

Given the above rules, the differential equations for scenario CB are then

$$
\begin{aligned}
\dot{M}_W &= \{f\} - R_a - R_i - \{E\}, \\
\dot{M}_H &= C_H\left(R_a + R_i\right) - \{V\}, \\
\dot{M}_{Ca} &= C_M R_a, \\
\dot{M}_{Ci} &= C_M R_i.
\end{aligned}
\tag{23}
$$

The awkward terms T and B have been avoided by working with the total water and hydrogen inventories rather than separate inventories for the annulus and interior.

(4) Approximation of the magnetic profile in the annulus

Given the successive magnetite masses in the annulus, an approximation to the profile of the magnetite layer in the annulus can be constructed. The corrosion profile will not necessarily be uniform, if liquid water is present in the annulus at any time, then galvanically enhanced corrosion beneath the water level will cause the magnetite profile there to be thicker. Suppose that $m = [m_0, m_1, ..., m_i, m_{i+1}, ..., m_n]$ are the total masses of magnetite in the annulus, so that m_i is the mass of magnetite at time t_i (the ith timestep). Defining α to be the volume of magnetite produced per unit volume of steel consumed by the corrosion process,

$$
\alpha = \frac{1}{3}\frac{\mathrm{M}_{\mathrm{Fe_3O_4}}}{\mathrm{M}_{\mathrm{Fe}}}\frac{\rho_{\mathrm{Fe}}}{\rho_{\mathrm{Fe_3O_4}}},
\tag{24}
$$

and the fraction of the total magnetite volume intruding in the annulus is $(\alpha - 1)/\alpha$. Then $v = [v_0, v_1, ..., v_i, v_{i+1}, ..., v_n]$, where

$$
v_i = \frac{\alpha - 1}{\alpha}\frac{m_i}{\rho_{\mathrm{Fe_3O_4}}}
\tag{25}
$$

is a vector of volumes of magnetite intruding into the annulus at successive timesteps. Also let $h = [h_0, h_1, ..., h_i, h_{i+1}, ..., h_n]$ be the corresponding vector of water heights in the annulus.

We approximate the increase in thickness of the magnetite profile in the annulus as follows. Let k_i denote the increase in thickness of magnetite that would have occurred from time t_{i-1} to time t_i in the presence of purely non-galvanically enhanced corrosion. Then increase in magnetite thickness over the same timestep due to purely galvanically enhanced corrosion will be $2k_i$. We make the assumption that, over the timestep, for any particular point in the annulus the corrosion is either purely non-galvanically enhanced or purely galvanically enhanced. This will obviously not be the case for a point which is submerged at the beginning at the timestep and above the water level at the end of the timestep (or *vice versa*), but since the rate of change of water height is generally small compared to the timesteps being used (usually 1 year), the assumption is not a bad one. Since the thickness of the corrosion profile is small compared to the radius of the canister, we approximate the profile at time t_{i-1} by a cylinder of radius r_c (i.e. the cylinder is the inner steel canister). Then using the assumptions above, the thickness k_i is approximated by the solution of

$$v_i - v_{i-1} = 2\pi r_c(h + h_i)k_i + \pi(3h_i + h)k_i^2. \tag{26}$$

Here, h is the height of the canister. Many approximations have been made in the derivation of the approximation k_i, the following section compares some analytical arguments and some experimental data which suggest that the approximation is nevertheless an accurate one.

(5) Time taken for magnitite to fill the annulus

In the presence of liquid water in the canister, the rate of consumption of water in the interior of the canister, R_i (Kg s^{-1}), is constant, and the rate in the annulus, R_a (Kg s^{-1}), can be bounded by $R_a^* \le R_a \le 2R_a^*$, where R_a^* is the non-galvanically enhanced rate of corrosion in the absence of (liquid) water in the annulus.

Given the corrosion rate υ μm/year, the water is consumed at the rate,

$$\begin{aligned} R &= \left(\frac{10^{-6}}{S_y}\rho_{\mathrm{Fe}} \times \frac{4}{3}\frac{\mathrm{M}_{\mathrm{H_2O}}}{\mathrm{M}_{\mathrm{Fe}}}\right)\upsilon, \\ &= 1.0683 \times 10^{-10}\upsilon \ \ \mathrm{Kg\ m^{-2}s^{-1}}, \end{aligned} \tag{27}$$

where S_y is the number of seconds in a year. The minimum rate of consumption in the annulus occurs when the annulus is free of (liquid) water, so that

(28) $$R_a^* = R \times A_a,$$

where A_a is the surface area of the annulus, which for the case of the proposed SKB canister is given by

(29) $$A_a = 2\pi r_c h = 2\pi \times 0.473 \times 4.47 \,\mathrm{m}^2,$$

and so,

(30) $$R_a^* = 1.4192 \times 10^{-9} \upsilon \ \mathrm{Kg\ s^{-1}}.$$

Magnetite is generated in the annulus at the rate $C_M R$, where

(31) $$C_M = \frac{\mathrm{M}_{\mathrm{Fe_3O_4}}}{4\ \mathrm{M}_{\mathrm{H_2O}}} = 3.211,$$

and hence a lower bound on the rate of magnetite production is $C_M \times R_a^* = 4.5572 \times 10^{-9} \upsilon \ \mathrm{Kg\ s^{-1}}$. Some of the magnetite occupies space that was vacated by the corroded steel, and the remainder intrudes into the annulus. If α is defined to be the volume of magnetite produced per unit volume of steel consumed, then

(32) $$\alpha = \frac{1}{3} \frac{\mathrm{M}_{\mathrm{Fe_3O_4}}}{\mathrm{M}_{\mathrm{Fe}}} \frac{\rho_{\mathrm{Fe}}}{\rho_{\mathrm{Fe_3O_4}}} \ ,$$

and the fraction of the total volume of magnetite that intrudes into the annulus is $(\alpha - 1)/\alpha$. In the presence of only vapour-corrosion, the corrosion rate is uniform across the whole of the steel surface area in the annulus, and so the magnetite is distributed evenly across the steel surface. The rate at which the thickness of the magnetite increases in the presence of purely vapour-corrosion is given by

(33) $$\frac{C_M \times R_a^*}{\rho_{Fe_3O_4} \times A_a} \frac{\alpha - 1}{\alpha} = 3.4515 \times 10^{-14} \upsilon \text{ ms}^{-1}.$$

Similarly, whilst the annulus is entirely full of water, magnetite thickness due to the galvanically enhanced corrosion increases at the rate

(34) $$\frac{C_M \times 2R_a^*}{\rho_{Fe_3O_4} \times A_a} \frac{\alpha - 1}{\alpha} = 6.9029 \times 10^{-14} \upsilon \text{ ms}^{-1}.$$

These two rates of corrosion (which are independent of the surface area of the annulus) are the maximal and minimal rates of corrosion in the annulus whilst liquid water is present, and hence can be used to bound the thickness of the actual corrosion profile for the times when liquid water is present in the canister. For example, Figure 2.5 shows the corrosion profiles for each scenario when the intrusion in the copper overpack is at the bottom of the canister, the area of the intrusion is $5 \times 10^{-6} \text{m}^2$ and $\upsilon = 0.01\,\mu\text{m/year}$. For the model CB, liquid water is only at the height of the crack in the steel container, so that the remainder of the annulus is only free to vapour corrosion. Thus the thickness of the magnetite layer grows at the minimum rate above. Liquid water is present in the canister for 15,406 years in this case. At the end of this time, the thickness of the magnetite layer is expected to be

$$15,406 \times S_y \times 3.4515 \times 10^{-14} \times 0.01 = 1.6769 \times 10^{-4} \text{ m},$$

which agrees closely with the computed magnetite thickness of 1.6763×10^{-4}m (giving a relative error of 3.5×10^{-4}). Similarly the thickness of magnetite at the bottom of the annulus in scenario CT for the same parameter values is expected to be 2.7253×10^{-4}m since here, all corrosion is galvanically enhanced (if the water in the interior had dried out significantly later than that in the annulus we would also expect some corrosion at the minimum rate due to vapour corrosion at the bottom of the annulus). Again this agrees well with the computed value of 2.7239×10^{-4}m (with relative error 5.2×10^{-4}m).

(6) Bentonite gel intrusion – model CTBi

In each of the models CTB, CT, CB discussed so far, it has been assumed that water enters the penetration in the copper overpack through an immobile bentonite interface located at the exterior of the penetration. This assumption can be unrealistic. Experiments by Pusch **[9]** have shown that the viscosity of bentonite is very much dependent on its water content, and thin bentonite gel can intrude relatively quickly into even very narrow gaps, 0.1mm for example. Since the size of the penetrations being considered here are larger than 0.1mm, it would be expected that, rather than remaining immobile at the exterior of the penetration, bentonite gel will intrude into the canister.

Once inside the canister the bentonite gel will give up water to the corrosion process, thus the density of the bentonite in the canister will increase as it loses water and hydrogen will be produced. As the gas accumulates, the pressure will increase and the rate of inflow of bentonite gel due to the pressure differential will decrease. Eventually the bentonite gel level will begin to decrease and the bentonite density in the canister will increase more rapidly as the bentonite gel is re-consolidated.

Two situations are then possible. If the bentonite level in the canister has fallen below the penetration, hydrogen will continue to be generated (and possibly vented) as was the case for each of the previous scenarios. However, if the bentonite level is still above the penetration when a critical bentonite density ρ_{crit} is attained in the canister, capillary forces can suck water through small pores in the reconsolidated bentonite from the exterior bentonite buffer, and this water can continue (or restart) the supply of water to the canister and prolong the corrosion process. Once the pressure in the canister reaches the breakthrough pressure $P_{\text{hydro}} + P_{\text{swell}}$, hydrogen can be vented through the larger pores in the reconsolidated bentonite to the exterior of the canister. In this case the supply of water to the canister is not limited by the gas cushioning effect of the other models, and the corrosion process can proceed until either mechanical breakdown of the canister occurs, or the annulus fills with magnetite.

We will describe this new scenario in the case that there is a crack in both the top and bottom of the steel canister. This model will be referred to as model CTBi.

Firstly we assume that the rate of inflow of water to the canister is unchanged from the previous scenarios, that is

$$f = \begin{cases} 0, & p \geq P_{\text{hydro}}, \\ 2\pi r_h \dfrac{k}{\mu}\left(P_{\text{hydro}} - p\right)\rho_{\text{H}_2\text{O},} & p < P_{\text{hydro}}, \end{cases} \tag{35}$$

is the rate (Kg s^{-1}) at which water enters the canister. However it will be assumed here that this water enters the canister in the form of bentonite gel. Then given the density of this inflowing bentonite gel, ρ_{gel}, and the density of water, $\rho_{\text{H}_2\text{O}}$, the water fraction F_{W} of the total inflow I_{tot} satisfies

$$F_{\text{W}} I_{\text{tot}} = f, \tag{36}$$

and is given by

$$F_{\text{W}} = \frac{\rho_{\text{H}_2\text{O}}}{\rho_{\text{gel}}}. \tag{37}$$

The bentonite fraction of the inflow, F_{B} is similarly given by

$$F_{\text{B}} = \frac{\rho_{\text{gel}} - \rho_{\text{H}_2\text{O}}}{\rho_{\text{gel}}}, \tag{38}$$

so that rate (Kg s^{-1}) at which bentonite enters the canister is

$$F_{\text{B}} I_{\text{tot}} = \frac{F_{\text{B}}}{F_{\text{W}}} f. \tag{39}$$

If the true density of bentonite is ρ_{TRUE}, and the masses of bentonite and water in the canister, M_{B} and M_{W} are known, then the bulk volume of the mixture is

$$V_{\text{B+W}} = \frac{M_{\text{W}}}{\rho_{\text{H}_2\text{O}}} + \frac{M_{\text{B}}}{\rho_{\text{TRUE}}}. \tag{40}$$

Thus, the density of the bentonite in the canister, ρ_{B}, is given by

$$\rho_{\text{B}} = \frac{M_{\text{B}}}{V_{\text{B+W}}}. \tag{41}$$

If $\rho_{\text{B}} > \rho_{\text{crit}}$, where ρ_{crit} is the critical bentonite density described above, then water can be sucked from the exterior bentonite buffer into the interior of the canister through the small pores in the reconsolidated bentonite. Both ρ_{gel} and ρ_{crit} should be considered as variables for sensitivity analysis, and have been given preliminary values of 1,300 Kg m^{-3} and 1,800 Kg m^{-3} respectively.

The differential equations describing this system are,

$$\begin{aligned}
\dot{M}_W &= \{f\} - \left(R_a + R_i\right) - \{E\} + \{S\}, \\
\dot{M}_B &= \frac{F_B}{F_W} f, \\
\dot{M}_H &= C_H\left(R_a + R_i\right) - \{V\}, \\
\dot{M}_{C_a} &= C_M R_a, \\
\dot{M}_{C_i} &= C_M R_i.
\end{aligned} \tag{42}$$

Once again the term γ has been ignored for simplicity, but should be used wherever appropriate. The term S refers to the suction of water through the small pores, the water expulsion term, E, needs to be slightly reformulated. Otherwise all terms are as previously defined. E is now also zero whenever the water (gel) level in the annulus is above the hole and the bentonite density in the canister is above the critical value, ρ_{crit}. Hence

$$(43)\quad E=\begin{cases} 0, & p<P_{\text{hydro}},\ \text{or } P_{\text{hydro}}\le p \ \text{ and } w_a\le h_h,\\ & \text{or } w_a>h_h \text{ and } \rho_B\ge\rho_{\text{crit}}\\ 2\pi r_h\dfrac{k}{\mu}\left(p-P_{\text{hydro}}\right)\rho_{H_2O}, & P_{\text{hydro}}\le p,\ w_a>h_h \text{ and } \rho_B<\rho_{\text{crit}}. \end{cases}$$

The suction term S compensates for the fact that water is sucked into the canister to replace that used up in the corrosion process, whenever the pressure in the canister exceeds the hydrostatic pressure, the water (gel) level in the annulus is above the hole and the bentonite density in the canister is above the critical value. Then the rate of change of water mass in the canister is zero, so that

$$(44)\quad S=\begin{cases} R_a+R_i, & w_a>h_h \text{ and } \rho_B\ge\rho_{\text{crit}},\\ 0, & \text{otherwise,} \end{cases}$$

(i.e. whenever $S\neq 0,\ \dot{M}_W=0$).

2.2 Results

(1) A zero corrosion rate reference scenario

As a refernce we consider a case where the corrosion rate is zero. This case serves as a basis for comparison, since it gives the minimum time for canister saturation. If it is assumed that the interior of the canister is initially a vacuum, as is assumed for models CTB, CT, CB, and CTBi, then this calculation is trivial. Since the corrosion rate is zero, there is no pressure buildup in the canister, and hence water flows into the canister at a constant rate until the canister is full. In this case, the time (in years) taken until canister saturation, T, is

$$(45)\quad T=\frac{1}{r_{\text{h}}}\frac{V_{\text{i}}+V_a}{2\pi\left(\dfrac{k}{\mu}\right)P_{\text{hydro}}}\frac{1}{S_{\text{y}}}.$$

For example, when the penetration area is 2×10^{-5} m^2, the above formula gives $T=17{,}067$ years, and when the penetration area is 5×10^{-6} m^2, $T=34{,}133$ years.

It could also be assumed that the interior of the canister initially contained gas at atmospheric pressure. If this is the case, the gas volume will be squeezed as water fills the canister, until it reaches a pressure equal to the external hydrostatic pressure. At this point the inflow of water to the canister will stop. This case is depicted in the following figures for the two penetration areas considered above. Since pressure is inversely proportional to gas volume, the initial pressure buildup is slow, but increases quickly when the canister is almost full of water, and so the time taken until the canister contains the maximum possible amount of water is not greatly different from the times calculated with the constant flow assumption above.

Figure 2.4: Presure and water height curves for the reference zero-corrosion rate scenarios, with initial gas at 1 atmosphere

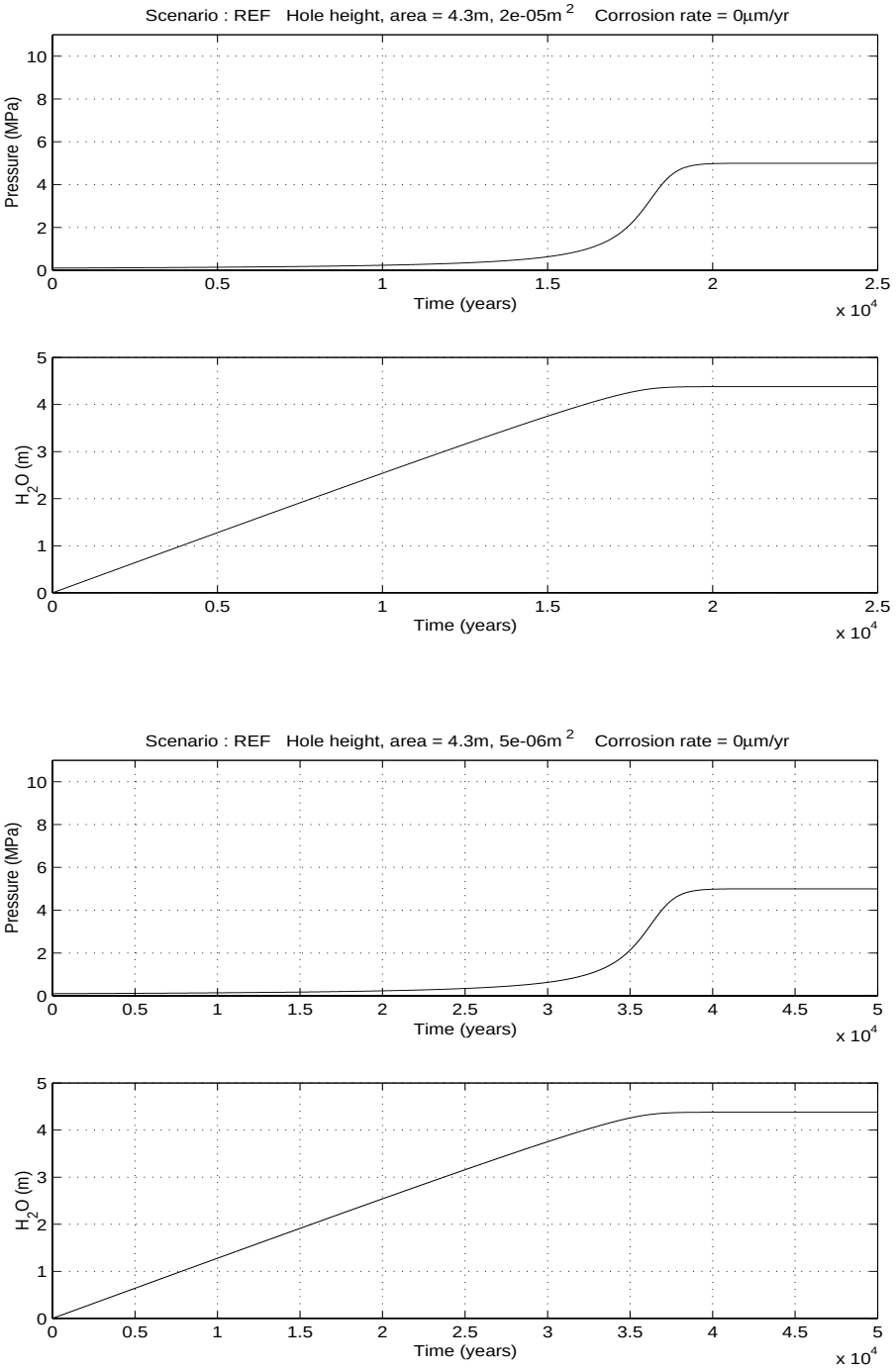

(2) Results – models CTB, CT and CB

Results for the models CTB, CT and CB are given for the parameter variations in the following table.

Table 2.1: Parameter variations

Parameter	Values taken
Corrosion rate (υ)	0.01, 0.1 μm/year
Penetration height (h_h)	0, 2.235, 4.3 m
Peteration area (πr^2)	5×10^{-6}, 2×10^{-5} m
Crack positions	0 m (i.e scenario CB) 4.7 m (i.e. scenario CT) 0 m and 4.7 m (i.e. scenario CTB)

All possible combinations of parameter values were taken, so that 36 simulations were run in total.

(i) Penetration area = 5×10^{-6} m^2, $\upsilon = 0.01\,\mu$m/year

Graphs of these results are shown in Figure 2.5 – Figure 2.7.

(i-a) Penetration at 0m

Model CTB : The inflowing water enters both the annulus and interior of the canister, where the water level rises to a maximum of 0.427m at 7,300 years. After this time the rate of consumption of water in the corrosion process exceeds the rate of inflow of water, and the water level begins to fall. The internal pressure in the canister reaches the external hydrostatic pressure of 5 MPa after 8,413 years. The water inventory then begins to fall as water is expelled from the canister, until it is all reduced to zero at 15,113 years when the pressure is 8.2 MPa. Since the pressure in the canister does not rise above the total external pressure of 10 MPa, no hydrogen is vented from the canister in this case. The magnetite layer for this case has the largest maximum thickness, since this is the case for which the water inventory in the canister remains the longest. For each of the experiments in this document, the magnetite profiles were calculated at 200 points along the height of the canister. The magnetite profile is at its thickest value of 0.327mm at the bottom of the canister, where galvanically enhanced corrosion took place, and has a uniform thickness of 0.165mm above the maximum water height of 0.427m.

Model CT : In this case, inflowing water initially enters the annulus. The crack at the top of the canister, which is assumed to have width 1mm, is reached after 3,264 years, after which time water begins to enter the interior of the canister. The rate of loss of water in the interior of the canister exceeds the rate of water inflow to the

interior of the canister after 6010 years at which point the water level in the interior is 0.079m. The water level in the interior then begins to fall. In the annulus, the water level begins to fall after 6,650 years. The external hydrostatic pressure of 5 MPa is reached after 7,136 years, and water begins to be expelled from the annulus. The interior water inventory is exhausted after 12,460 years, whilst the inventory in the annulus is zero by 12,518 years. The final pressure in the canister is 8 MPa. Again no hydrogen leaves the canister. The magnetite profile in the annulus is thicker nearer the bottom of the canister, where galvanically enhanced corrosion took place for the longest period of time. The magnetite has a maximum thickness of 0.272mm and a minimum thickness of 0.176mm.

Model CB : Inflowing water initially enters the annulus and interior of the canister. Since the ratio S_a / V_a (where V_a is the volume of the annulus) is larger than the ratio S_i / V_i (where V_i is the volume of the interior), the actual values being approximately $499m^{-1}$ and $85m^{-1}$ respectively, the rate of hydrogen generation per unit volume is much greater in the annulus than in the interior. Thus, in order to equilibrate the pressure throughout the canister, as soon as the crack in the steel canister is submerged, which takes 9 years, hydrogen bubbles from the annulus to the interior of the canister, and the water height in the interior is held at the top of the crack, which is assumed to be 1mm high. The water inventory in the interior of the canister rises to a maximum height of 0.463m at 7,445 years, after which time the rate of consumption of water in the corrosion process is greater than the rate of inflow of water, and the water level begins to fall. The pressure in the canister reaches the external hydrostatic pressure of 5MPa at 8557 years, at which point water begins to be expelled from the canister. The water inventory in the canister is reduced to zero by 15,400 years, when the pressure in the canister is 8.2 MPa. Again no hydrogen leaves the canister. Since all corrosion in the annulus is due to vapour, the corrosion profile in the annulus is uniform and has a thickness of 0.167mm by the time that all the water in the annulus is used up.

(i-b) Penetration at 2.235m

Model CTB : In this case, the maximum water height of 0.427m in both the interior and the annulus as achieved at 7,300 years. The pressure in the canister reaches the external hydrostatic pressure of 5MPa after 8,413 years, but since the water height is never as high as the penetration in the canister, no water is expelled from the canister. At 17,241 years the pressure in the canister reaches the total external pressure of 10 MPa and hydrogen is vented from the canister at the rate required to maintain a constant pressure of 10 MPa in the canister. The water inventory is exhausted at 32,958 years. The maximum magnetite thickness in the annulus is 0.709mm at the bottom of the annulus and is uniform at 0.359mm above the maximum water height.

Model CT : Water initially enters the annulus, and reaches the crack in the steel canister at 3,264 years. The interior water level then begins to rise and attains its

maximum value of 0.079m at 6010 years (as in the case of the penetration at 0m). The water height in the annulus begins to fall at 6,650 years. At 7,136 years, the internal pressure reaches the external hydrostatic pressure of 5MPa and water begins to be expelled from the canister, until 10,662 years when the water level in the annulus falls below the penetration. The interior water inventory is used up by 12,460 years. At 15,463 years the internal pressure reaches the total external pressure of 10 MPa and hydrogen begins to be vented from the canister. By 19,580 years the water inventory in the annulus is exhausted. The maximum and minimum thickness of the magnetite profile are 0.426 mm and 0.253 mm respectively.

Model CB : As in the case of the penetration at 0m, it takes 9 years for the level of the water in the canister to submerge the crack, after which time the water level in the annulus is held at the top of the crack (1mm) and hydrogen bubbles from the annulus to the interior. The water level in the interior achieves its maximum value of 0.463m at 7,445 years. The external hydrostatic pressure of 5 MPa is reached at 8,556 years, but since the water level in the annulus is held at the top of the crack, no water is expelled. The total external pressure of 10 MPa is attained at 17,552 years. At this time, hydrogen begins to be expelled from the canister and the water level in the annulus begins to quickly rise as the gas volume in the interior grows to maintain the uniform pressure, and the water level in the interior begins to fall quickly. The water level in the annulus reaches the penetration at 18,450 after which time water begins to be expelled from the canister. The water level in the annulus continues to rise, as does the pressure since water cannot be expelled at a rate sufficient to maintain an internal pressure of 10 MPa. At 19,139 years the water level in the interior has dropped to the top of the crack and hydrogen begins to bubble from the interior to the annulus. At the same time the water level in the annulus is at its maximum value of 2.495 m. Then the level begins to fall until it returns below the penetration at 19,241 years, hydrogen begins to be vented again, and the pressure, which has risen to 10.17 MPa, quickly drops to 10 MPa. The level continues to fall until the water inventory is exhausted at 27,609 years. The maximum and minimum thickness of the magnetite profile are 0.365 mm and 0.278 mm respectively.

(i-c) Penetration at 4.3m

Model CTB : The results for this case are exactly the same as those for the case when the penetration is at 2.235m since in neither case does the water height ever reach the penetration. The results are given again for completeness. A maximum water height of 0.427m in both the interior and the annulus as achieved at 7,300 years. The pressure in the canister reaches the external hydrostatic pressure of 5MPa after 8,413 years, but since the water height is never as high as the penetration in the canister, no water is expelled from the canister. At 17,241 years the pressure in the canister reaches the total external pressure of 10 MPa and hydrogen is vented from the canister at the rate required to maintain a constant pressure of 10 MPa in the canister. The water inventory is exhausted at 32,958 years. The maximum

magnetite thickness in the annulus is 0.709 mm at the bottom of the annulus and is uniform at 0.359 mm above the maximum water height.

Model CT : Again the results prior to the pressure reaching the external hydrostatic pressure are exactly the same as in the cases of penetrations at 0m and 2.235m. Water enters the annulus, and reaches the crack in the steel canister at 3,264 years. The interior water level rises to a maximum value of 0.079m at 6010 years (as in the case of the penetration at 0m). The water height in the annulus begins to fall at 6,650 years. At 7,136 years, the internal pressure reaches the external hydrostatic pressure of 5MPa, but since the water level in the annulus has already fallen below the penetration height, no water is expelled from the canister. The interior water inventory is used up by 12,460 years. At 14,561 years the internal pressure reaches the total external pressure of 10MPa and hydrogen begins to be vented from the canister. By 24,600 years the water inventory in the annulus is exhausted. The maximum and minimum thickness of the magnetite profile are 0.535mm and 0.308mm respectively.

Model CB : Again, the water height in the annulus is held at the top of the crack until the total external pressure is reached in the canister. The interior water height rises to a maximum of 0.463m at 7,445 years. The water height then falls slowly to 0.292m at 17,551 years, at which point the pressure in the canister reaches the total external pressure of 10 MPa. Then hydrogen is vented to maintain a constant pressure, and water is pushed from the interior to the annulus by the expanding gas volume in the interior. The water level in the annulus rises to its maximum height of 3.962m at 19,139 years. Since this maximum height is below the penetration, no water is expelled from the canister. The water continues to be consumed until it is used up at 33,878 years. The maximum and minimum thickness of the magnetite profile are 0.445mm and 0.318mm respectively.

(ii) Penetration area = $2\times10^{-5}\,\mathbf{m^2}$, $\upsilon = 0.01\,\mu\mathbf{m/year}$

Graphs of these results are shown in Figure 2.8 – Figure 2.10.

(ii-a) Penetration at 0m

Model CTB : The water in the canister reaches a maximum height of 0.877m at 6,840 years. After 7,330 years, the pressure in the canister exceeds the external hydrostatic pressure of 5MPa and so water is expelled from the canister. After 14,818 years the water inventory is exhausted at which point the pressure in the canister is 8.18 MPa. The final magnetite profile has a maximum and minimum thickness of 0.321mm and 0.161mm respectively.

Model CT : The water level in the annulus reaches the height of the crack in the steel container in 1,251 years. The interior water level then begins to rise until it reaches a maximum height of 0.488m at 5,794 years. At 6,083 years the water level in the annulus begins to fall as the rate of loss of water due to corrosion exceeds the

rate of inflow of water. After 6,308 years the external hydrostatic pressure of 5 MPa is attained and water begins to be expelled from the annulus until the annulus is dry at 10,093 years. After 15,078 years the pressure in the canister equals the total external pressure of 10 MPa and hydrogen begins to be vented from the canister, until the water inventory in the interior is exhausted at 34,372 years. The final magnetite profile has a maximum and minimum thickness of 0.484mm and 0.429mm respectively.

Model CB : The water level in the canister submerges the crack at 5 years, and is held at the top of the crack until the total external pressure is reached in the canister. The interior water inventory reaches a maximum height of 0.963m at 7,062 years. At 7,555 years the pressure is equal to the external hydrostatic pressure and water begins to be expelled from the canister. After 15,337 years the water inventory in the canister is completely exhausted and the pressure is 8.17 MPa. The final magnetite profile has a uniform thickness of 0.167mm.

(ii-b) Penetration at 2.235m

Model CTB : The water in the canister reaches a maximum height of 0.877m at 6,840 years. After 7,330 years, the pressure in the canister exceeds the external hydrostatic pressure of 5MPa but no water is expelled because the water level is below the penetration height. After 14,952 years the pressure in the canister reaches the total external pressure and hydrogen begins to be vented from the canister. The water inventory is exhausted after 58,041 years. The final magnetite profile has a maximum and minimum thickness of 1.256mm and 0.632mm respectively.

Model CT : The water level in the annulus reaches the height of the crack in the steel container in 1,251 years. The interior water level then begins to rise until it reaches a maximum height of 0.488m at 5,794 years. At 6,083 years the water level in the annulus begins to fall as the rate of loss of water due to corrosion exceeds the rate of inflow of water. After 6,308 years the external hydrostatic pressure of 5 MPa is attained and water begins to be expelled from the annulus until the water level in the annulus falls below the penetration height at 8,812 years. After 13,949 years the pressure in the canister equals the total external pressure of 10 MPa and hydrogen begins to be vented from the canister. The water inventory in the annulus is used up in 32,830 years, and the water inventory in the interior is exhausted at 40,752 years. The final magnetite profile has a maximum and minimum thickness of 0.799mm and 0.498mm respectively.

Model CB : The water level in the canister submerges the crack at 5 years, and is held at the top of the crack until the total external pressure is reached in the canister. The interior water inventory reaches a maximum height of 0.963m at 7,062 years. At 7,555 years the pressure is equal to the external hydrostatic pressure but no water is vented since the water level in the annulus lies below the penetration. At 15,496 years the total external pressure is attained, hydrogen is vented, the water level in the interior begins to fall quickly and the level in the annulus begins to rise until it

reaches the height of the crack at 16,398 years, when water is expelled. The pressure in the canister is sufficiently high to expel water at the rate required to maintain the water level in the annulus at the height of the penetration. At 19,941 years the water level in the interior falls to the height of the crack and hydrogen bubbles from the interior to the annulus. At this point the water level in the annulus begins to fall until the total water inventory is used up by 28,301 years. The final magnetite profile has a maximum and minimum thickness of 0.383mm and 0.276mm respectively.

(ii-c) Penetration at 4.3m

Model CTB : The results for this case are exactly the same as those for the case that the penetration is at 2.235m. The water in the canister reaches a maximum height of 0.877m at 6,840 years. After 7,330 years, the pressure in the canister exceeds the external hydrostatic pressure of 5 MPa but no water is expelled because the water level is below the penetration height. After 14,952 years the pressure in the canister reaches the total external pressure and hydrogen begins to be vented from the canister. The water inventory is exhausted after 58,041 years. The final magnetite profile has a maximum and minimum thickness of 1.256mm and 0.632mm respectively.

Model CT : The water level in the annulus reaches the height of the crack in the steel container in 1,251 years. The interior water level then begins to rise until it reaches a maximum height of 0.488m at 5,794 years. At 6,083 years the water level in the annulus begins to fall as the rate of loss of water due to corrosion exceeds the rate of inflow of water. After 6,308 years the external hydrostatic pressure of 5 MPa is attained but no water is expelled since the water level lies below the penetration. After 13,007 years the pressure in the canister equals the total external pressure of 10 MPa and hydrogen begins to be vented from the canister. The water inventory in the interior is used up in 43,843 years, and the water inventory in the annulus is exhausted at 44,665 years. The final magnetite profile has a maximum and minimum thickness of 0.972mm and 0.541mm respectively.

Model CB : The water level in the canister submerges the crack at 5 years, and is held at the top of the crack until the total external pressure is reached in the canister. The interior water inventory reaches a maximum height of 0.963m at 7,062 years. At 7,555 years the pressure is equal to the external hydrostatic pressure but no water is vented since the water level in the annulus lies below the penetration. At 15,496 years the total external pressure is attained, hydrogen is vented, the water level in the interior begins to fall quickly and the level in the annulus begins to rise until it reaches the height of the crack at 17,230 years, when water is expelled. The pressure in the canister is sufficiently high to expel water at the rate required to maintain the water level in the annulus at the height of the penetration. At 19,941 years the water level in the interior falls to the height of the crack and hydrogen bubbles from the interior to the annulus. At this point the water level in the annulus begins to fall until the total water inventory is used up by 35,979 years. The final magnetite profile has a maximum and minimum thickness of 0.469mm and 0.319mm respectively.

(iii) Penetration area = $5\times10^{-6}\mathrm{m}^2$, $\upsilon = 0.1\,\mu$m/year, all penetration heights

For all of these cases (shown in Figure 2.11 – Figure 2.13) the rate of inflow of water is so small, compared to the rate at which water is used up by the corrosion process, that no liquid water inventory forms for any of the scenarios (CTB, CT and CB) and so corrosion is limited by the supply of water. Since there is no build-up of water, each case exhibits exactly the same behaviour. The issue of whether the water supply due to the pressure differential is greater than the water supply due to diffusion of water vapour at the bentonite surface is debatable and should be considered further. If we assume that the supply of water by the pressure differential is the greater for a significant initial time then the differential equation models can be applied and the pressure in the canister tends asymptotically to the external hydrostatic pressure P_{hydro} and the magnetite thickness tends to approximately $1.0292\times10^{-4}\mathrm{m}$.

(iv) Penetration area = $2\times10^{-5}\mathrm{m}^2$, $\upsilon = 0.1\,\mu$m/year, all penetration heights

In each of these cases (shown in Figure 2.14 – Figure 2.16) there is an initial build-up of a water inventory in the canister, because the larger hole size in this scenario than the one described above gives rise to a greater initial inflow of water. In all cases however, the high corrosion rate causes the pressure to rise so quickly that the inflow of water is soon suppressed and the water inventories are used up before the pressure reaches the external hydrostatic pressure. Hence in all cases the pressure in the canister tends asymptotically to P_{hydro}. Since the pressure never exceeds P_{hydro}, the position of the penetration plays no part in the simulation. The time taken for the rate of loss of water to corrosion to exceed the rate of inflow of water is 339 years for model CB, 328 years for model CT and 337 years for model CTB. The time taken is least for model CT since here, all of the water inventory is confined to the annulus, and so the galvanically enhanced corrosion causes the pressure to rise more quickly than in the other cases. The reason that the time taken in model CTB less than that taken in model CB is similar. Again the issue of whether the water supply due to the pressure differential is greater than the water supply due to diffusion of water vapour at the bentonite surface is debatable.

(3) Comparing models CTB and CB

Model CTB is similar to the scenario used in **[1]** to simulate the case when there is a crack in (only) the bottom of the steel canister. It has been argued here that an alternative description of this case is given by model CB. Model CB supports the possibility of varying water heights in the annulus and interior of the canister due to

the differing gas volumes in the interior and annulus required to support a uniform gas pressure throughout the canister, whereas model CTB assumes that there is really an additional crack at the top of the canister, through which gas transfer is possible, so that the water levels in the interior and annulus are always equal. In model CB, if gas is to transfer from the annulus to the interior (or interior to annulus), the water level in the annulus (interior) must lower to the top of the crack. Then gas can 'bubble' from one side of the crack to the other.

The consequences of using model CB rather than CTB are most obvious when the corrosion rate υ is 0.01 μm/year. (For the larger rate, 0.1 μm/year there is little no water build-up in either scenario, and so both CTB and CB behave similarly). Since the annulus has a large surface area, relative its volume, whereas the interior has a smaller surface area relative to its volume, the water level in the annulus does not initially rise above the crack in model CB. Instead it is held constant at the top of the crack, and hydrogen generated in the annulus bubbles into the interior. This has the effect lessening the amount of galvanically enhanced corrosion in the annulus than that in model CTB, where there water inventory in the annulus is above the top of the crack for the majority of the simulation time. Thus the initial build-up of magnetite in the annulus is least for model CB.

Once the pressure in the canister reaches the external hydrostatic pressure, water is expelled from the canister if the water level in the annulus is above the height of the penetration. However, if the penetration is above the height of the crack, then no water is expelled in model CB, since the water level is being held at the top of the crack, and the water level in the annulus will not increase until the total external pressure is reached. Thus water can be expelled from the canister sooner in model CTB, provided that he penetration height is below the water level in model CTB.

Provided that the penetration is above the crack height, once the total external pressure has been reached, the water level in the annulus will rise in model CB, since hydrogen will begin to be vented from the annulus and the hydrogen volume in the interior will expand to maintain a constant pressure of 10 MPa. For the case when the penetration area is 5×10^{-6}m^2, the maximum water height attained in the annulus is 3.962m. Thus, for any penetration below 3.962m, water will be expelled from the canister. In contrast, the maximum penetration height beyond which no water can be expelled in model CTB is less than 0.427m, the maximum water height obtained at a pressure lower than the external hydrostatic pressure. Thus in general it can be concluded that a greater amount of water will be expelled from the canister in model CB.

In summary, model CB generally has a final magnetite profile in the annulus that is thinner , and more water is expelled from the canister than that in model CTB.

(4) Results - model CTBi

In these simulations, ρ_{gel} and ρ_{crit} are taken to be 1,300 Kg m^{-3} and 1,800 Kg m^{-3} respectively. Graphs of the results are shown in Figure 2.17.

(i) Penetration area = $2\times10^{-5}\,\mathbf{m^2}$, $\upsilon = 0.01\,\mu$m/year, penetration height = $0\,\mathbf{m}$

Water and bentonite (bentonite gel) initially enter the canister. As the water is used up in the corrosion process, the pressure in the canister increases, the inflow of bentonite and water reduces, and the density of the bentonite in the canister increases. At 7,121 years, the internal pressure reaches the external hydrostatic pressure and the inflow of water and bentonite stops, the bentonite inventory in the canister is 28.41 Kg. The density of the bentonite reaches ρ_{crit} after 14,106 years, when the pressure is 8.12 MPa. Capillary forces then begin to draw water through small pores in the bentonite and the water level in the canister remains fixed from this point onwards at 0.1653m. After 17,732 years, the pressure reaches the total external pressure and hydrogen is vented through the bentonite in the interior of the canister to the exterior of the canister. The simulation stops after 91,874 years when the thickness of the magnetite at the bottom of the canister is 2mm (the thickness of the annulus).

(ii) Penetration area = $2\times10^{-5}\,\mathbf{m^2}$, $\upsilon = 0.01\,\mu$m/year, penetration height > $0\,\mathbf{m}$

From the above case, it can be deduced that for penetration heights below the final water level of 0.1653m, the critical bentonite density will be reached before the water level falls below the penetration. Bentonite will continue to draw water from the external bentonite buffer and corrode the canister and the annulus will block after 91,874 years.

(iii) Penetration area = $5\times10^{-6}\,\mathbf{m^2}$, $\upsilon = 0.01\,\mu$m/year, penetration height = $0\,\mathbf{m}$

Water and bentonite (bentonite gel) initially enter the canister. As the water is used up in the corrosion process, the pressure in the canister increases, the inflow of bentonite and water reduces, and the density of the bentonite in the canister increases. At 8,276 years, the internal pressure reaches the external hydrostatic pressure and the inflow of water and bentonite stops, the bentonite inventory in the canister is 16.08 Kg. The density of the bentonite reaches ρ_{crit} after 14,557 years, when the pressure is 8.08 MPa. Capillary forces then begin to draw water through small pores in the bentonite and the water level in the canister remains fixed from this point onwards at 0.0936m. After 17,993 years, the pressure reaches the total

external pressure and hydrogen is vented through the bentonite in the interior of the canister to the exterior of the canister. The simulation stops after 91,874 years when the thickness of the magnetite at the bottom of the canister is 2mm (the thickness of the annulus).

(iv) Penetration area = $5\times10^{-6}\mathbf{m^2}$, $\upsilon = 0.01\,\mu\mathbf{m/year}$, penetration height > $0\,\mathbf{m}$

Similar to the case above where penetration sizes of $2\times10^{-5}\mathrm{m}^2$ are considered, the annulus will block after 91,874 years for penetration heights below 0.0936m.

(v) Penetration area = $2\times10^{-5}\mathbf{m^2}$, $\upsilon = 0.1\,\mu\mathbf{m/year}$, penetration height = $0\,\mathbf{m}$

Drawing of water through small pores in the interior bentonite inventory from the external bentonite begins at 605 years, when the water level is at 0.0182m and the pressure is 3.207 MPa. At this point the system becomes stiff and unsolvable. It can be deduced however, that the water level will never fall below 0.0182m since the pressure differential at 605 years is still forcing water and bentonite into the canister, in addition to the water supply due to the capillary forces in the interior bentonite inventory. It can also be deduced from the discussion in section [-] that the thickness of the magnetite in the annulus will reach 2mm after 9,187 years.

(vi) Penetration area = $5\times10^{-6}\mathbf{m^2}$, $\upsilon = 0.1\,\mu\mathbf{m/year}$, penetration height = $0\,\mathbf{m}$

In this case, all water that initially enters the canister is immediately used up by the corrosion process, so that any inflowing bentonite gel is reconsolidated as soon as it enters the canister. The resulting system is very stiff, and is not solvable in the present framework.

(5) Comparison with results in [1]

The following table shows the cases considered in this document and the corresponding scenarios from **[1]**.

Table 2.2: Comparison with scenarios in **[1]**

Models	Penetration at 0m	Penetration at 2.235m	Penetration at 4.3m
CT	Scenario 4	Scenario 1	Scenario 5
CTB	Scenario 3	Scenario 2	---
CB	---	---	---
CTBi	---	---	---

(i) Penetration area = $5\times10^{-6}\mathbf{m^2}$, $\upsilon = 0.01\,\mu$**m/year**

Scenario 1 : The results qualitatively agree, both assessments predict that the final canister pressure will be equal to the total external pressure, and that hydrogen will be vented from the canister after approximately 15,400 years. The time taken for the water inventory to dry out in SKB 97-19 is approximately 1,500 years shorter than that in this assessment.

Scenario 2 : The results agree fairly closely with the times taken to reach the total hydrostatic pressure and total external pressure varying by less than 160 years. Again, the time taken for the water inventory to dry out in **[1]** is approximately 1,400 years shorter than that in this assessment.

Scenario 3 : The results agree within similar margins to scenario 2. The final pressure of 8.2MPa predicted here agrees well with the final pressure of 8.13MPa given in **[1]**.

Scenario 4 : The results agree within similar margins again. The final pressure given here is 8MPa compared with 7.971MPa in **[1]**.

Scenario 5 : Results vary significantly. **[1]** predicts that water is present in the annulus for 93,550 years, and that the annulus fills with magnetite at this time, whereas this assessment predicts that the internal water inventory is used up after 12,460 years and that the magnetite layer in the annulus has a maximum thickness of 0.709mm. This difference is most likely due to the fact that, in **[1]** it is assumed that no corrosion of the interior of the steel canister takes place once the interior water inventory is reduced to zero (**[1]**, Appendix A). Here it is assumed that if zero water inventory is present in the interior, vapour generated by evaporation in the annulus can be transported to the interior of the canister through the crack in the steel canister and continue the corrosion process there.

(ii) Penetration area = 2×10^{-5} m², $\upsilon = 0.01\,\mu$m/year

No results for these scenarios are given in **[1]**.

(iii) Penetration area = 5×10^{-6} m², $\upsilon = 0.1\,\mu$m/year

For both assessments, there is no build-up of water in the canister, and the pressure increases asymptotically to the external hydrostatic pressure. This result will also apply for any corrosion rate greater than $0.1\,\mu$m/year. In **[1]**, maximum penetration areas up to which this behaviour must continue are also given for these scenarios. The maximum sizes quoted are 8.25×10^{-6} m² when the corrosion rate is $0.1\,\mu$m/year, and 8.25×10^{-4} m² when the corrosion rate is $0.01\,\mu$m/year.

(iv) Penetration area = 2×10^{-5} m², $\upsilon = 0.1\,\mu$m/year

Both assessments predict that there will be an initial build-up of water that will dry out before the external hydrostatic pressure can be exceeded, and so the pressure tends asymptotically to the external hydrostatic pressure.

Model CB

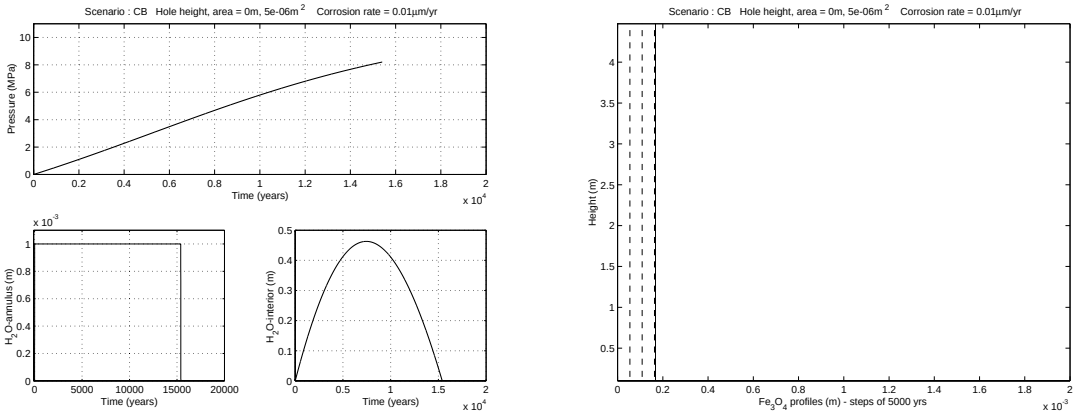

Model CTB

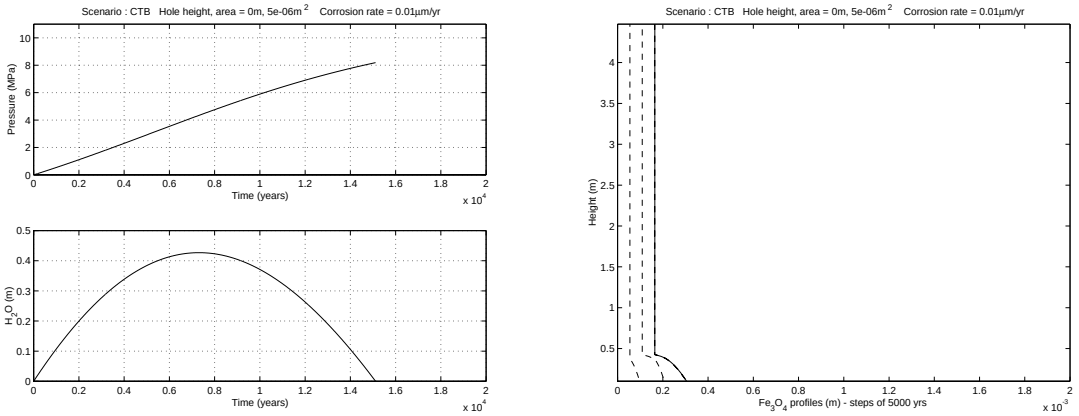

Model CT

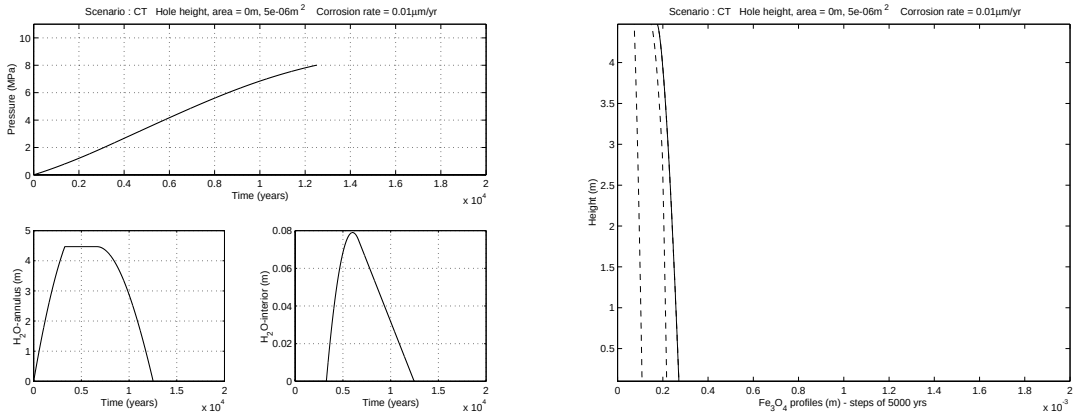

Figure 2.5: Penetration at 0m, Penetration area = $5\times10^{-6}m^2$,
Corrosion rate = $0.01\mu m/year$

Model CB

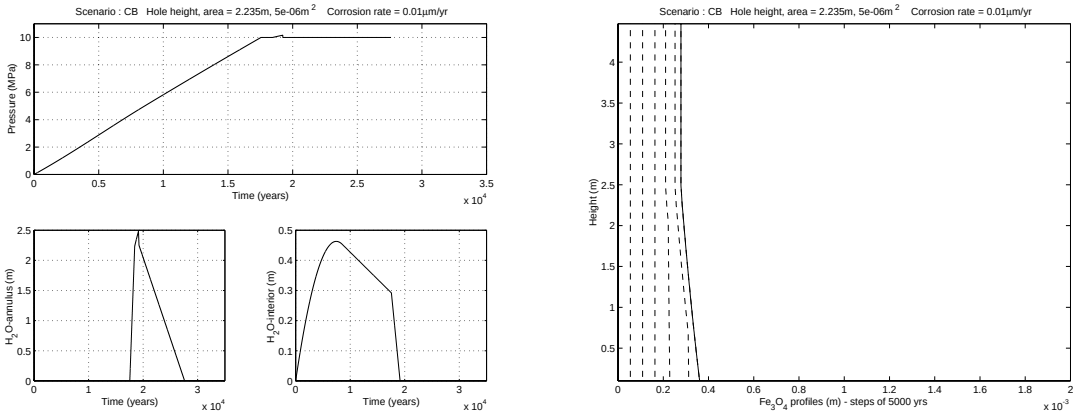

Model CTB

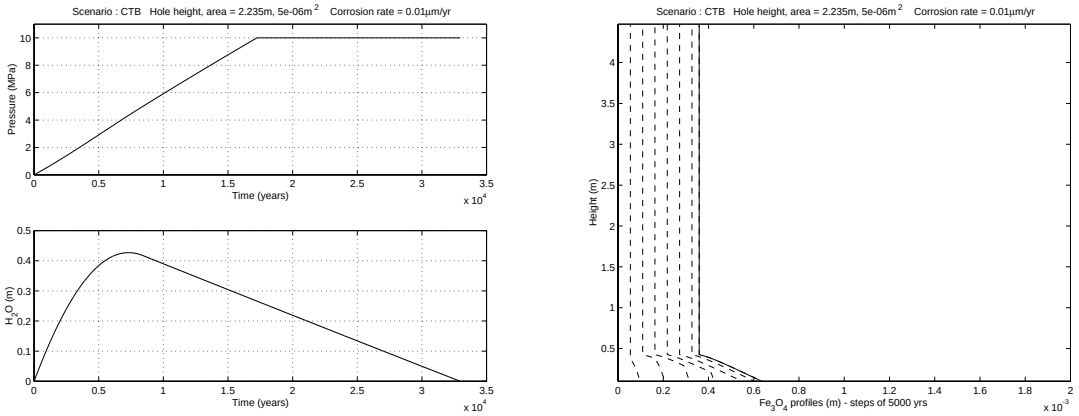

Model CT

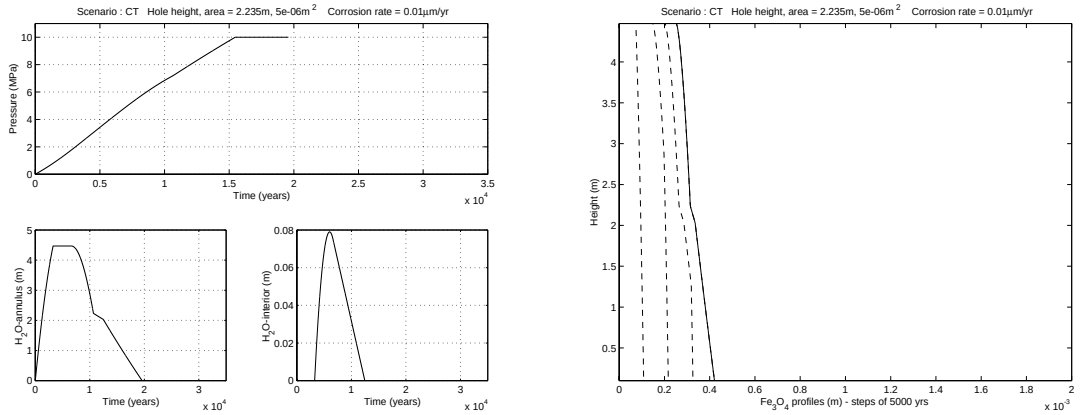

Figure 2.6:Penetration at 2.235m, Penetration area = $5\times10^{-6}m^2$,
Corrosion rate = $0.01\mu m/year$

Model CB

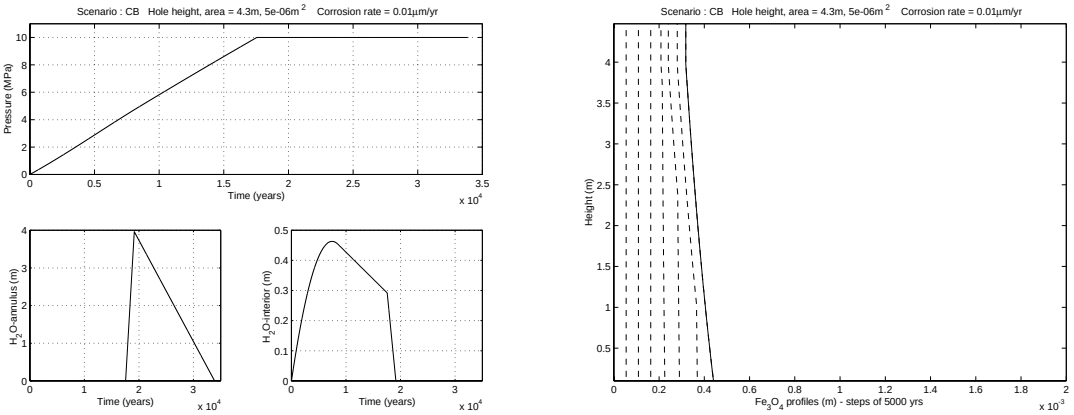

Model CTB

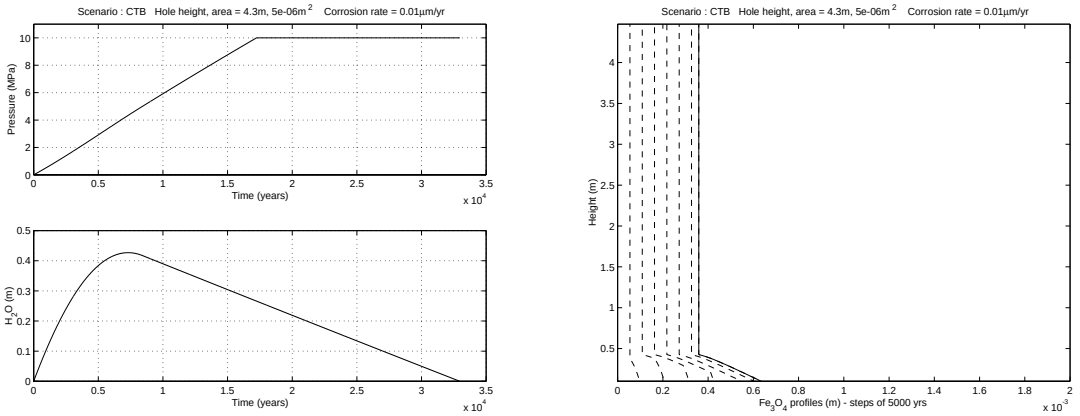

Model CT

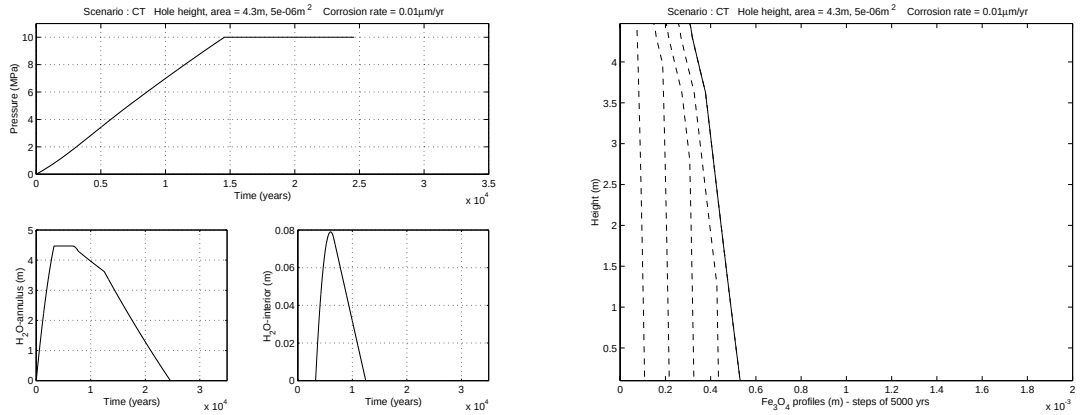

Figure 2.7:Penetration at 4.3m, Penetration area = $5\times10^{-6}m^2$,
Corrosion rate = $0.01\mu m/year$

Model CB

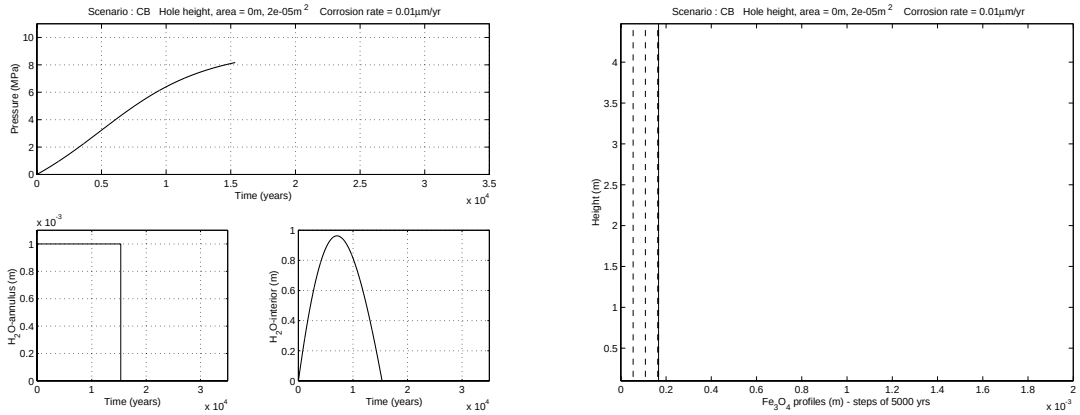

Model CTB

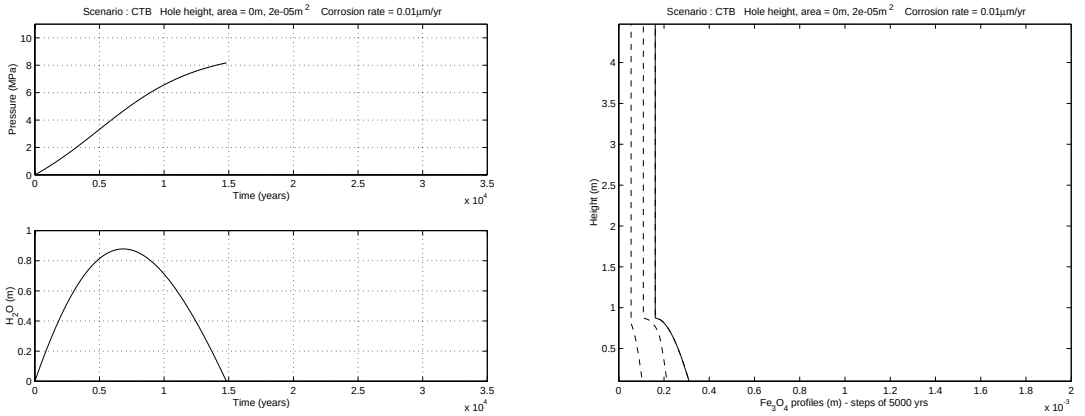

Model CT

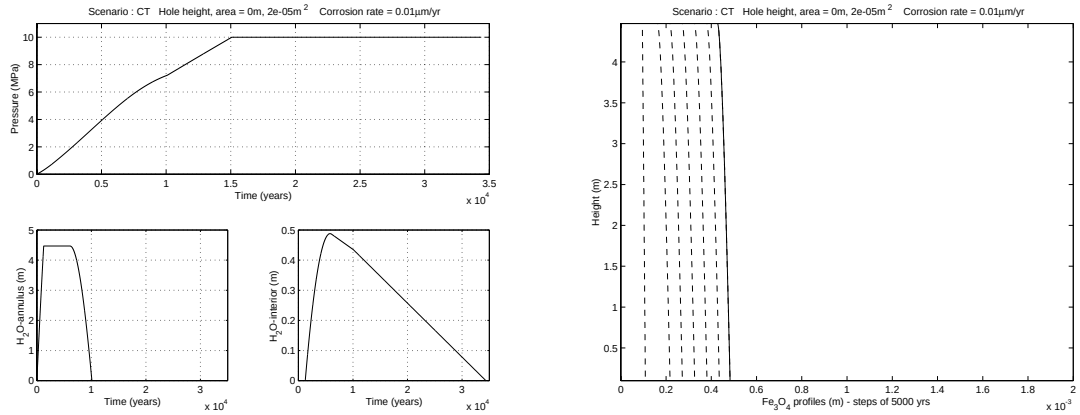

Figure 2.8:Penetration at 0m, Penetration area = $2 \times 10^{-5} m^2$,
Corrosion rate = $0.01 \mu m / year$

Model CB

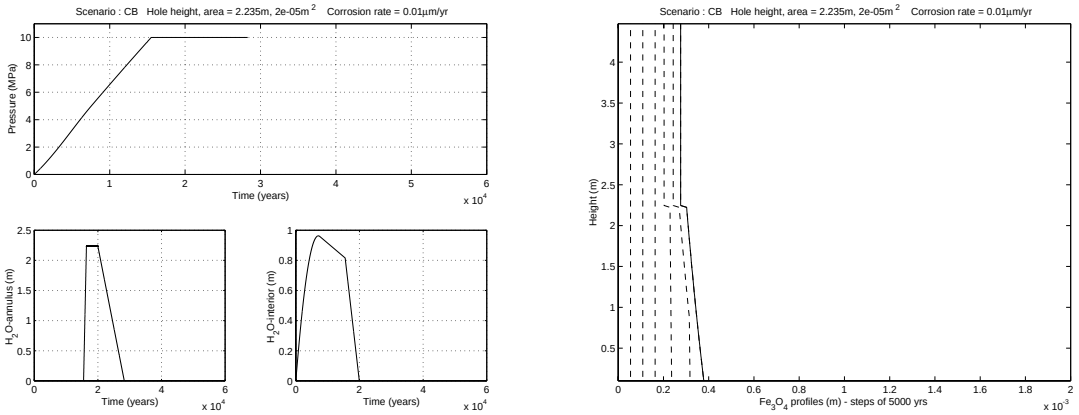

Model CTB

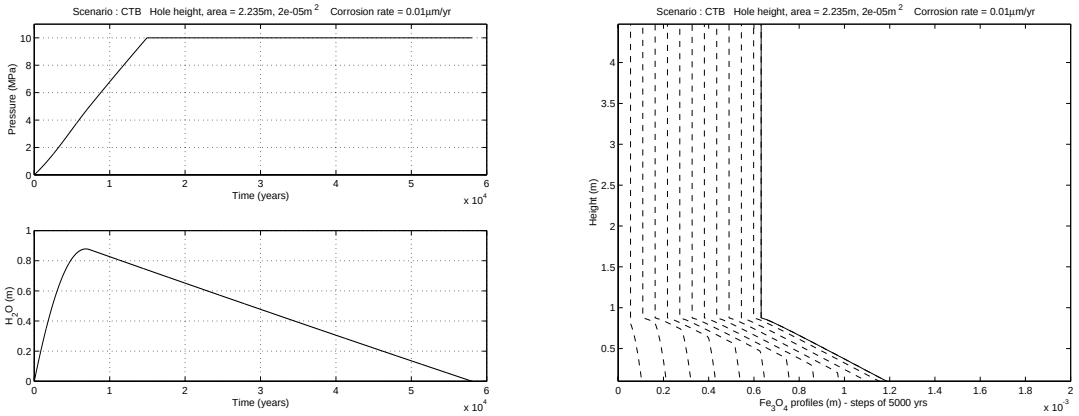

Model CT

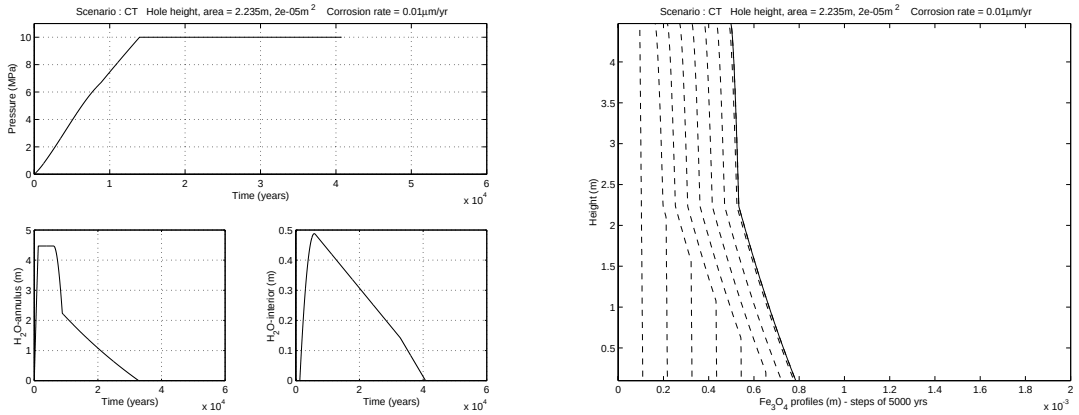

Figure 2.9: Penetration at 2.235m, Penetration area = $2\times10^{-5}m^2$, Corrosion rate = $0.01\mu m/year$

Model CB

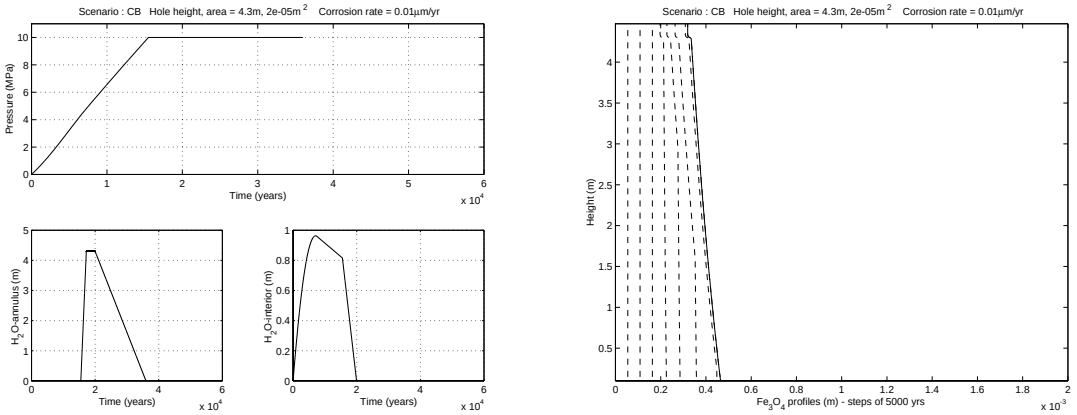

Model CTB

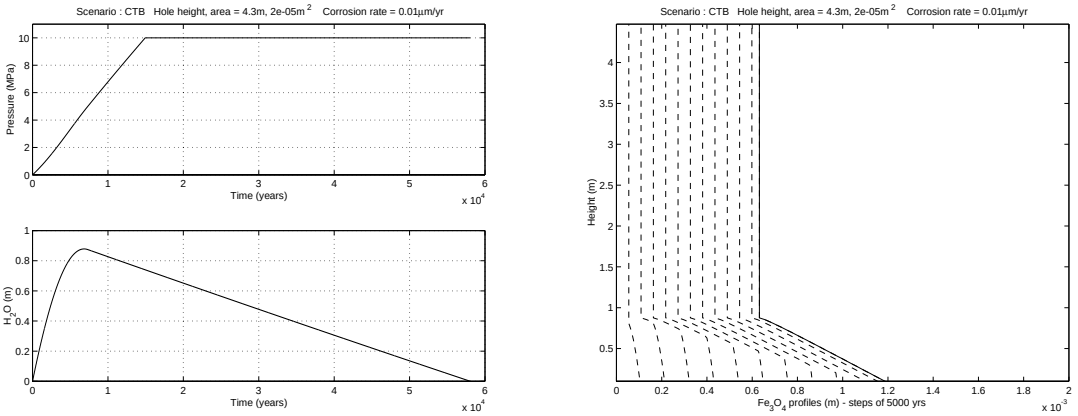

Model CT

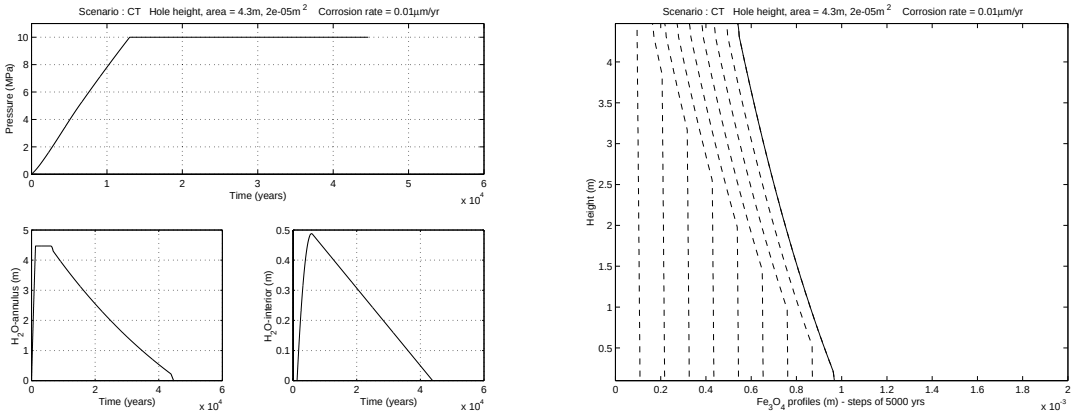

Figure 2.10:Penetration at 4.43m, Penetration area = $2\times10^{-5}m^2$,
Corrosion rate = $0.01\mu m/year$

Model CB

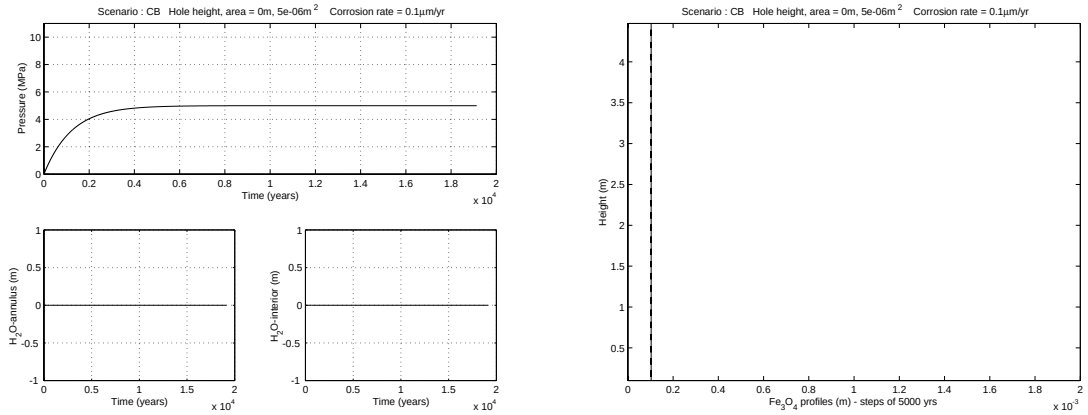

Model CTB

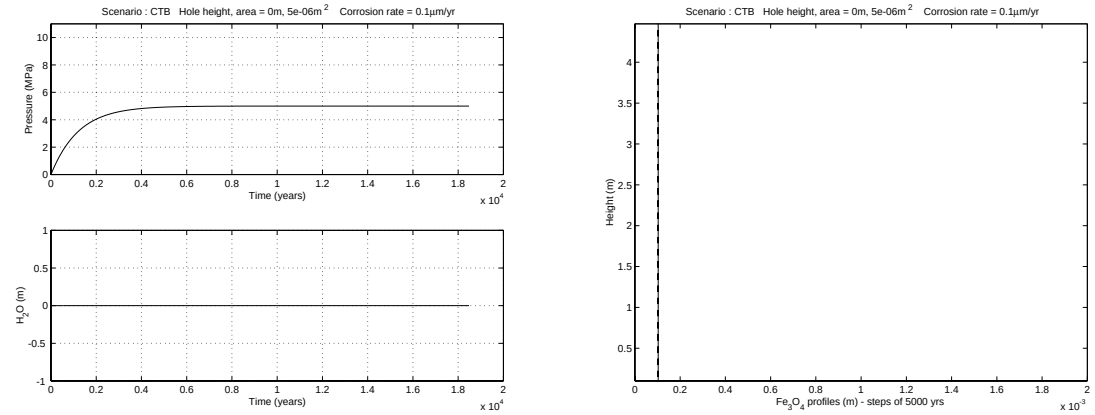

Model CT

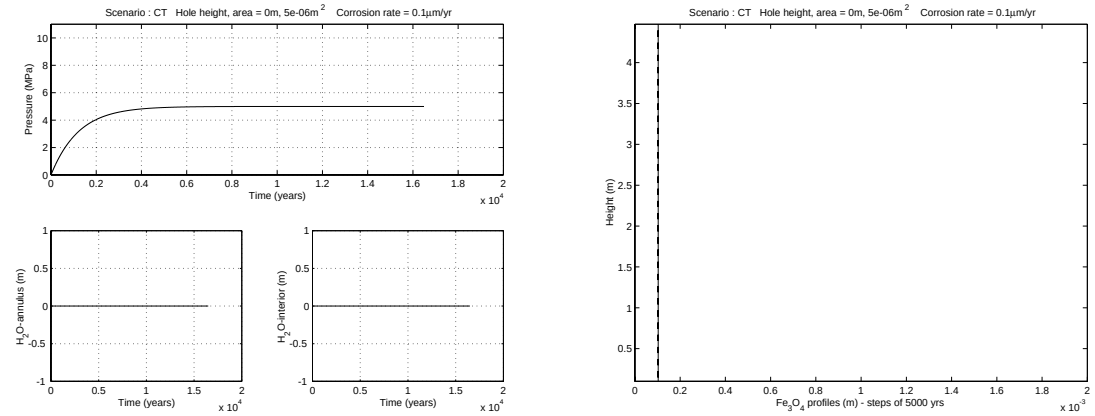

Figure 2.11:Penetration at 0m, Penetration area = $5\times10^{-6}m^2$, Corrosion rate = $0.1\mu m/year$

Model CB

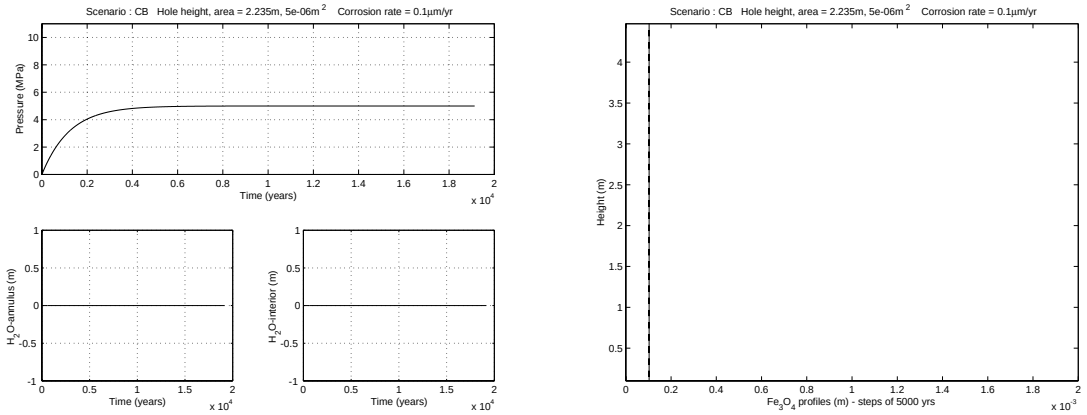

Model CTB

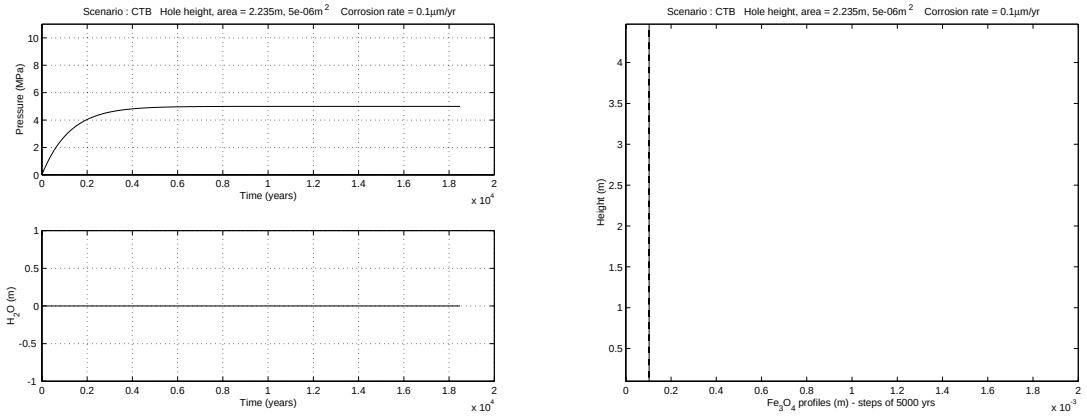

Model CT

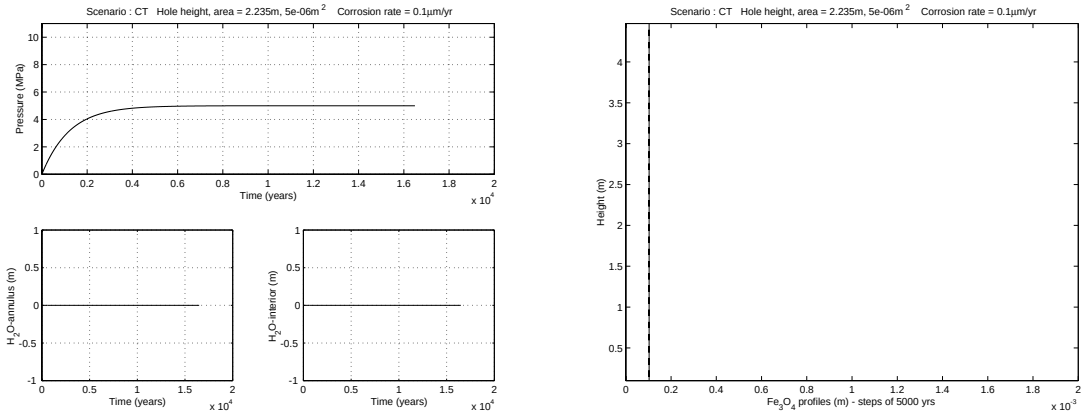

Figure 2.12:Penetration at 2.235m, Penetration area = $5\times10^{-6}m^2$,
Corrosion rate = $0.1\mu m/year$

Model CB

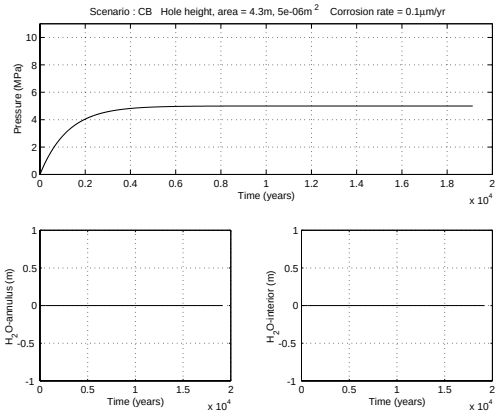

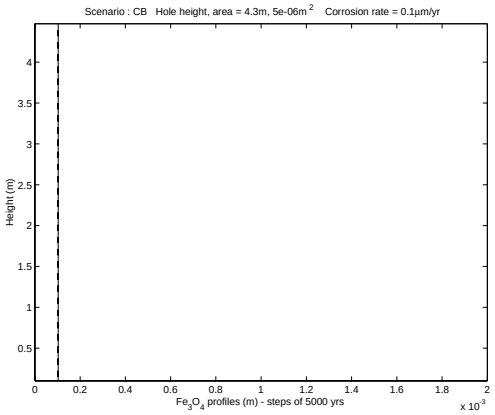

Model CTB

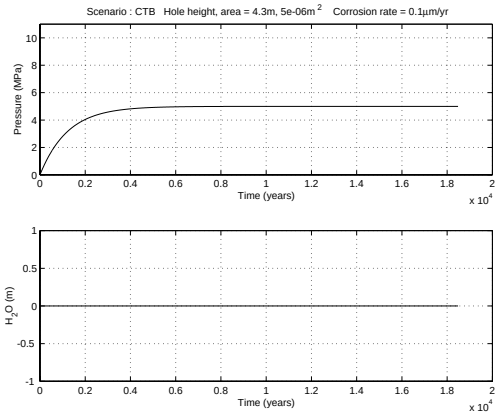

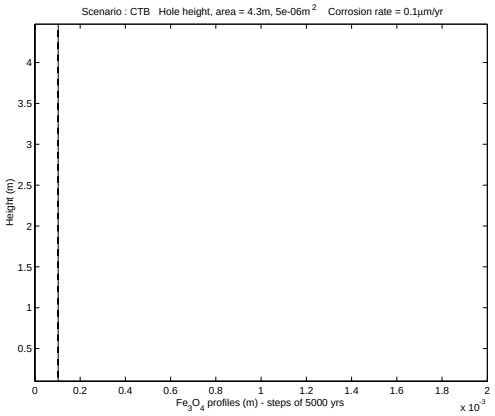

Model CT

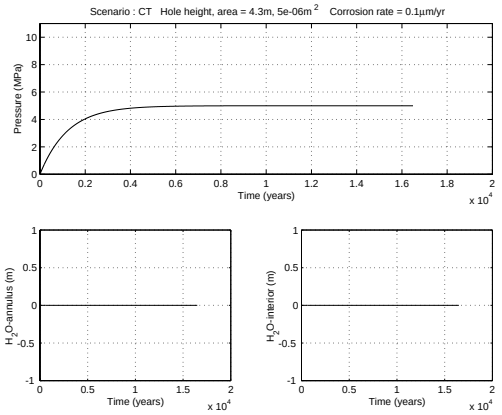

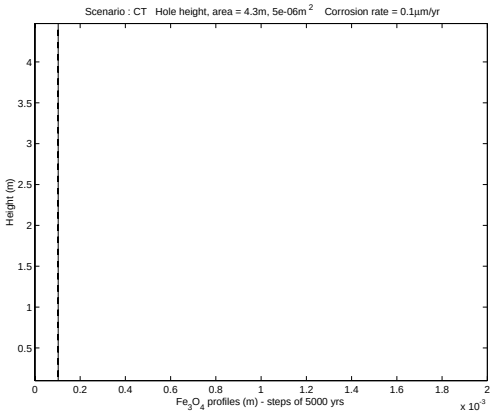

Figure 2.13:Penetration at 4.3m, Penetration area = $5\times10^{-6}m^2$, Corrosion rate = $0.1\mu m/year$

Model CB

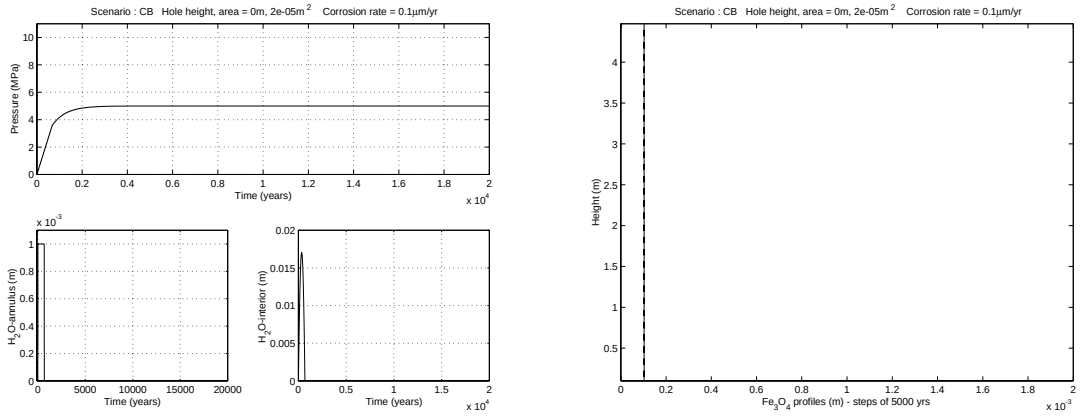

Model CTB

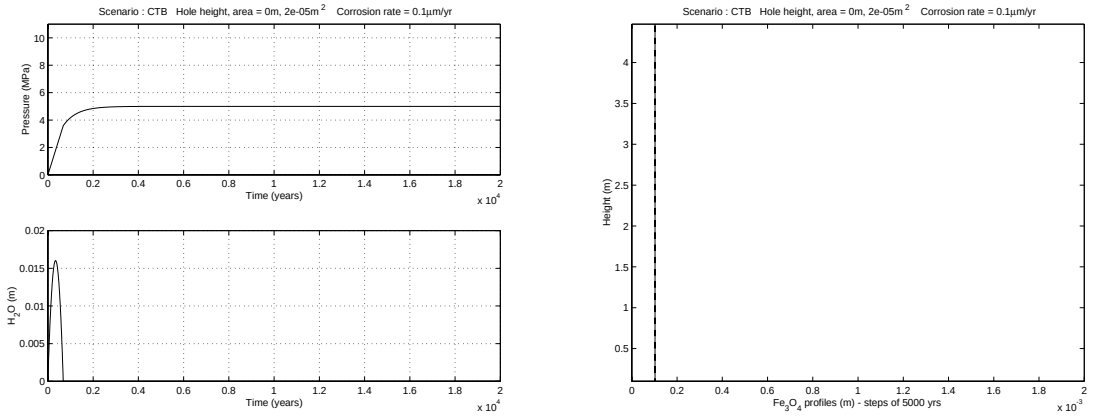

Model CT

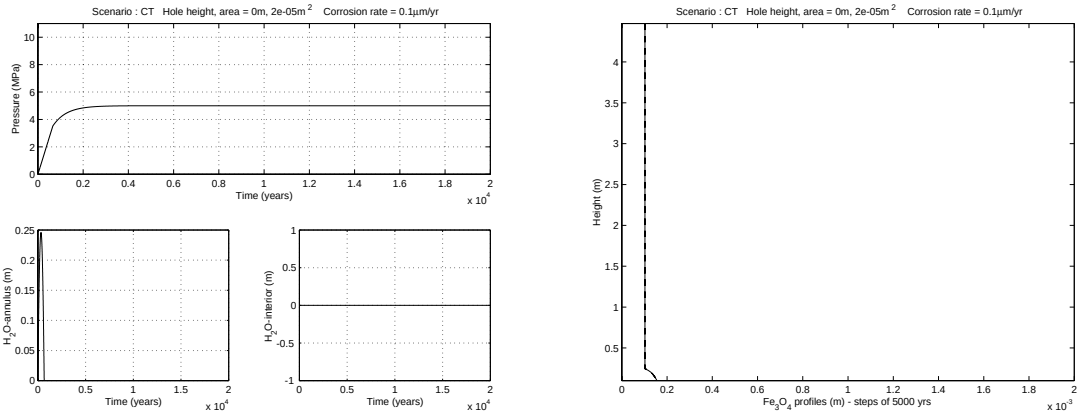

Figure 2.14:Penetration at 0m, Penetration area = $2\times10^{-5}m^2$,
Corrosion rate = $0.1\mu m/year$

Model CB

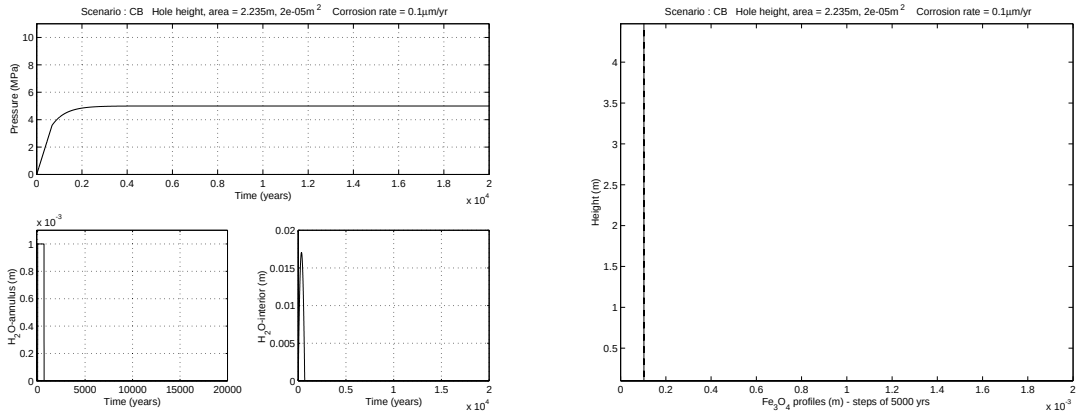

Model CTB

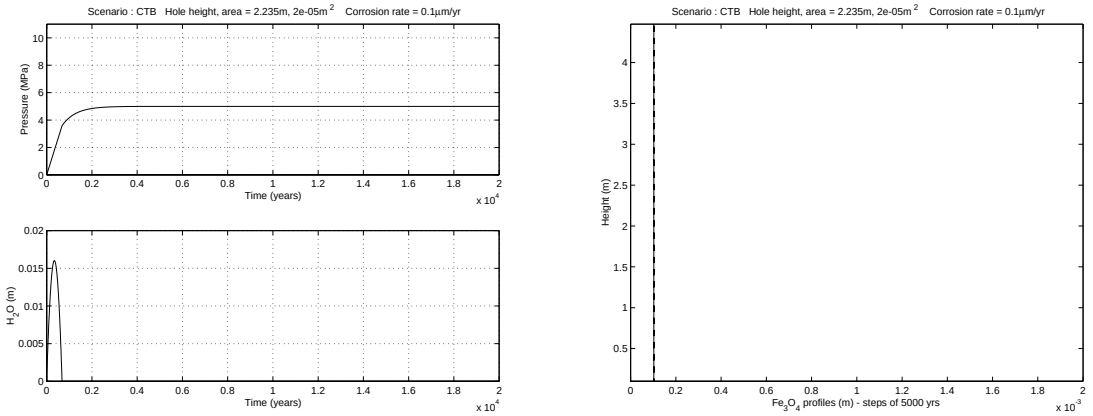

Model CT

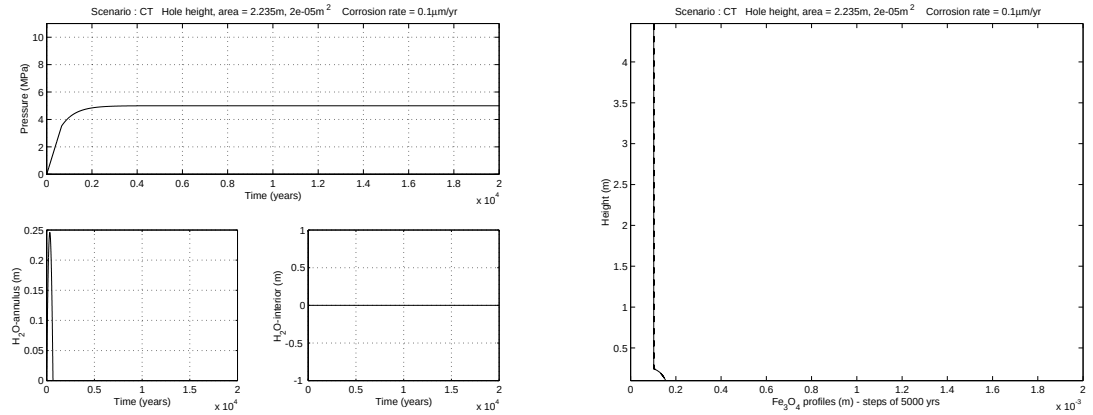

Figure 2.15:Penetration at 2.235m, Penetration area = $2\times10^{-5}m^2$, Corrosion rate = $0.1\mu m/year$

Model CB

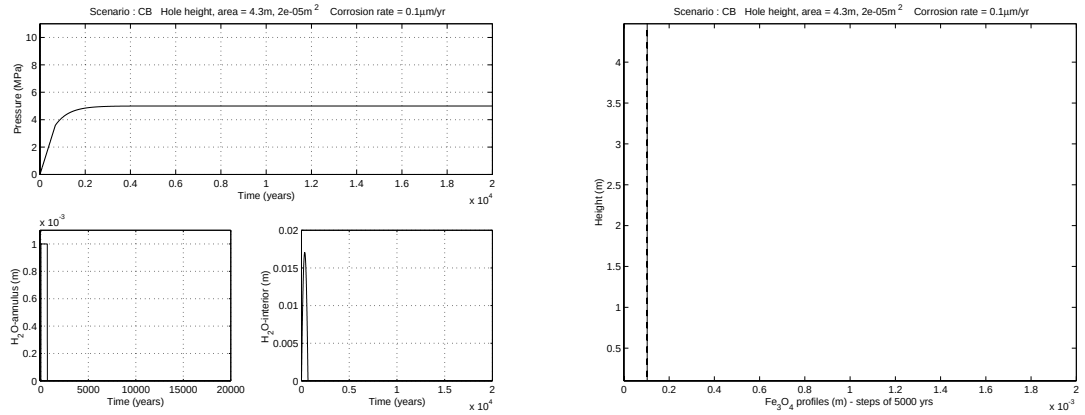

Model CTB

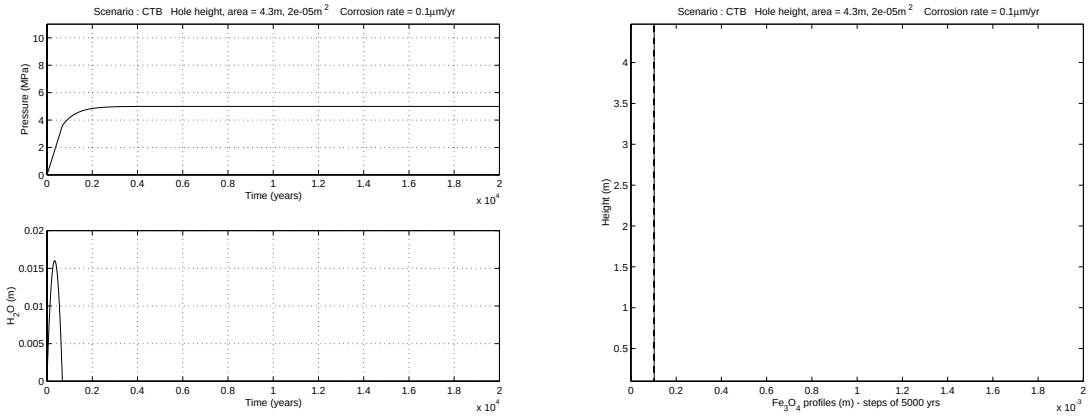

Model CT

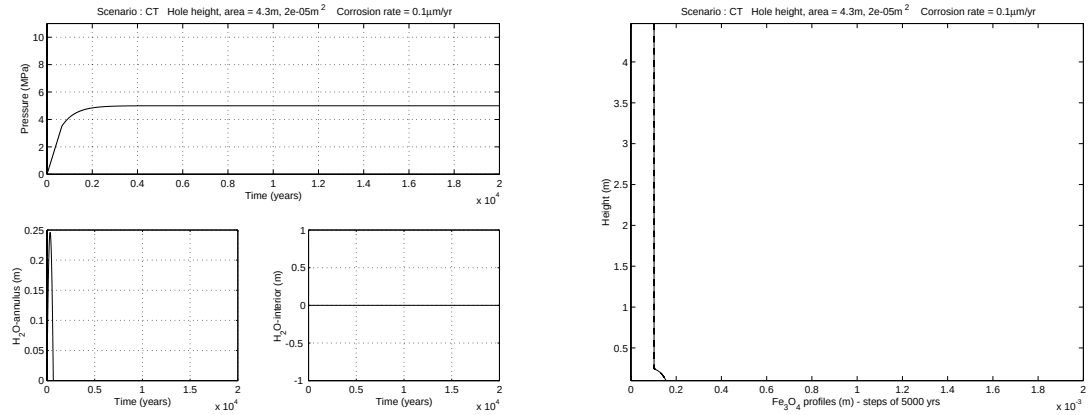

Figure 2.16:Penetration at 4.3m, Penetration area = $2\times10^{-5}m^2$,
Corrosion rate = $0.1\mu m/year$

Penetration area = $2\times10^{-5}\mathbf{m^2}$ **Penetration area =** $5\times10^{-6}\mathbf{m^2}$

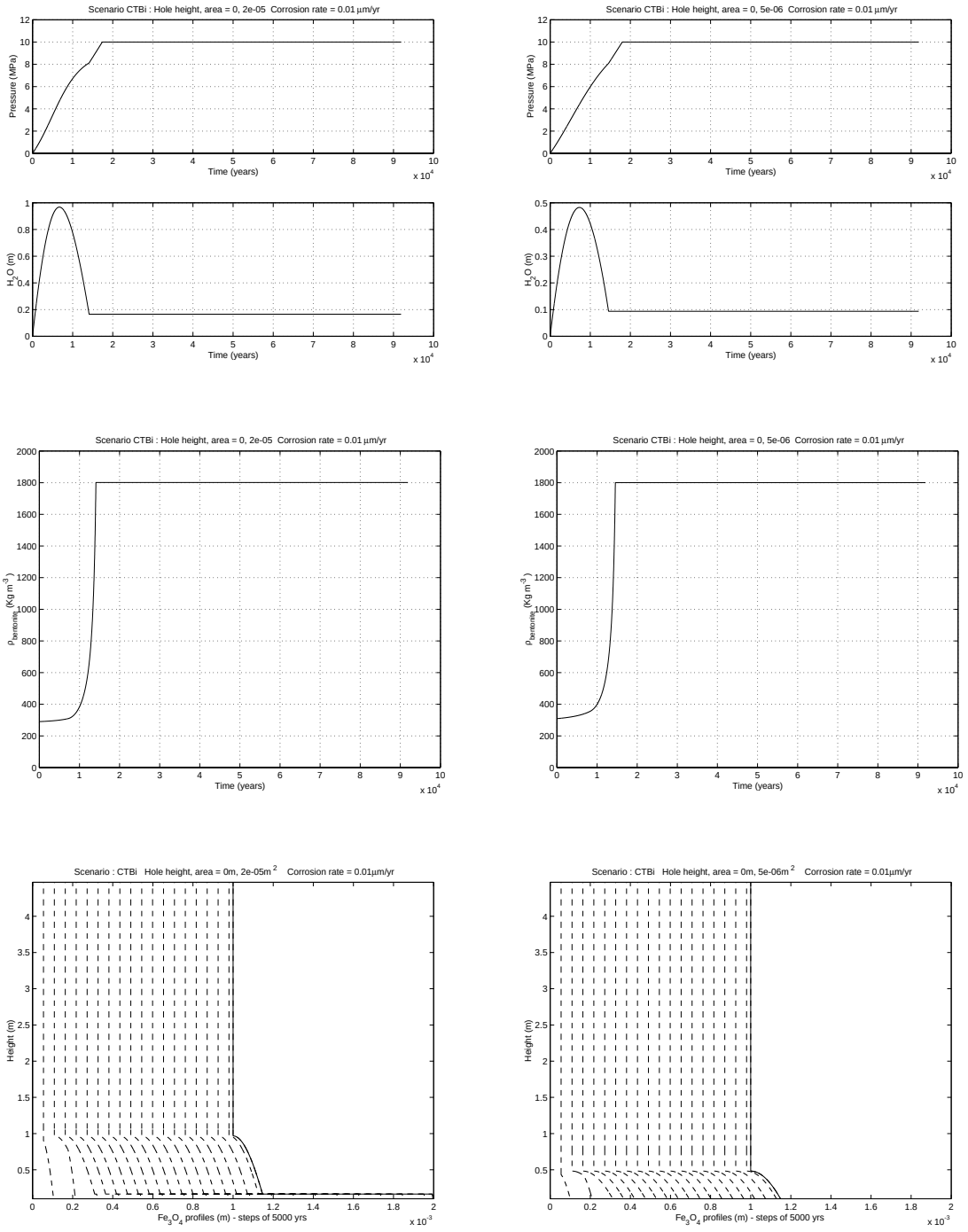

Figure 2.17:Model CTBi $v = 0.01\mu$m/year Penetration height =0m

3 Diffusion-limited corrosion of steel container after desaturation

3.1 Conceptual model

We consider the situation where the gas pressure within the canister reaches the hydrostatic pressure and no (liquid) water can flow into the system. In this situation though, water is transported as vapour. Since the anaerobic corrosion of the steel produces hydrogen gas and it flows out of the system, we need to consider the following two transport mechanisms for the vapour;

1. diffusion,

2. counter advection due to gas flow.

We conceptualise geometry of the system by a disk of constant thickness connected with a cylinder corresponding to the annular gap and the penetration through the copper overpack respectively (Figure 14).

Figure 3.1: Geometry of the system

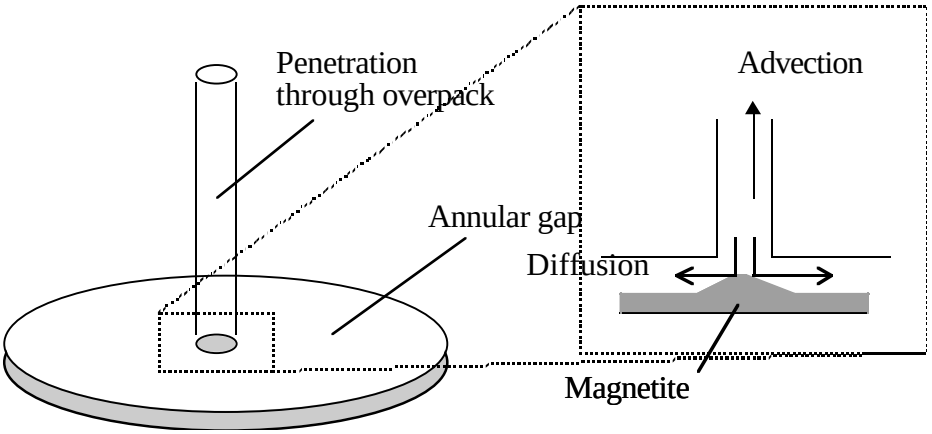

The vapour transported into the disk reacts with the steel and is consumed, producing hydrogen gas and magnetite. Generation of hydrogen gas increases the gas pressure in the system and gas break through will occur when it exceeds a threshold level. In reality, gas flow is intermittent. However, since the time scale associated with this intermittent behaviour is much smaller than the global time scale, we only consider a flow rate which is averaged in time. The magnetite layer formed at the steel surface acts as a protective barrier against further corrosion. Moreover, consumption of the vapour due to corrosion decreases the local vapour density and hence the rate of corrosion. Hence, in order to model the self-inhibiting effect of the corrosion, we need to relate the corrosion rate with the local vapour density and the magnetite thickness.

3.2 Mathematical formulation

(1) Equations for vapour transport through the penetration

Transport of vapour through the cylindrical penetration is described by the following advection-diffusion equation

$$
\begin{aligned}
&\tilde{u}_t = D\tilde{u}_{zz} - v_0\tilde{u}_z, \quad 0 \le z \le l, 0 < t \\
&\tilde{u}(0,t) = U(t), \quad 0 < t \\
&\tilde{u}(l,t) = \rho_{sat}, \quad 0 < t \\
&\tilde{u}(z,0) = \rho_{sat}, \quad 0 \le z \le l
\end{aligned} \tag{46}
$$

where

$\tilde{u}(z,t)$: vapour density in the cylinder,

D : diffusion coefficient for vapour,

$v_0(z,t)$: gas flow velocity through the cylinder,

$U(t)$: vapour density at the interface of the cylinder with the disk,

l : length of the cylinder,

ρ_{sat} : saturation level of vapour density at the given temperature.

In what follows, we assume that the vapour density profile always achieves the stationary condition and that the flow velocity (yet to be determined) is independent from z. Thus, by solving

$$
\begin{aligned}
&0 = D\tilde{u}_{zz} - v_0\tilde{u}_z, \quad 0 \le z \le l, \\
&\tilde{u}(0,t) = U(t), \\
&\tilde{u}(l,t) = \rho_{sat},
\end{aligned} \tag{47}
$$

we have

$$
\tilde{u}(z,t) = \frac{e^{\frac{v_0 l}{D}} - e^{\frac{v_0 z}{D}}}{e^{\frac{v_0 l}{D}} - 1} U(t) + \frac{e^{\frac{v_0 z}{D}} - 1}{e^{\frac{v_0 l}{D}} - 1} \rho_{sat}. \tag{48}
$$

Equation (48) implies that we have the following estimate for the vapour flux density, $F(t)$

(49) $$F(t) = D\tilde{u}_z - v_0\tilde{u} = \frac{\rho_{sat} - e^{\frac{v_0 l}{D}} U(t)}{e^{\frac{v_0 l}{D}} - 1} v_0.$$

(2) Equations for vapour transport and magnetite growth at the interface

We consider a small (sub)disk of the same radius as the cylindrical penetration, r_0, and regard this as the interface between the cylinder and the disk. Assuming that the disk is so small and, thence, well-stirred, we have the following system of ordinary differential equations

$$\frac{d}{dt}\Big[U\big(h_g - (\alpha-1)W\big)\Big] =$$

$$-\gamma R(U,W) + F + \frac{2}{r_0}\big(h_g - (\alpha-1)W\big)\Big[Du_r|_{r=r_0} + v(r_0,t)U\Big], \quad 0 < t$$

(50) $$\frac{dW}{dt} = R(U,W),\ 0 < t$$

$$U(0) = \rho_{sat},$$

$$W(0) = c^* /(\alpha - 1),$$

where

$U(t)$: vapour density in the subdisk,

h_g : initial gap width,

W : accumulated loss of steel due to corrosion,

α : volumetric ratio of magnetite to steel,

γ : mass of water consumed by unit corrosion,

$R[x,y]$: corrosion rate due to vapour of density x
adjacent to magnetite layer of thickness y

$$R[x,y] = \frac{\mu}{1 + \frac{y}{l_s}}\left(\frac{x}{\rho_{sat}}\right)^n$$

μ : corrosion rate of wet steel surface
without magnetite layer,

l_s : corrosion suppression length,

n : constant,

c^* : initial thickness of the magnetite layer.

(3) Equations for vapour transport and magnetite growth in the rest of the disk

Behaviour of the vapour and the magnetite in the rest of the disk is formulated by the following reaction-advection-diffusion equations, assuming a radial symmetry

$$\frac{\partial}{\partial t}\left[u\left(h_g-(\alpha-1)w\right)\right]=$$

$$\frac{1}{r}\frac{\partial}{\partial r}\left[r\left(h_g-(\alpha-1)w\right)\left(D\frac{\partial u}{\partial r}+v\,u\right)\right]-\gamma\,R(u,w),\quad r_0\le r\le r_1,\ 0<t$$

(51)
$$\frac{\partial w}{\partial t}=R(u,w),\quad r_0\le r\le r_1,\ 0<t$$

$$u(r_0,t)=U(t),\quad \left.\frac{\partial u}{\partial r}\right|_{r=r_1}=0,\quad 0<t$$

$$u(r,0)=\rho_{sat},\quad w(r,0)=c^*,\quad r_0\le r\le r,$$

where

$u(r,t)$: *vapour density in the disk at* (r,t),
$w(r,t)$: *magnetite thickness in the disk at* (r,t),
r_1 : *radius of the disk*.

As for the average gas flow velocity, $v(r,t)$, we have the following estimate based on the volumetric balance of the gas within an arbitrary ring $r\le\xi\le r_1$, at the fixed pressure*

(52)
$$v(r,t)=\frac{1}{r\left(h_g-(\alpha-1)w\right)}\int_r^{r_1}\left[\beta R\left(u(\xi,t),w(\xi,t)\right)+\frac{\partial w(\xi,t)}{\partial t}\right]d\xi$$

$$\frac{1+\beta}{r\left(h_g-(\alpha-1)w\right)}\int_r^{r_1}R\left(u(\xi,t),w(\xi,t)\right)d\xi.$$

where

β: volume (at the given pressure) of hydrogen gas generated by unit corrosion.

Remark

The gas pressure oscilates between the hydrostatic pressure and the gas break through pressure according to the intermittent gas flow. However, for the purpose of calculating time-averaged gas flow, we can assume the average gas pressure all the time for the estimate of β.

3.3 Results

In order to simulate diffusion-limited corrosion of the steel container, the system of integro-differential equations needs to be solved numerically. To do this, we spatially discretise $u(r,t), w(r,t)$ and express the integration in (52) as sum of finite terms. Then, the system of integro-differential equations (49) to (52) reduces to a set of simultaneous ordinary differential equations. We solve this system of ODEs by using Gear's method.

Calculations are made for the cases taken from the previous section which are summarised in Table 3.1, where as conditions common to all the cases are listed below;

$$
\begin{aligned}
& r_1 = 2.06[m] \,(steel\ surface\ area = 13.285\, m^2) \\
& h_g = 2.0 \times 10^{-3}\,[m], \\
& D = 28.4\left[m^2 / yr\right], \\
& \rho_{sat} = 3.27 \times 10^{-2}\left[kg / m^3\right], \\
& \alpha = 3.0[-], \\
& \beta = 83.8[-], \\
& \gamma = 3366.
\end{aligned}
$$

Remark

1. Saturation level of the vapour density is estimated at 30 degrees Celsius.
2. β is calculated assuming that the time averaged gas pressure is equal to the hydrostatic pressure 5 Mpa.

The power included in the corrosion rate expression, n, was set to be unity. In fact, n needs to be equal to or greater than one in order to guarantee Lipshitz continuity of the nonlinearity in the system and, hence, uniqueness of the solution. However, with the given initial and boundary conditions, vapour density is nonzero everywhere provided n is strictly positive. Hence we can treat the sublinear case as well.

Table 3.1: Summary of the cases considered

	Penetration height (m)	Crack position	Penetration area (m^2)	Initial corrosion rate (m/yr)	Initial magnetite thickness (m)	Corrosion suppression length (m)
1	0	CT	5 E-6	1 E-7	0	1 E-3
2	0	CT	5 E-6	1 E-7	0	1 E-4
3	0	CT	5 E-6	1 E-8	0	1 E-3
4	0	CT	5 E-6	1 E-8	0	1 E-4
5	0	CB	5 E-6	1 E-7	1.03 E-4	1 E-3
6	0	CB	5 E-6	1 E-7	1.03 E-4	1 E-5
7	0	CT	2 E-5	1 E-8	4.84 E-4	1 E-3
8	0	CT	2 E-5	1 E-8	4.84 E-4	1 E-5

Remark

1. The values for magnetite thickness when the diffusion-limited corrosion starts are based on the results calculated for the corresponding cases in **[3]**.

2. CT: Crack at the top, CB : Crack at the bottom.

Results are shown in Figures 3.2 to 3.9. As can be seen from the figures, magnetite thickness possesses the maximum at r_0 and is nonzero everywhere in the disk. In all the cases, vapour density is monotonically decreasing (within peripheral regions in the ring, in particular). This is mainly due to the fact that the gas velocity is greater at later times because of the decreased gap width.

Table 3.2 summarises time required for the magnetite layer to fill the annular gap. It varies by three orders of magnitude and appears to be most sensitive to the initial corrosion rate and the corrosion suppression length among the input parameters considered in Table 3.1. The corrosion suppression length also affects the spatial profile of the magnetite layer, i.e. the larger the suppression length, more localised the magnetite accumulation. This spatial pattern of the magnetite growth may affect the mode of mechanical failure of the outer copper overpack as described in **[1]**.

Table 3.2: Time for magnetite layer to fill the annular gap

1	8.3 E3 years
2	4.7 E4 years
3	7.6 E4 years
4	4.8 E5 years
5	6.8 E3 years
6	4.8 E5 years
7	6.9 E4 years
8	4.6 E6 years

Figure 3.2:
Case 1
(a) and (b) are 20 snapshots of vapour density in [kg/m3] and magnetite thickness in [m] distribution in the disk taken at a regular interval from t=0 to 8.3 E3 years respectively.
(c): Comparison of the maximum thickness of magnetite and the average thickness both as functions of time [years].

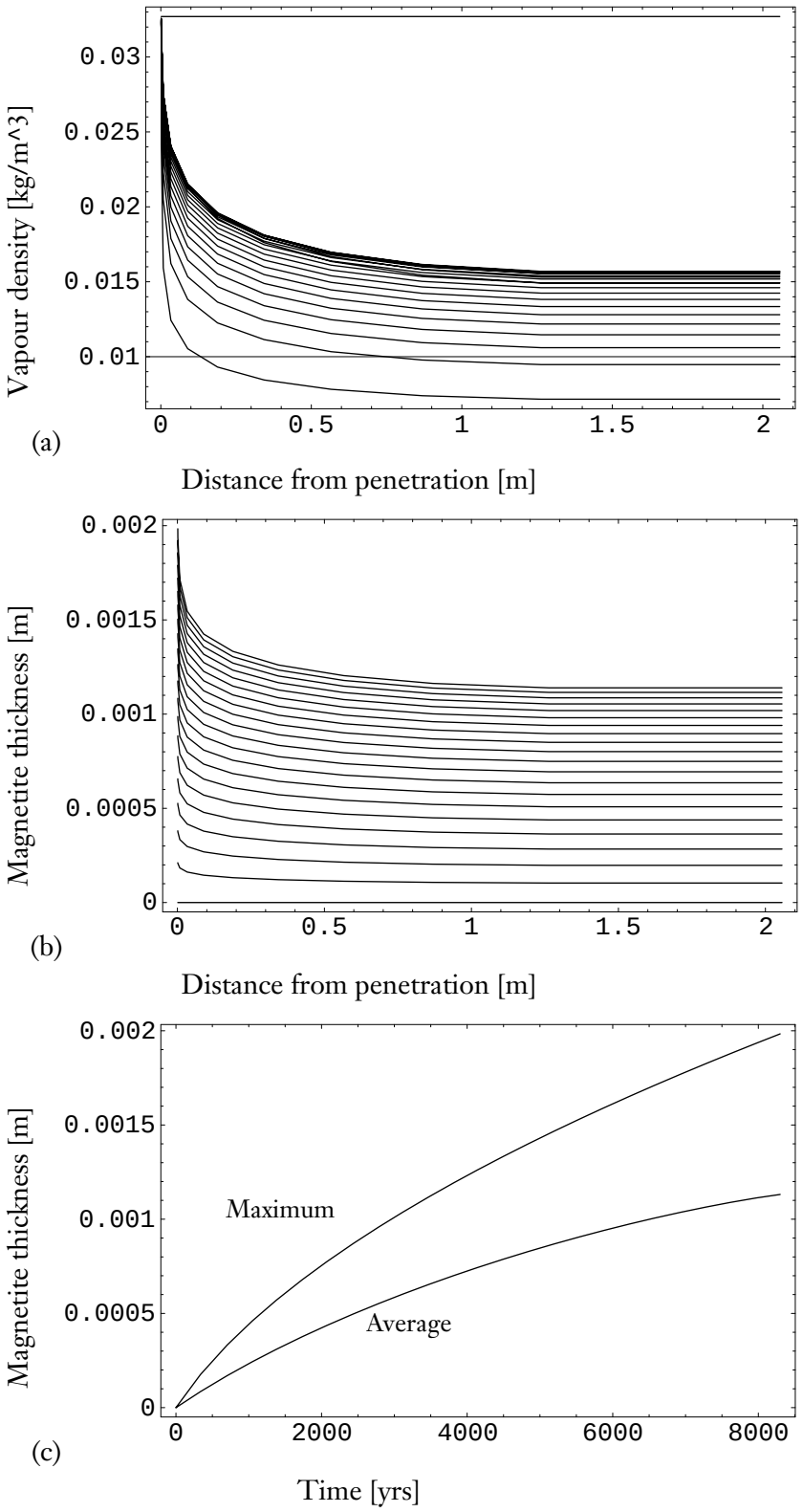

Figure 3.3:
Case 2
(a) and (b) are 20 snapshots of vapour density in [kg/m3] and magnetite thickness in [m] distribution in the disk taken at a regular interval from t=0 to 4.7 E4 years respectively.
(c): Comparison of the maximum thickness of magnetite and the average thickness both as functions of time [years].

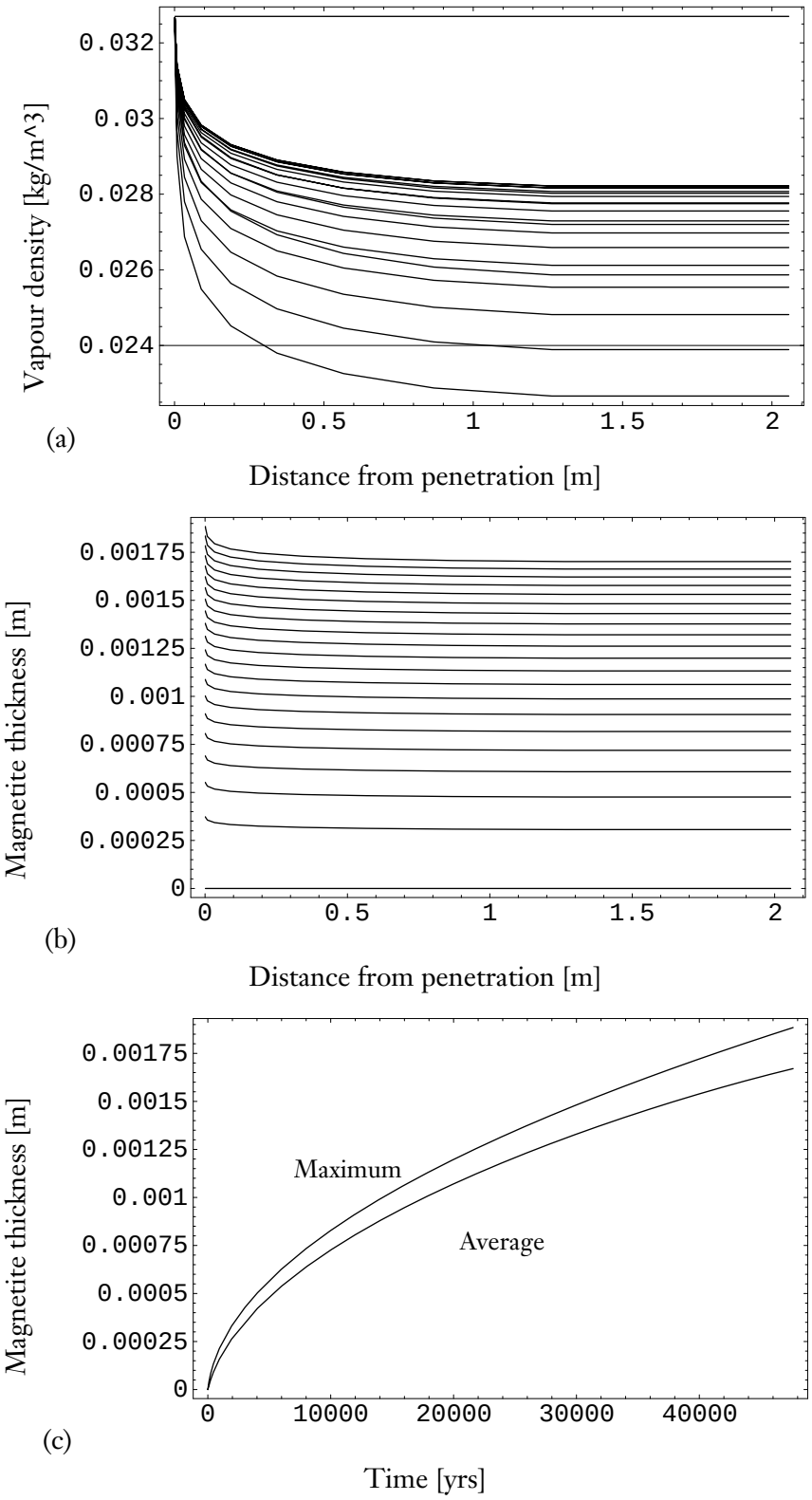

Figure 3.4:
Case 3
(a) and (b) are 20 snapshots of vapour density in [kg/m3] and magnetite thickness in [m] distribution in the disk taken at a regular interval from t=0 to 7.6 E4 years respectively. (c): Comparison of the maximum thickness of magnetite and the average thickness both as functions of time [years].

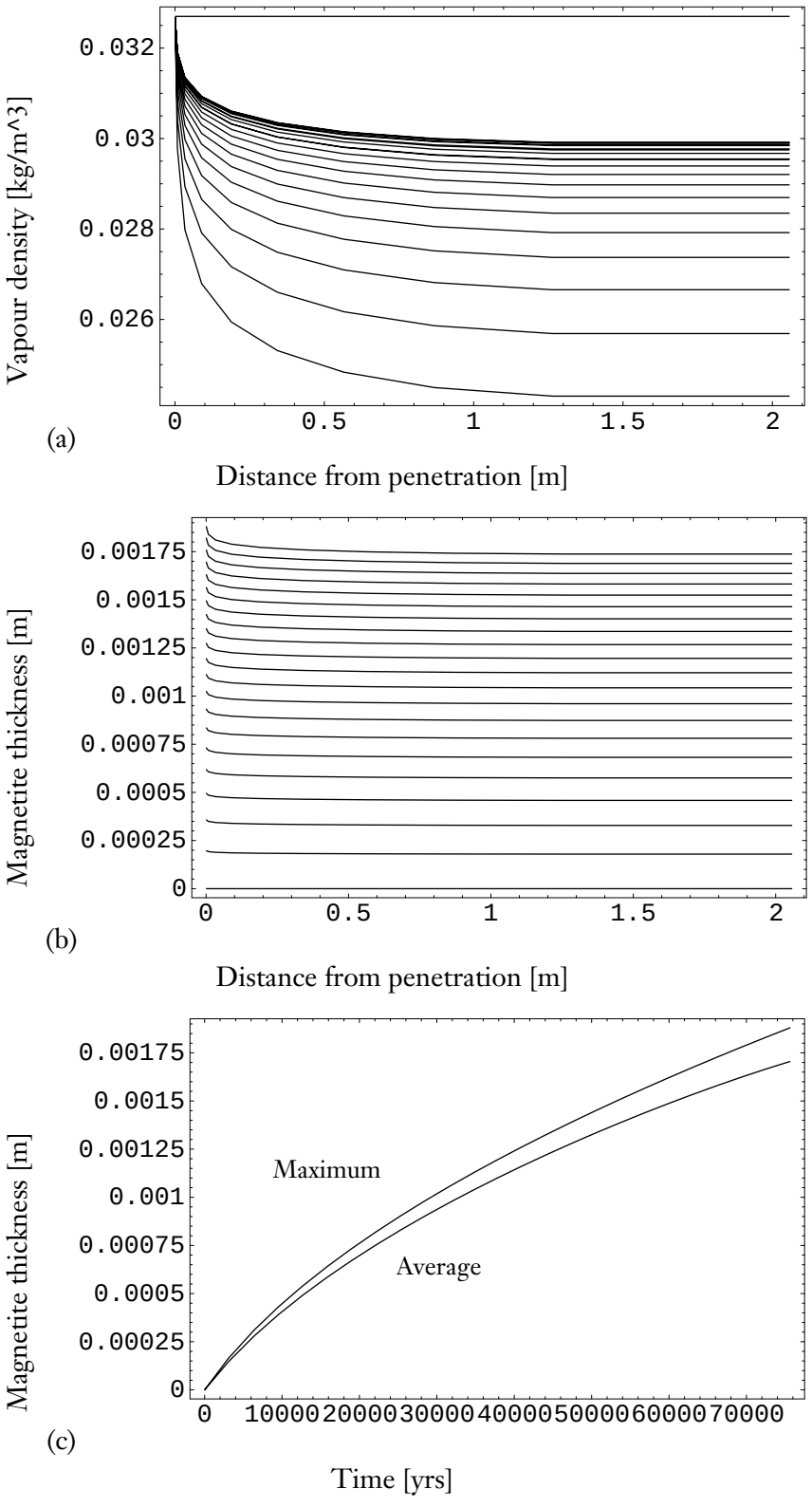

Figure 3.5:
Case 4
(a) and (b) are 20 snapshots of vapour density in [kg/m3] and magnetite thickness in [m] distribution in the disk taken at a regular interval from t=0 to 4.8 E5 years respectively.
(c): Comparison of the maximum thickness of magnetite and the average thickness both as functions of time [years].

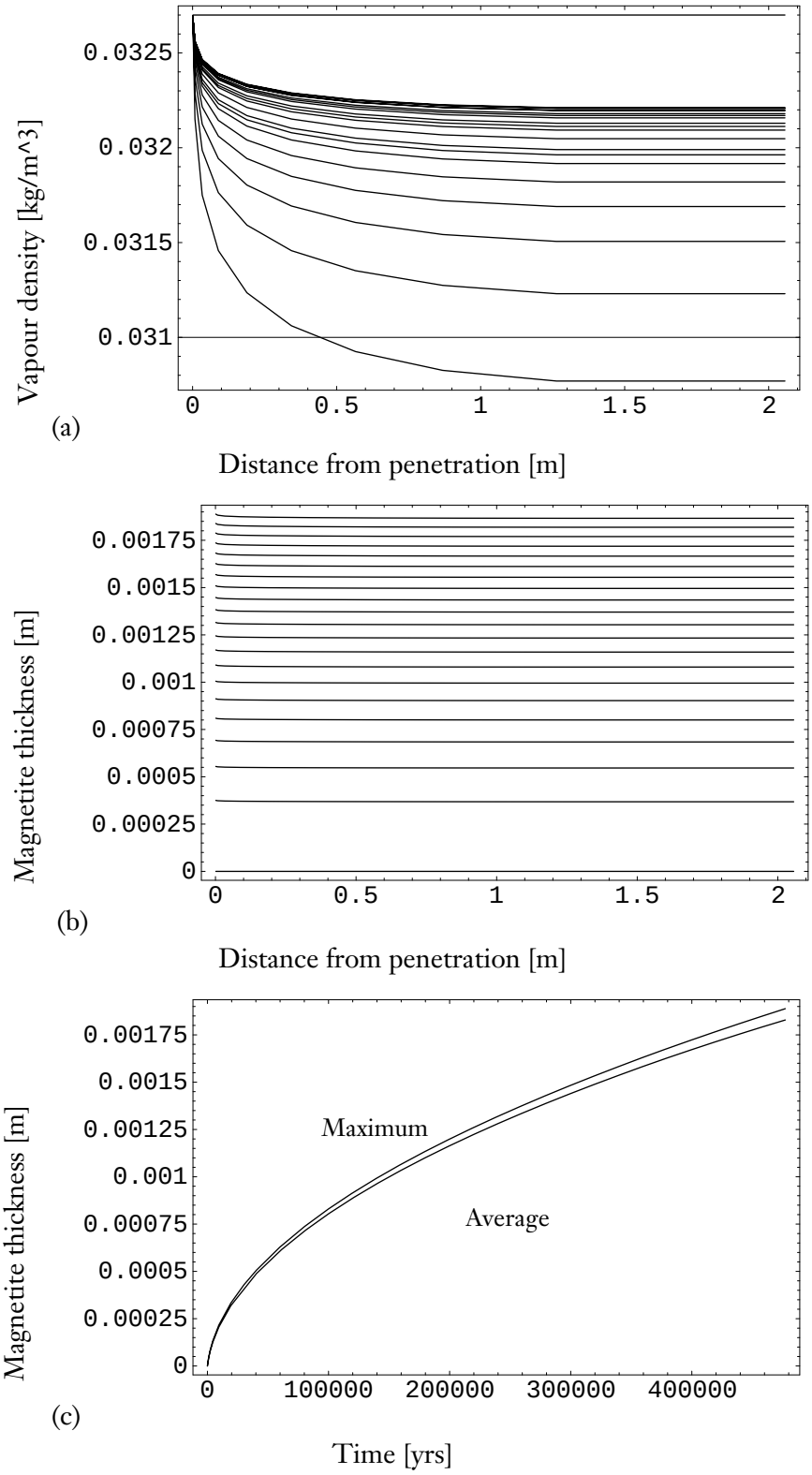

Figure 3.6:
Case 5
(a) and (b) are 20 snapshots of vapour density in [kg/m3] and magnetite thickness in [m] distribution in the disk taken at a regular interval from t=0 to 6.8 E3 years respectively. (c): Comparison of the maximum thickness of magnetite and the average thickness both as functions of time [years].

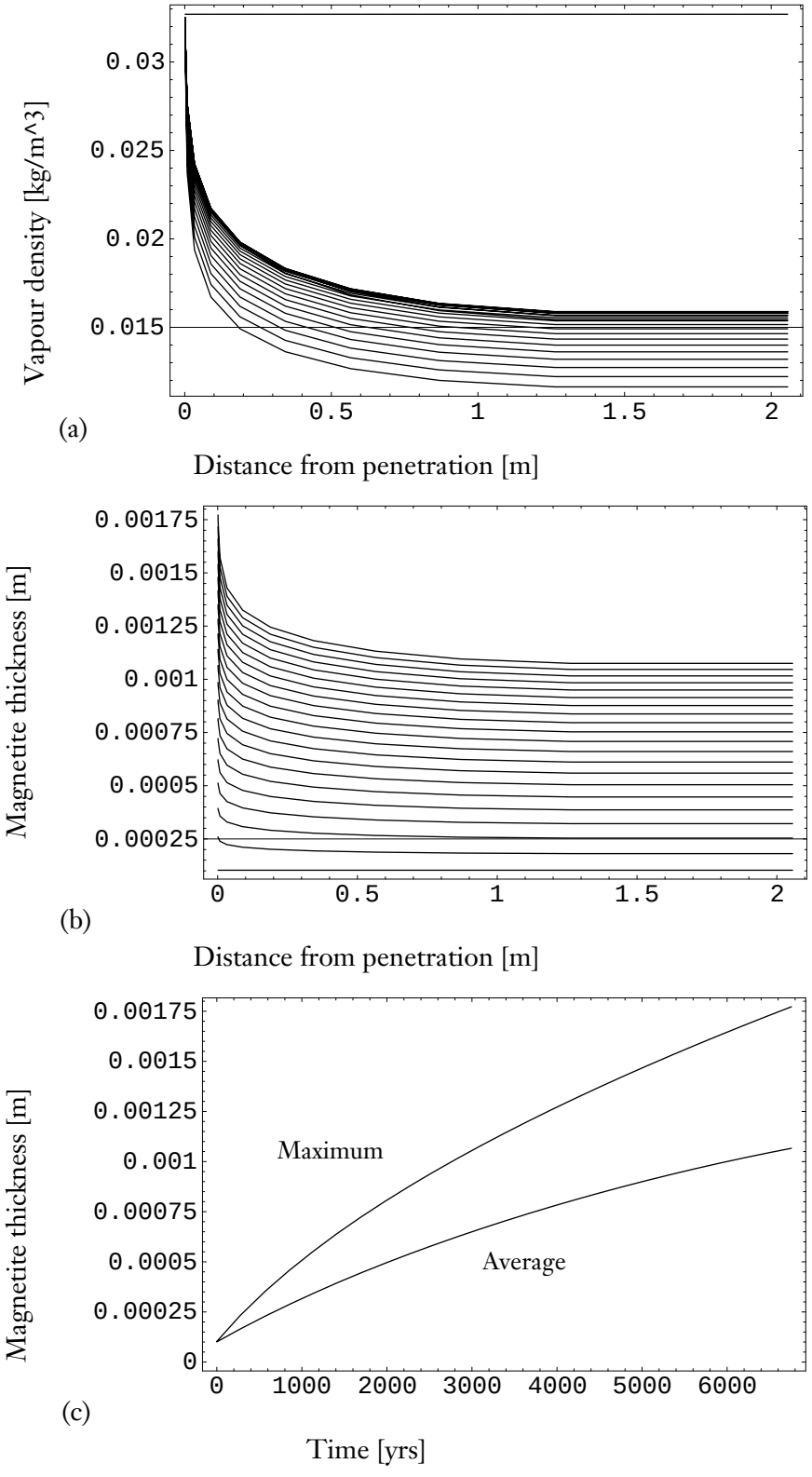

Figure 3.7:
Case 6
(a) and (b) are 20 snapshots of vapour density in [kg/m3] and magnetite thickness in [m] distribution in the disk taken at a regular interval from t=0 to 4.8 E5 years respectively.
(c): Comparison of the maximum thickness of magnetite and the average thickness both as functions of time [years].

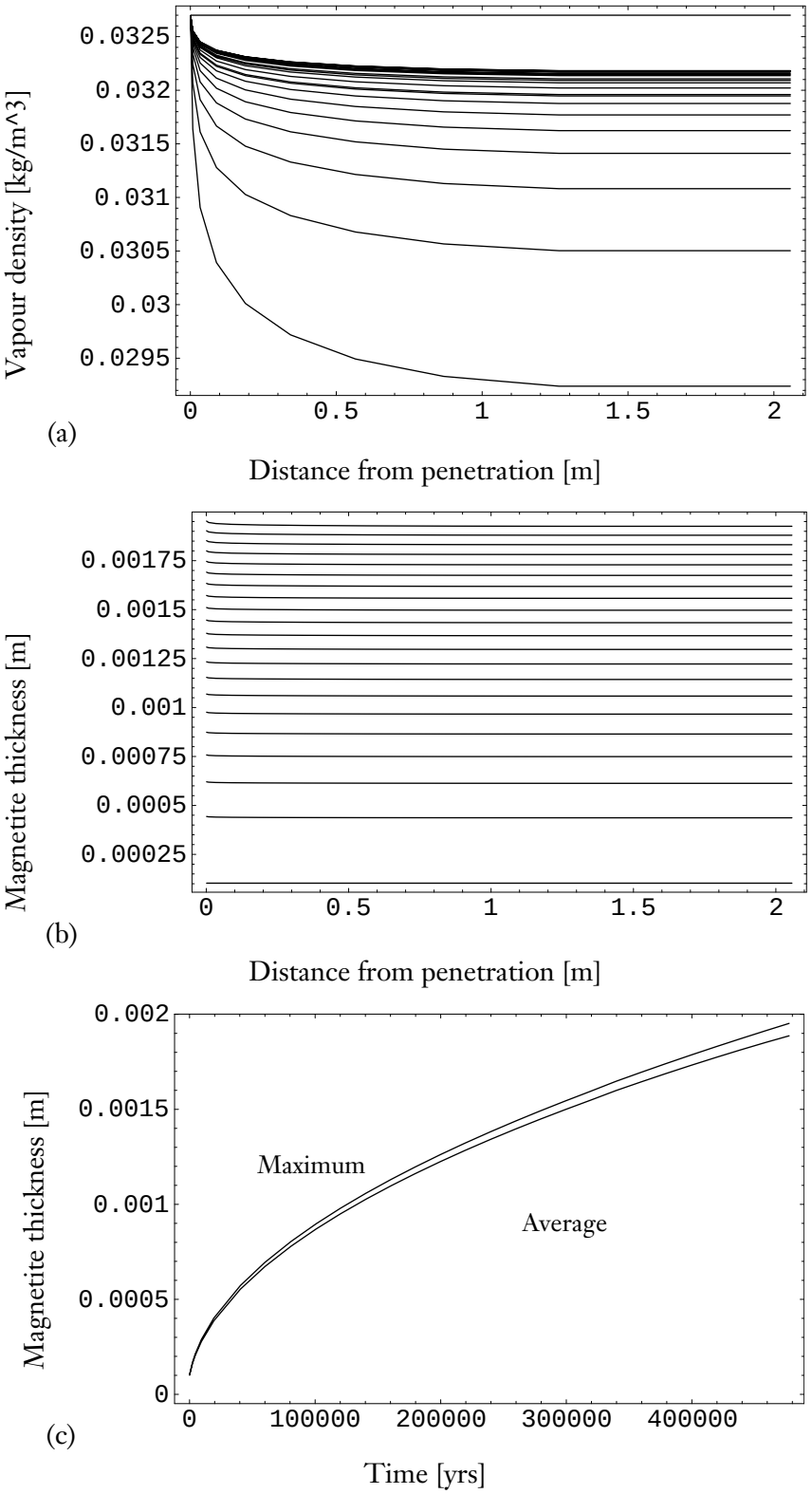

Figure 3.8: Case 7 (a) and (b) are 20 snapshots of vapour density in [kg/m3] and magnetite thickness in [m] distribution in the disk taken at a regular interval from t=0 to 6.9 E4 years respectively. c):Comparison of the maximum thickness of magnetite and the average thickness both as functions of time[years].

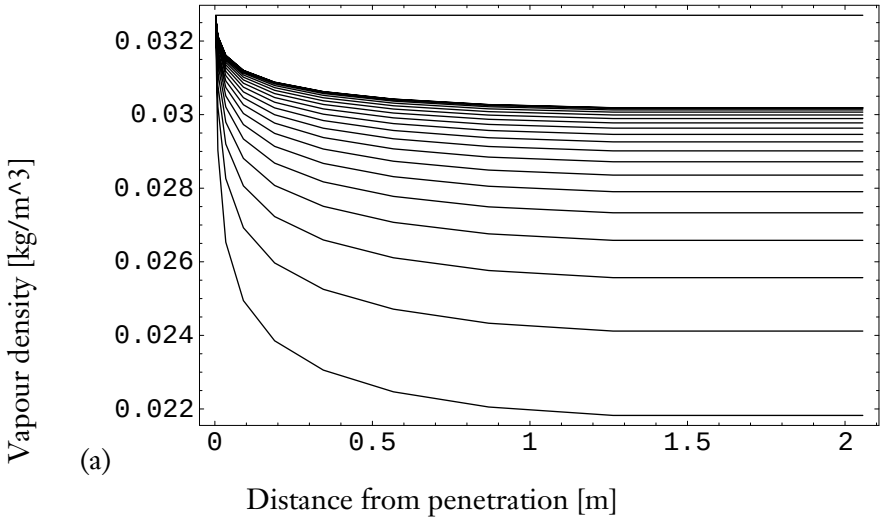

(a)

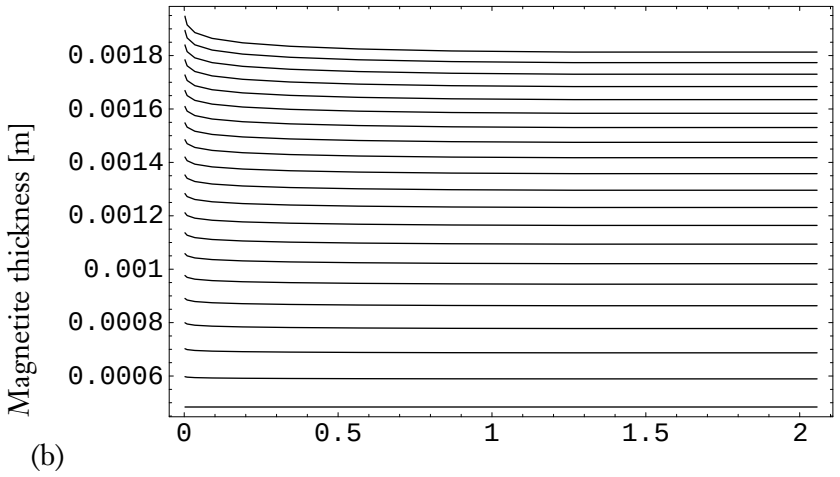

(b)

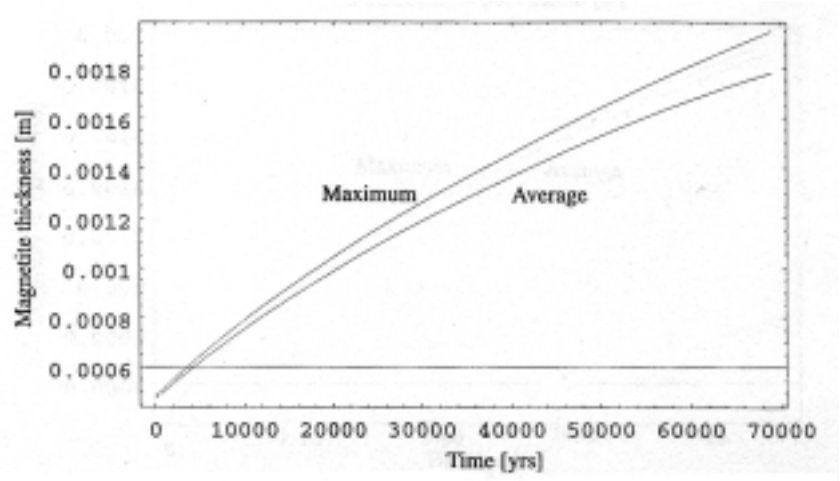

(c)

Figure 3.9:
Case 8
(a) and (b) are 20 snapshots of vapour density in [kg/m3] and magnetite thickness in [m] distribution in the disk taken at a regular interval from t=0 to 4.6 E6 years respectively.
(c): Comparison of the maximum thickness of magnetite and the average thickness both as functions of time [years].

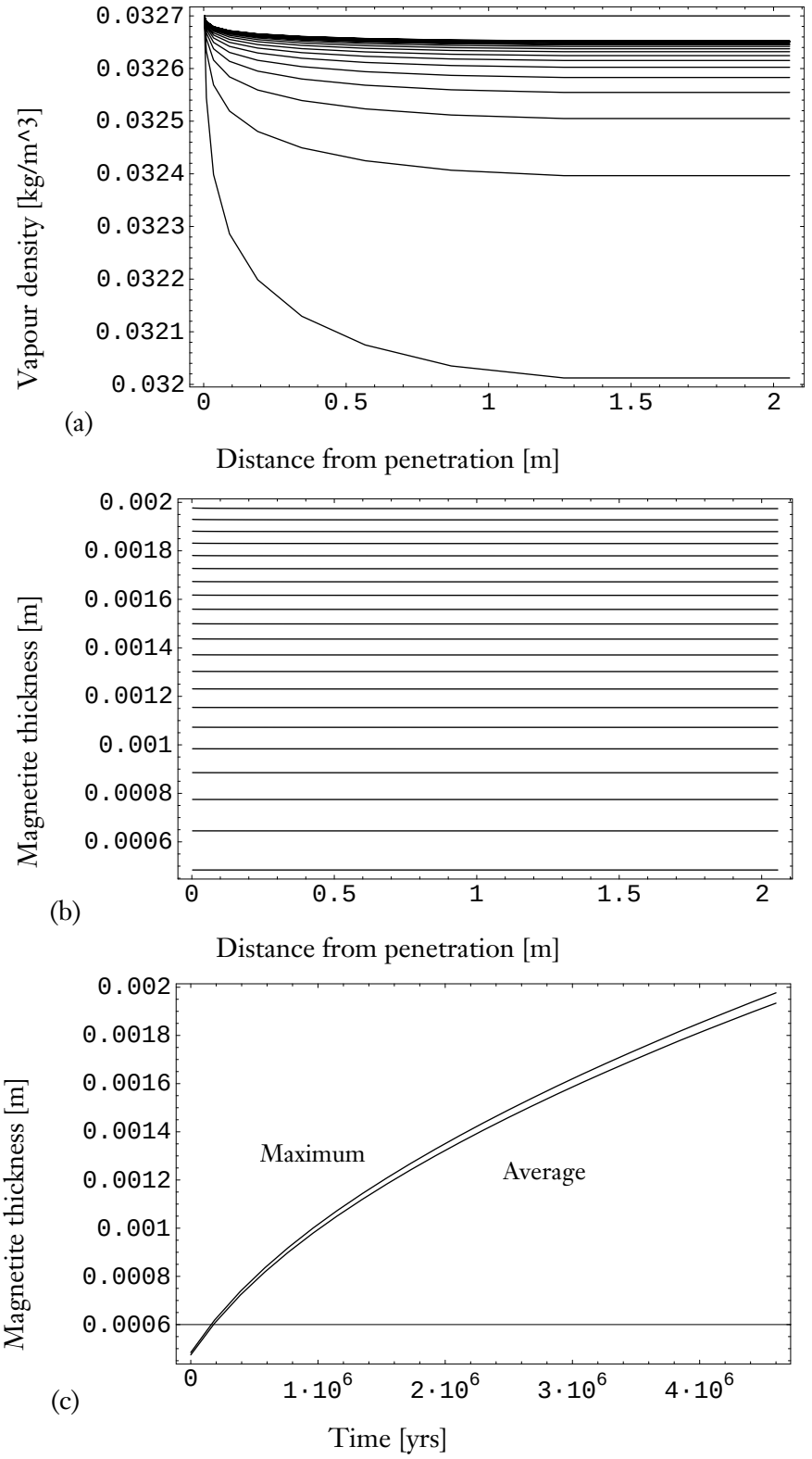

4 Conclusion of consequence analysis

As was discussed in sections 2 and 3, there are a number of alternatives in scenario, mathematical models, and parameter values. These variations at different levels make the system's behaviour bifurcate both in qualitative and quantitative manner. In particular, questions such as

- whether bentonite gel can migrate into the penetration through the copper overpack and stay in the annular gap without fully expelled by the gas pressure?
- how large is the long term corrosion rate of the steel and, in particular, how does the magnetite layer act as a protective layer against further corrosion?

seem to be of high importance.

References

[1] Alex E Bond, Andrew R Hoch, Gareth D Jones, Aleks J Tomczyk, Richard M Wiggin, William J Worraker, *Assessment of a spent fuel disposal canister: Assessment studies for a copper canister with cast steel inner component*, SKB Technical Report 97-19, 1997

[2] NAGRA, *Kristalline-1 Safety Assessment Report*, NAGRA Technical Report 93-22, 1994

[3] Ivars Neretnieks, *Modelling Oxidative Dissolution of Spent Fuel*, Mat. Res. Soc. Symp. Proc. Vol. 465, 573 - 580, Materials Research Society, 1997

[4] J. Bruno, E. Cera, L. Duro, T.E. Eriksen and L.O. Werme, *A Kinetic Model for the Stability of Spent Fuel Matrix under Oxic Conditions*, Journal of Nuclear Materials 238, 110 - 120, 1996

[5] J. Glimm, B. Lindquist, O. McBryan and G. Tryggvason, *Sharp and diffuse fronts in oil reservoirs: Front tracking and capillarity*, Proc. Math. and Comp. Methods in Seismic Exploration and Reservoir Modelling, SIAM, 1985

[6] Tamas Vicsek, *Fractal Growth Phenomen*a, World Scientific, 1989

[7] M. D. Impey, H. Takase, and B. M. Watkins, *Technical Evaluation of Gas Effects for the Rokkasho Phase II Shallow Land Burial Facility; Review Report*, QuantiSci Report IE5011A-2, 1997

[8] S.T. Horseman and J. F. Harrington, Study of Gas Migration in MX-80 Bentonite, BGS WE/97/7 1997

[9] Roland Pusch, Stability of Bentonite Gels in Crystalline Rock; Physical Aspects, KBS Technical Report 83-04

ISSN 1404-0344

CM Gruppen AB, Bromma, 1999